RETROFIT TECHNIQUES FOR DISTORTION-INDUCED FATIGUE DAMAGE IN STEEL BRIDGE GIRDERS

By

Say Hak Bun

Submitted to the graduate degree program in Civil Engineering and the Graduate Faculty of the University of Kansas in partial fulfillment of the requirements for the degree of Master of Science.

_____	_____
Co- Chairperson Dr. Caroline Bennett	Co- Chairperson Dr. Adolfo Matamoros
	_____
	Dr. Stanley Rolfe

Date Defended: 12/20/2013

The Thesis Committee for Say Hak Bun

certifies that this is the approved version of the following thesis:

RETROFIT TECHNIQUES FOR DISTORTION-INDUCED FATIGUE DAMAGE IN STEEL BRIDGE GIRDERS

_____	_____
Co- Chairperson Dr. Caroline Bennett	Co- Chairperson Dr. Adolfo Matamoros

_____

Dr. Stanley Rolfe

Date approved: 03/12/2014

EXECUTIVE SUMMARY

A large number of steel bridges constructed before the mid-1980s are susceptible to *distortion-induced fatigue* damage. Repairing distortion-induced fatigue cracking in two framing systems was explored within this thesis: cross-frame-to-girder connection and stringer-to-floorbeam connections. Several different retrofit measures have been developed to either stop further crack growth or to slow the rate of crack propagation. The cross-frame-to-girder connection has been identified as a severe connection in term of fatigue cracking induced by out-of-plane forces delivered by the cross-frame.

Distortion-induced fatigue has been a primary research topic in the Fatigue and Fracture research group at the University of Kansas, with an aim of determining the efficacy of several different retrofit measures to halt crack growth. Girder subassemblies were chosen for study to evaluate for the effectiveness of various retrofits using both an analytical approach and physical experimentation.

This thesis is organized into four chapters. The first three chapters describe the analytical and experimental programs used to evaluate the uses of a composite block retrofit, a carbon fiber reinforced polymer (CFRP) retrofit, and crack-arrest holes to effectively repair distortion-induced fatigue cracking on 3-m (9-ft) steel girder segments under fatigue loading. The fourth chapter details a literature review and an analytical study of a retrofit to repair distortion-induced fatigue damage at floorbeam-to-stringer connections.

ACKNOWLEDGEMENTS

This research would not have been accomplished without the contributions from the following people:

Special appreciation is due to Drs. Caroline Bennett, Adolfo Matamoros, Stanley Rolfe, and Ronald Barrett- Gonzalez for their guidance and assistance.

I would like to thank KDOT and the Mid America Transportation Center for their funding. Additionally, the assistance of the University of Kansas Transportation Research Institute (KU TRI) and its staff is greatly appreciated.

The experimental research described in this thesis was made possible by the assistance of laboratory personnel Jim Weaver and Matt Maksimowicz. Also, I would like to thank my fellow graduate students: Gary G. Simmons, Amanda Hartman, Alisha Elmore, and Eric Bonet. Furthermore, I would also like to thank undergraduate research assistant Zach Olson.

Lastly, I would also like to thank my family and friends for their support and encouragement.

TABLE OF CONTENTS

Chapter Three: Use of Crack-Arrest Holes as a Distortion–Induced Fatigue Mitigation Measure

Chapter Four: Repairing Distortion–Induced Fatigue Damage at Floorbeam-Stringer Connections in Steel Bridge Girders

LIST OF FIGURES

LIST OF TABLES

Chapter One:

Use of Composite Block Retrofit for Repairing Distortion –Induced Fatigue Damage at Cross-Frame Connection Plates

Say Hak Bun
Adolfo Matamoros
Caroline Bennett
Ron Barrett-Gonzalez
Stan Rolfe

Abstract

Distortion-induced fatigue damage is a complex issue that has adversely affected many bridges built prior to the mid-1980s. Numerous retrofit techniques have been applied to steel girder bridges with varying levels of success to stop or slow crack initiation and propagation due to distortion-induced fatigue.

This paper presents and demonstrates the use of a composite material as one retrofit measure to extend the fatigue life of steel bridges under distortion-induced fatigue damage. The composite used in the physical experiment was a combination of WEST epoxy and Matt fiberglass. The results both from FE model and experimental testing were shown with great reduction in stress demand after installing the composite block retrofit.

Introduction and Background

Thousands of aging steel bridge girders throughout the United States are susceptible to fatigue damage. Many of these bridges are in need of fatigue rehabilitation and repairs to maintain their useful service life. A significant amount of fatigue cracking is due to a phenomenon termed *distortion-induced fatigue,* which often occurs due to large stress demand and geometric discontinuities in *web-gap regions*.

A web-gap region is the portion of a girder's web between a connection plate and adjacent flange when the connection plate is not connected to the flanges. This connection detail was widely used in the United States before the mid-1980s. Distortion-induced fatigue cracks

that occur at this detail typically start from the connection plate weld toes and then often progress along the stiffener-to-web welds, and sometimes propagate outwards into the web base metal. Retrofit measures applied to this detail must be carefully analyzed. Effective repairs will halt crack propagation, while ineffective retrofits may allow cracks to continue to grow, and may even increase the stress demand at the crack tip.

Some common retrofits used to mitigate distortion-induced fatigue cracking are drilling crack-arrest holes, grinding (and sometimes welding) the cracks, and applying steel overlay elements to provide a new load path. The retrofit measure introduced in this research paper differs from these methods in that it involves the use of fiber reinforced polymer (FRP) materials (i.e., composite materials) to enhance fatigue life.

The composite material used in this research was comprised of fibrous materials and a binding agent (an epoxy resin). There are many different choices regarding the composite material available to use for this purpose. The epoxy resin chosen for use within this study was a West System™ two-part epoxy. The West System™ two-part epoxy is widely available, relatively inexpensive, and is most often used in boatbuilding / boat repair applications. This epoxy was chosen for use in this study as it was known to have high strength, low cost, and fatigue resistance under impact damage. In addition to the epoxy, mat-type fiberglass was chosen as the other primary component in the FRP material to comprise the composite block retrofit in this research.

The composite material was used to provide an alternate load path between the connection stiffener and the girder web, and was applied to the web gap in the form of a block. This geometry was chosen for its simplicity.

Objective and Scope

The primary objective of this research was to investigate the effectiveness of a fiberglass composite block retrofit technique to increase the distortion-induced fatigue life of web-gap regions within steel bridge girders. This study included a physical test of the FRP composite block applied to a girder segment tested in distortion-induced fatigue and a corresponding finite

element analysis. The girder test system used in this study was modeled using the commercially-available computer application, Abaqus v6.10.2 (Simulia 2010), to compare the stress state in the web gap region before and after the retrofit was applied.

Research Approach

A comprehensive approach was used to determine the effectiveness of the fiberglass composite block retrofit, relying on the results both from Finite Element Analysis (FEA) and experimental testing. Because application of this FRP composite block was performed as a pilot study to determine the feasibility and effectiveness of such a retrofit for repairing distortion-induced fatigue damage, this test was performed on a girder segment. Alemdar (2011) and Hassel (2011) at the University of Kansas have shown the validity of the test set-up used in the laboratory test program through comparison with highly detailed 3D FEA of full bridge systems.

Finite Element Analysis

The girder and the tie-down system used in the physical tests as well as the concrete floor in the laboratory were modeled using the commercially-available software, Abaqus v6.10.2 (Simulia 2010), to analyze the variation of stresses at the web-gap region on the girder's web. The finite element (FE) model was analyzed as linear-elastic using eight-node brick elements with the overall degrees of freedom varying from 1 to 3 million depending on the crack type and retrofit measures modeled. To mimic the laboratory test set-up, the load was applied vertically upwards through the unrestrained end of the cross-frame, as shown in Figure 1-1. The concrete floor was included in the model (fixed at its base), and the connection between the test girder and the concrete floor was modeled. Since the test specimen was bolted to the floor through its bottom flange, any strong axis bending of the girder was eliminated. The linear-elastic material properties assigned in the finite element model are listed in Table 1-1.

Table 1-1 Material properties used in FE model

Type of Material	*Poisson's Ratio*	*Modulus of Elasticity Mpa (Ksi)*
Concrete	0.2	27,800 (4,000)
Steel	0.3	200,000 (29,000)
Composite	0.1	34,500 - 69,000 (5,000 - 10,000)

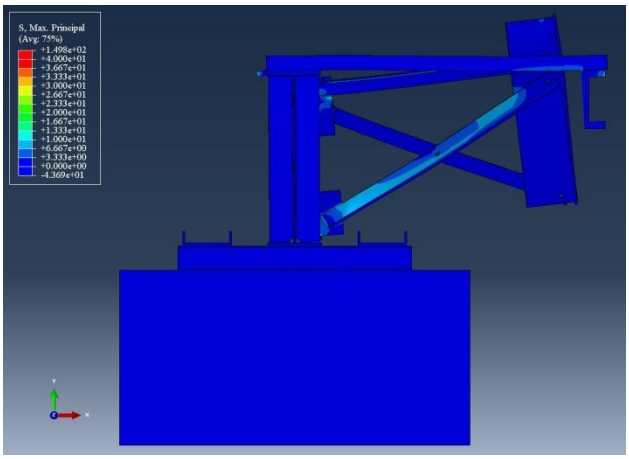

Figure 1- 1 Side view of the test assembly modeled in Abaqus

Two cracks were included in the model using the Extended Finite Element Method (XFEM): a horseshoe-shaped crack at the toe of the web-to-connection plate weld, on the girder web, and a crack at the toe of the web-to-flange weld, also on the girder web. The web-to-stiffener weld crack was modeled with a length of 102-mm (4-in), and the web-to-flange weld crack was modeled with a length of 204-mm (8-in.). The advantages of using the XFEM method rather than explicitly modeling the cracks is that the mesh in XFEM is independent of the crack geometry, and a crack modeled using XFEM is allowed to propagate and does not need to align with element boundaries.

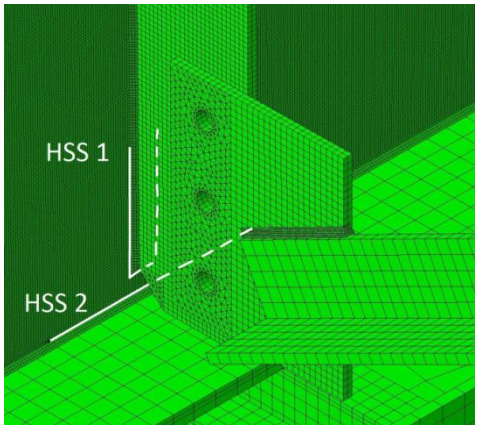

Figure 1- 2 Sampling hot spot stress paths used in the FE model (both paths parallel cracks along welds)

To interpret the model results, maximum principal stresses were computed along two paths in the models. Maximum principal stresses were selected at specific elements based upon a hot spot stress analysis technique used by Hassel et al. (2011) and Alemdar et al. (2011). The resulting stresses were designated as HSS1 and HSS2; these stresses were computed at a distance of 5-mm (3/16-in.) from the stiffener-to-web weld crack and flange-to-web weld crack, respectively (Fig.1-2). Therefore, the two paths shown in Figure 1-2 used to compute HSS1 and HSS2 parallel the two modeled cracks. The two cracking patterns that were modeled were intended to mimic two common modes of distortion-induced fatigue cracking that commonly occur in web-gap regions: cracking along the connection plate-to-web weld (sometimes referred to as horseshoe-shaped cracking) and horizontal cracks developing along the web-to-flange weld.

Composite blocks were then modeled as a retrofit in models that included cracked girder geometry (Richardson 2012). Each block was assigned dimensions of 114 x 114 x 127 –mm (4.5 x 4.5 x5.0 –in.) and was modeled as attached to both sides of the connection plate in the bottom web gap (Fig 1-3). Tie constraints were used to tie the composite block surfaces to the girder's web, bottom flange, and connection plate. This type of restraint was intended to represent one extreme bounding of possible behavior.

An upward load of 22.2-kN (5-kip) was applied to the actuator in the model to simulate the loading applied in the experimental tests.

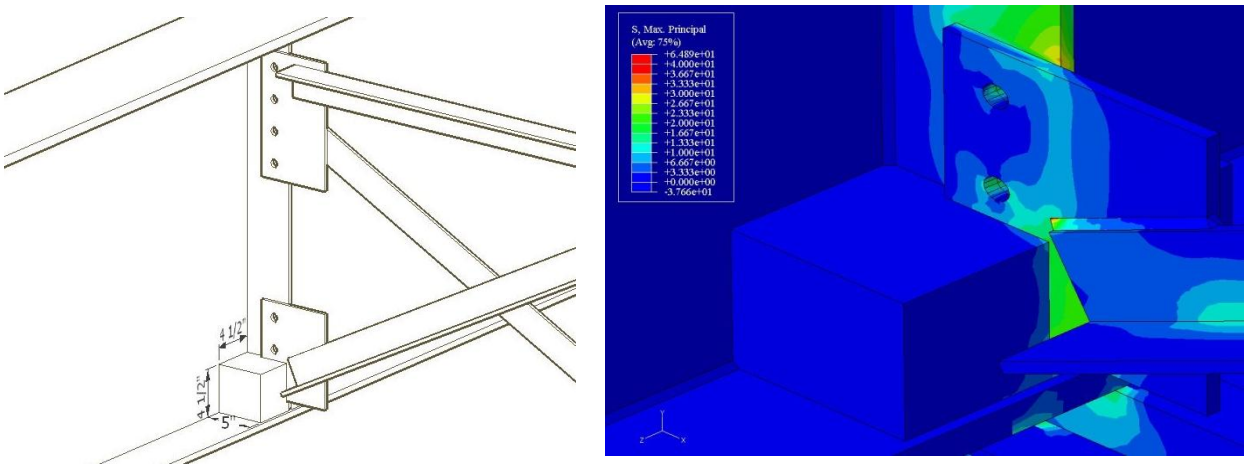

Figure 1- 3 Composite block retrofit applied to the test girder (Richardson 2012)

Experimental Test Set-Up

The 3-m (9-ft) long girder segment was connected to the concrete laboratory floor through a series of C5x9 channels post-tensioned to the 0.9-m (3-ft) thick concrete floor as shown in Figure 1-4. The subassembly was tested upside-down such that concrete laboratory floor simulated the lateral stiffness of a concrete deck on the bridge. The top flange of the test girder was restrained by the presence of L3x3x$^{3}/_{8}$ angles secured at each end of the girder. Full-depth stiffeners were provided at the girder ends to prevent web instability at those regions. The subassembly was tested by applying an upwards (tensile) cyclic load that ranged from 2.2-kN (0.5-kip) to 25.3-kN (5.7-kip) on a WT section that was attached to the end of the cross-frame that was not attached to the connection plate (Fig. 1-5).

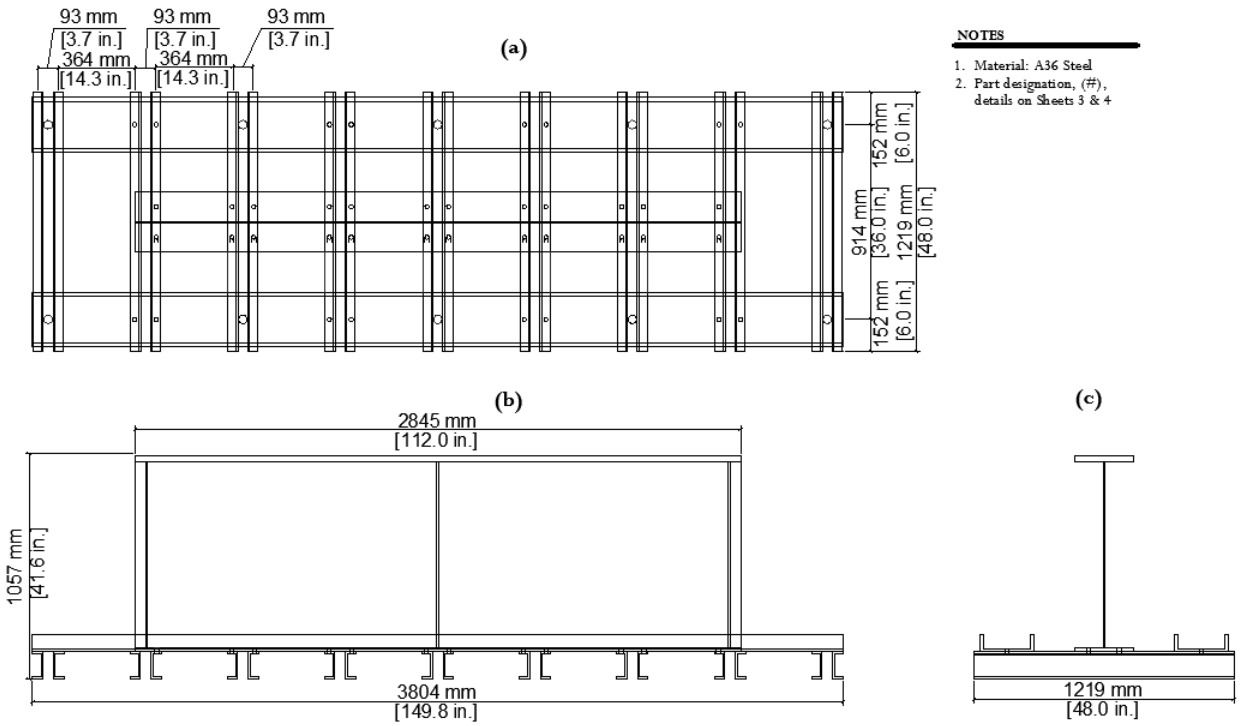

Figure 1-4: Girder Specimen: a) Plan view b) Elevation view c) Section view

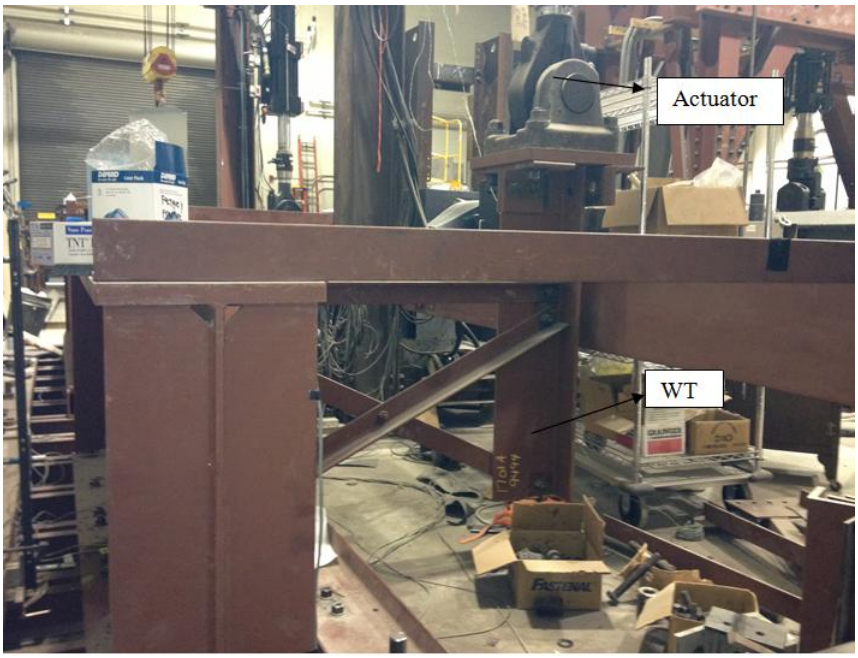

Figure 1-5 Cross-sectional view of the girder segment test assembly

Specimen Dimensions and Material Properties

The built-up steel girder used in this study was 2.7-m (9-ft) long and 918-mm (36-in) tall. The web had cross-section dimensions of 10 x 876-mm ($^3/_8$ x 34 ½ -in). The bottom and top flanges had cross-sections of 279 x 25-mm (11 x $^5/_8$-in) and 279 x 25-mm (11x1-in), respectively. The web, bottom flange and top flange were fabricated from steel with nominal 345-MPa (50-ksi) yield strength. At each end of the girder, there were two stiffeners welded to the web and flanges. A connection plate was welded to the web at the mid-length location of the girder. The four stiffeners were 876-mm (34 ½ -in) tall, 127-mm (5-in) wide, and 10-mm ($^3/_8$-in) thick. The connection plate was 873-mm (34 $^3/_8$-in.) tall, 127-mm (5-in) wide and 10-mm ($^3/_8$-in) thick. All stiffeners had a cropped end of 32-mm (1 ¼-in), and the weld thickness was 10-mm ($^3/_8$-in). The built-up girder was attached to the laboratory concrete floor through a series of C5x9 channels. A cross-frame was used to connect the connection plate and a WT segment. The cross-frame was made up of three L76x76x10-mm (L3x3x$^3/_8$-in) of which two were in an X-configuration, and one was used as a horizontal member. The tensile load was applied on the WT by an actuator.

Instrumentation

The test girder was instrumented with three linear variable differential transformers (LVDTs) and seven Micro-Measurements WK-06-250BG-350 strain gages (Fig.1-6). The LVDTs were powered using a 15V power supply and were used to measure the out-of-plane deflection at three different locations along the height of the girder.

Two strain gages were placed at the top and bottom web-gaps where cracks were expected to initiate, as shown in Figure 1-6. The locations of other gages used in the instrumentation plan have also been shown in Fig.1-6. All data was recorded using a single data acquisition system manufactured by National Instruments (NI 9236 module). A program was written in Labview 2011 to read and record data in a text file. The data was recorded using a sampling rate of approximately 20 samples/second. All calibration factors were applied within the Labview program.

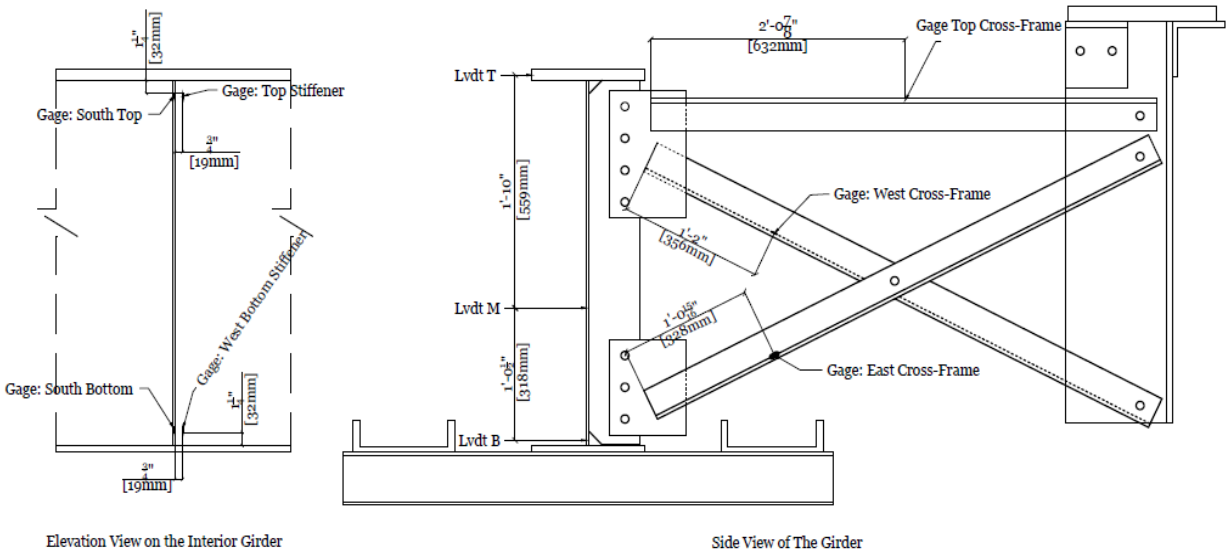

Figure 1-6 Instrumentation applied on 9ft-steel girder segment

Experimental Program

The girder subassembly was tested under cyclic loading, ranging from 2.2-kN (0.5-kip) to 25.3-kN (5.7-kip). The test was divided into two trials: Trial 1 was performed on the girder subassembly without any applied retrofit, followed by Trial 2 in which the composite block retrofit was applied to the girder subassembly.

In Trial 1, the girder specimen was cycled in the unretrofitted condition so that cracking could be initiated and propagated. A crack formed along the connection plate-to-web weld and was allowed to propagate to a length of 57-mm (2 ¼-in). During Trial 1, the girder subassembly was inspected every one thousand cycles using UV light and dye penetrant. Once the desired crack length was achieved, the composite block retrofit was cast on the interior face of the girder on both sides of the connection plate (Fig. 1-7), and Trial 2 was begun.

After the composite retrofit was installed, the girder subassembly was tested over a period of 1.2 million cycles (Trial 2). This number of cycles corresponded to the number of cycles on AASHTO-LRFD Bridge Design Specifications (AASHTO 2010) S-N Curve for Fatigue Category A based on a stress of 193-MPa (28-ksi) measured experimentally on the fascia side of the girder in the bottom web gap region before cracking occurred (Alemdar 2011). At the

end of Trial 2, the composite blocks were removed, and the girder subassembly was then inspected for any possible crack growth using UV light and dye penetrant.

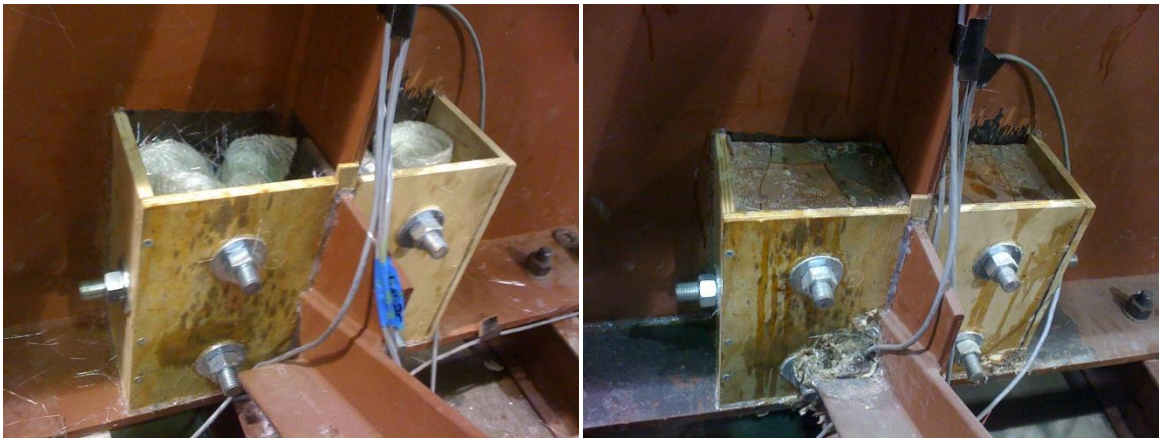

Figure 1- 7 View of the interior of the girder segment: a) FRP block formed; photograph taken prior to casting the WEST resin; b) Cured FRP blocks.

Composite Block Fabrication Processes

The composite block retrofit technique described in this paper was developed to take advantage of the fact that composite materials are light, tough, corrosion resistant, and highly shapeable. Two composite blocks were cast-in-place at the bottom web gap where the peak stress demands were located. The composite material was comprised of West System™ two-part epoxy (West System™ 105 Epoxy Resin and West System™ 206 Slow Hardener) and conventional mat fiberglass (Fig.1-8). The West System™ two-part epoxy was mixed using WEST 105 resin and WEST 206 hardener using a ratio of 5:1. The West System™ 206 Slow Hardener exhibited a pot life of 25 minutes, meaning that the chemical reaction in the epoxy could be expected to occur after this time frame, at which point the mix would no longer be workable.

The composite block was developed to hold the cracked surfaces together and to provide shear resistance while subjected to cyclic load. The mat fiberglass helped by providing some additional stiffness to the epoxy, and by adding cohesion to the mix. The FRP material had the

advantages of being lightweight, inexpensive, possessing moderate compressive and tensile strengths, and being resistant to both impact damage and cyclical loading. The mat fiberglass, which consists of glass fibers randomly laid across each other, was made cohesive by a styrene binder when used in conjunction with the resin.

The fabrication process used to create the composite blocks was as follows. First, to meticulously prepare the steel surfaces, the paint in the areas to be bonded was removed by sandblasting and then cleaned by degreaser. Then, two wooden forms were fabricated and placed on each side of the connection plate to form two rectangular molds, each with a dimension of 165 x 121 x 254-mm ($6^1/_2$ x $4^3/_4$ x 10-in). The forms were firmly held in position through use of 19-mm (¾-in) threaded rods. The threaded rods were snug-tightened. Next, the West System™ epoxy and mat fiberglass were combined to make 0.0102-m^3 (0.36-ft^3) of composite. The composite blocks were composed of about 30% mat fiberglass and 70% West System™ epoxy. The fiberglass content was first placed inside the molds, then the epoxy content was cast in the molds. Finally, the composite blocks were left to cure at room temperature for 24 hours before testing. It should be noted that no connection beyond that of naturally-occurring adhesion during the curing process was provided between the FRP block and the bottom flange of the test girder; however, mechanical connection was provided between the FRP blocks and the girder web via the threaded rods.

Figure 1- 8 Material used in the FRP block (a) West System™ two –part epoxy and (b) Mat fiberglass

Experimental Results

Fatigue Life Enhancement

Results of the physical testing showed that the distortion-induced fatigue life of this girder was significantly improved. The crack propagation rate was slowed significantly when compared to the crack growth rate observed in the test girder without the retrofit. Figure 1-9(a) presents the crack pattern that was recorded during the inspection performed directly before applying composite block retrofit (after Trial 1 and before Trial 2), and Figure 1-9(b) presents the crack pattern recorded after Trial 2 was completed with the retrofit. It can be seen that the only crack that initiated after application of the retrofit was a small spider crack on the right side of the transverse stiffener (Fig.1-10).

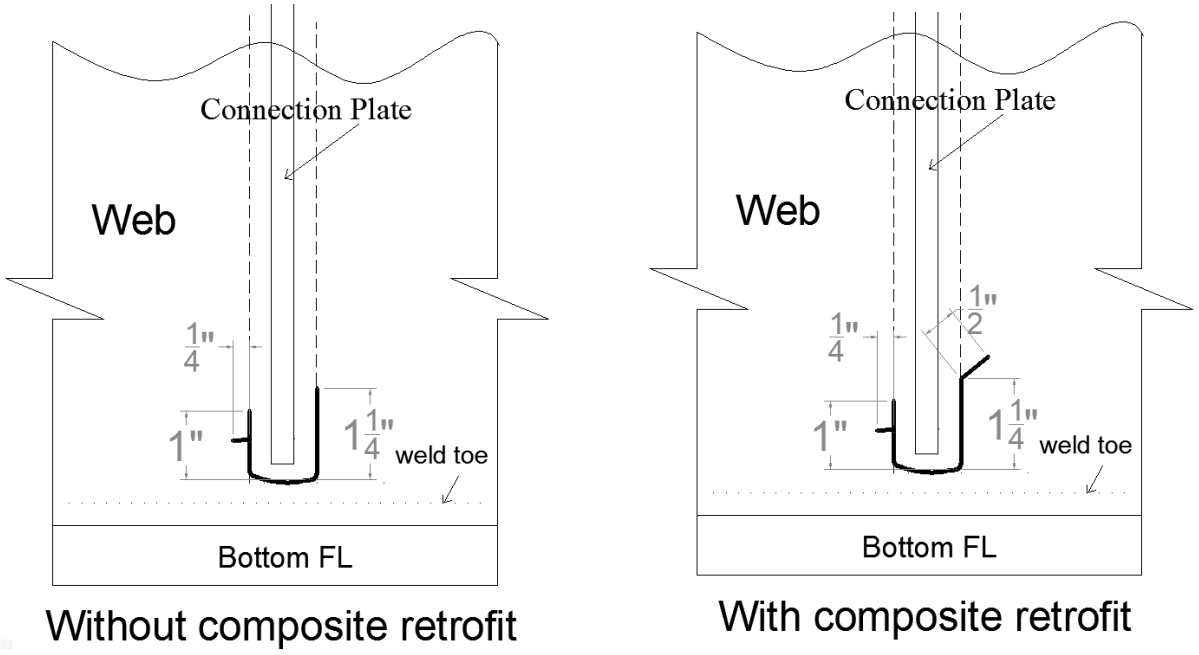

Figure 1-9 Recorded crack patterns: a) After Trial 1 (without composite retrofit – 1.2 million cycles) b) After Trial 2 (with composite retrofit – additional 1.2 million cycles)

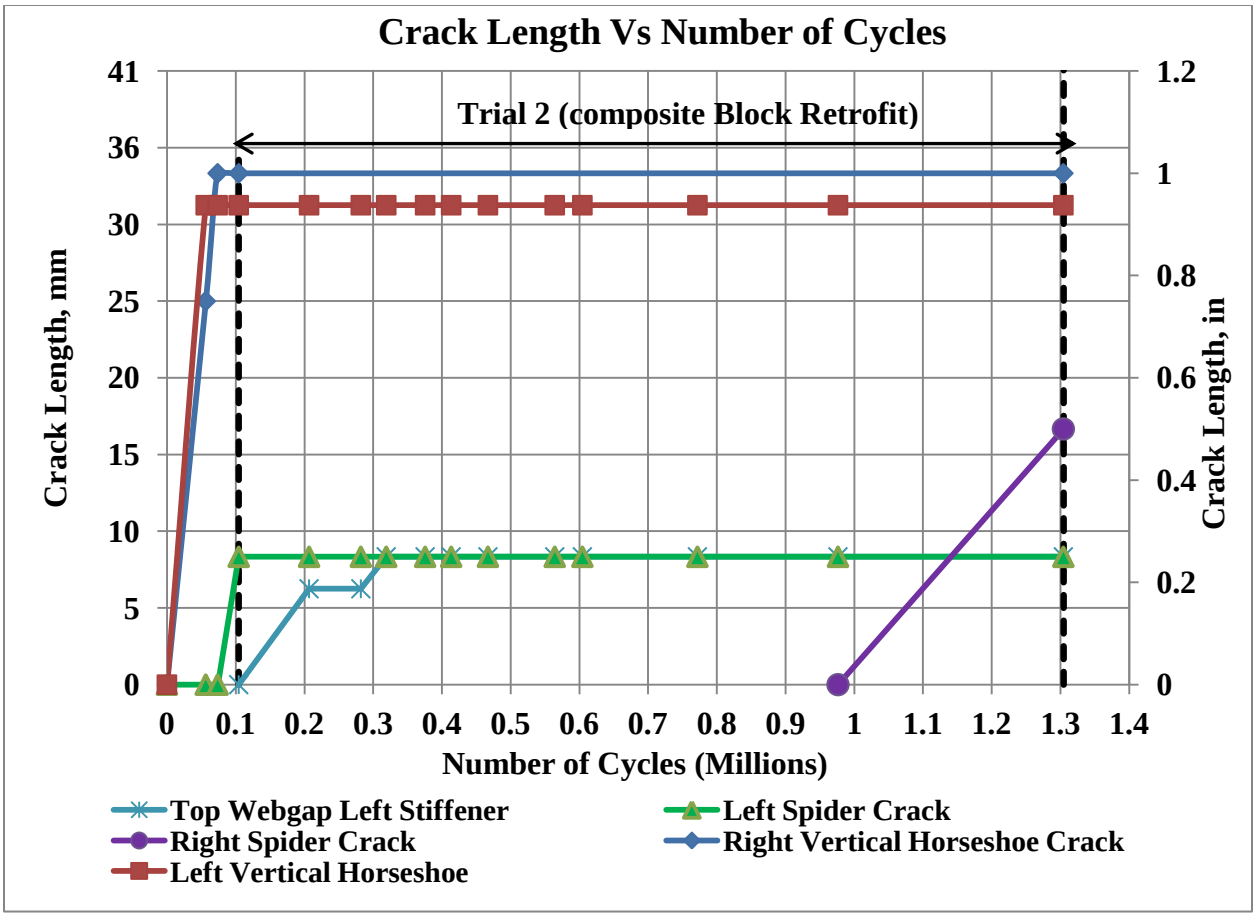

Figure 1-10: Plot of crack length versus cycle count

In the study performed by Richardson (2012) that included a finite element model of the test girder with the composite block retrofit, HSS1 was found to have decreased by 99%, and HSS2 was decreased by 96%. J-Integral values were also compared, and are shown in Table 1-2. The values in Table 1-2 indicate that the propensity for crack growth after application of the composite block was extremely small, close to zero. It should be emphasized here that debonding between the FRP block and the steel surfaces was noted during Test Trial 2 of the physical testing. Given that the FEA results reported here are only expected to be accurate if the bond is perfectly maintained between the FRP and the steel, these analysis results should be viewed as one extreme end of potential behavior, and not indicative of the testing performed in Trial 2 of this test sequence. It is expected that the physical test performed is far more indicative of the type of behavior that can be expected for this type of retrofit.

Table 1-2 J-Integral comparison before a retrofit was applied and after composite blocks were attached to both sides of the stiffener. All simulations contained a 102-mm (4-in.) web-to-stiffener weld crack and a 204-mm (8-in.) flange-to-stiffener weld crack (Richardson 2012)

Retrofit	*J*-Integral for 102-mm (4-in.) web-to-stiffener weld crack	*J*-Integral for 204-mm (8-in.) flange-to-stiffener weld crack
No Retrofit	0.41	0.58
Composite Block	1.6 E^{-3}	1.2 E^{-4}

Measurement of displacement data showed that inclusion of the composite block retrofit slightly decreased the measured out-of-plane deflections of the girder shown in Figure 1-11.

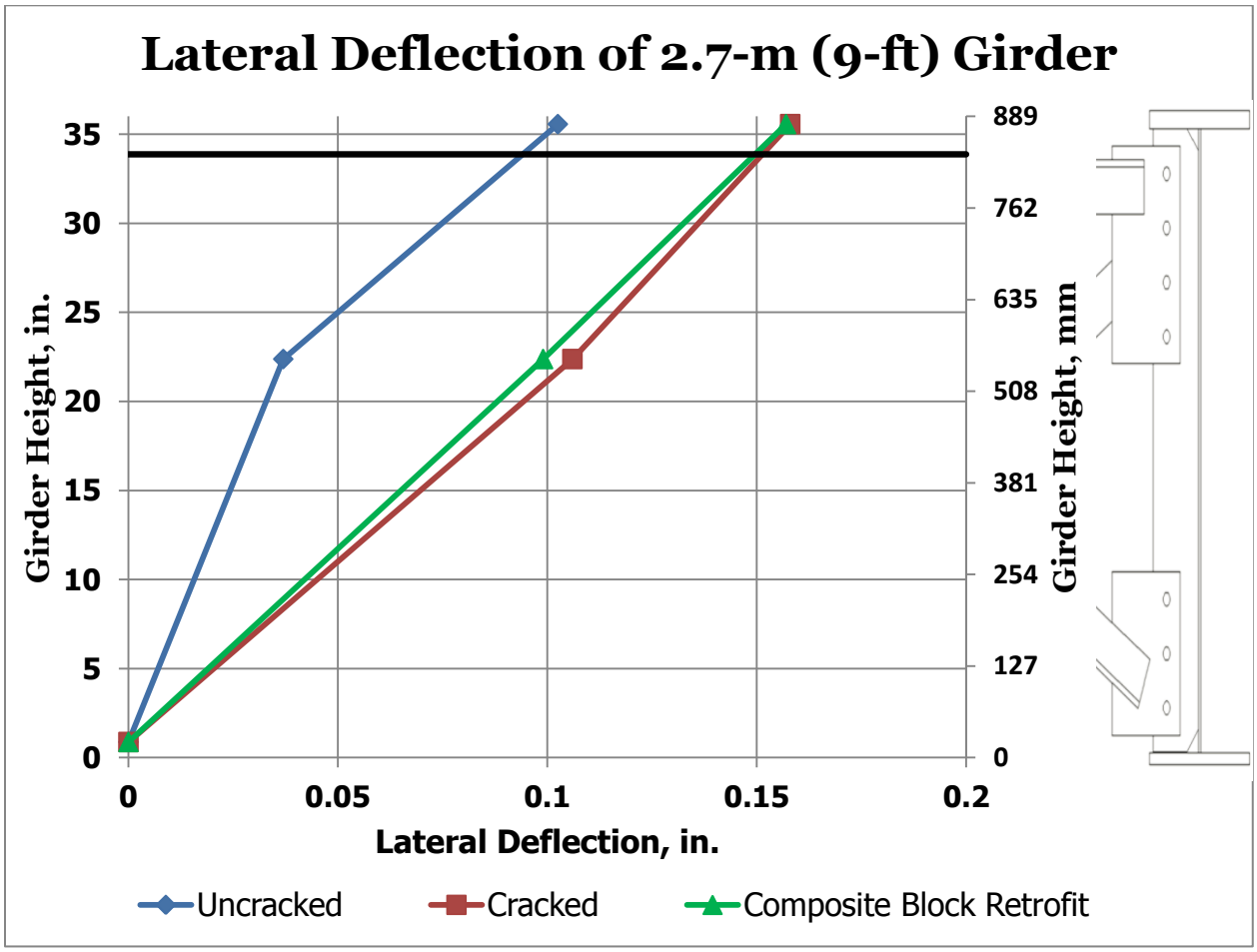

Figure 1-11: Lateral deflection of the specimen before and after the composite block retrofit was applied

Conclusions

The research presented in this paper was carried out to evaluate the effectiveness of a composite FRP block retrofit in repairing distortion-induced fatigue damage in steel girder bridges. Results from a physical test showed only a small reduction in the out-of-plane deflections of the girder, but showed a very significant reduction in crack growth propensity.

A finite element investigation was performed to show the potential effects of the composite block retrofit if 100% bond effectiveness was maintained between the steel and composite elements. The computational simulations showed that stresses in the web gap region could be reduced by more than 90% with those constraints.

The results of this study provided a meaningful understanding of the behavior of a FRP composite retrofit used as a distortion-induced fatigue retrofit. A FRP block composite comprised of mat fiberglass and WEST system epoxy was shown to significantly slow crack propagation rate. However, since the test was conducted at a load range producing a very high stress range in the web gap, the FRP block retrofit did not completely stop the crack from re-initiation. Further research should be performed to determine if the performance of the retrofit could be further improved with different bonding / connectivity mechanisms.

References

AASHTO (2010). "AASHTO-LRFD Bridge Design Specifications," 5th Edition, *American Association of State Highway and Transportation Officials* (AASHTO), Washington D.C.

Castiglioni, C., Fisher, J., and Yen, B. (1988). " Evaluation of Fatigue Cracking at Cross Diaphragms of a Multigirder Steel Bridge." *Elsevier Ltd*, 9(2):95-110.

Roddis, K., and Zhao, Y. (2001). "Out-of-plane Fatigue Cracking in Welded Steel Bridges." *Welding Inovations* 27 (2):2-7.

Hassel, H. (2011). "An Analytical Evaluation of Distortion-induced Fatigue in Steel Bridges," thesis, presented to the University of Kansas, at Lawrence, Kansas, in partial fulfillment of the requirements for the degree of Master of Science in Civil Engineering.

Richardson, T. (2012). "Analytical Investigation of Repair Methods for Fatigue Cracks in Steel Bridges." thesis, presented to The University of Kansas, at Lawrence, Kansas, in partial fulfillment of the requirements for the degree of Master of Science in Civil Engineering.

Alemdar, F. (2011). "Repair of bridge steel girders damaged by distortion-induced fatigue,"thesis, presented to The University of Kansas, at Lawrence, KS, in partial fulfillment of the requirments for the degree of Doctor of Philosophy in Civil Engineering.

Simulia. (2010). ABAQUS FEA Version 6.10-2. Providence, RI. http://www.simulia.com.

WEST SYSTEM, 105 Epoxy Resin®/206 Hardener®, 2013, http://www.westsystem.com

Chapter Two:

Use of CFRP Combined with Steel Angles and Back Plate for Repairing Distortion–Induced Fatigue Damage at Cross-Frame Connection Plates

Say Hak Bun
Regan Gangel
Adolfo Matamoros
Caroline Bennett
Ron Barrett-Gonzalez
Stan Rolfe

Abstract

Distortion-induced fatigue damage is a common problem in steel girder bridges built prior to the mid-1980s. The location in which damage is likely to occur and the type of damage pattern are affected by the bridge geometry and loading conditions. In this study the propensity for damage under the combined effects of girder bending and cross-frame loading, as well as the pattern of damage that is to be expected were evaluated by performing a suite of finite element analyses.

After fatigue damage is detected, some repair or retrofit method must be implemented to prevent further fatigue crack propagation and protect the structural integrity of the bridge. Three repair methods were evaluated to determine the reduction in stress demand that each method produced at two critical locations. The three methods evaluated were: (1) drilling of crack-arrest holes at crack tips, (2) attachment of bolted full-depth splice plates to the damaged web, (3) and attachment of adhesively bonded CFRP overlays reinforced by bolted steel cover plates. Results of finite element analyses showed that while both the full-depth steel splice plates and CFRP assemblage produced large reductions in stress, the latter outperformed the other repair methods and had the best potential for preventing further fatigue crack growth.

Introduction and Background

Many existing bridges built prior to the 1980s left connection stiffeners unattached to the adjacent top flange and are susceptible to fatigue cracking. Differential deflections of adjacent steel bridge girders can produce an out-of-plane rotation of the girder's web at the cross-frame connecting the connection plate. A result is that large stress demands can be produced at the connection plate-to-web weld toe.

While steel retrofits have been applied extensively as retrofit techniques on steel bridge girders experiencing distortion-induced fatigue cracking, Fiber Reinforced Polymer (FRP) composite materials have also been recognized by many researchers as having strong potential as a means of repairing fatigue cracking. Low strength-to-weight ratios and the crack growth inhibiting nature of fiber reinforced polymers make them ideal materials to repair and strengthen fatigue-critical details in steel bridges (Meier 1992). FRP materials can have distinct strength advantages over steel when loaded in their optimal orientation, and fiber composite materials such as graphite (carbon)-epoxy and Kevlar-epoxy can outperform steel when subjected to uniform tension (Mallick 1993).

In this research, a retrofit was developed to repair distortion-induced fatigue damage in steel bridge girders using Carbon Fiber Reinforced Polymers (CFRP) materials. The formability and high-strength of CFRP makes it an ideal choice for a distortion-induced fatigue retrofit, however, the effectiveness of such a technique is expected to be governed by the quality of the finished retrofit. Use of CFRP materials as a fatigue enhancement technique has proven challenging in past investigations due to localized delaminating failures experienced at the bond between the steel and composite materials (Colombi 2003). Thus, the application of CFRP on steel must be prepared and performed carefully to achieve satisfactory results.

Objective and Scope

The primary objective of this research was to investigate the effectiveness of using CFRP as a retrofit technique to increase the fatigue life of steel bridge girders. This investigation involved testing two retrofit techniques that were applied over deep web cracks formed under the

action of distortion-induced fatigue. The first retrofit examined consisted of steel angles with a back plate, and another retrofit consisted of steel angles, a steel back plate and a layer of 1.6-mm ($^1/_{16}$-in) thick CFRP material. The retrofits were tested on a 2.7-m (9-ft) length of steel girder that had fatigue cracks that had propagated deep into the web height.

Research Approach

To determine the effectiveness of the retrofits used, Finite Element Analysis (FEA) and physical testing were performed on a girder subassembly. The methodology used in these two approaches is described in the following.

Experimental Test Set-Up

The physical test setup used in this investigation was comprised of a built-up steel girder connected to the concrete floor through a series of C5x9 channels post-tensioned to the 0.9-m (3-ft) thick concrete floor as shown in Fig. 2-1. The girder subassembly was tested upside-down so that laboratory concrete floor simulated the lateral stiffness of the concrete deck on the bridge. The top flange was restrained from in-plane lateral movement by a L3x3x$^3/_8$ angle placed at each end of the girder. The subassembly was tested under the action of a cyclic tensile force ranging from 2.2-kN (0.5-kip) to 25.4-kN (5.7-kip) applied through a WT section that was connected to the cross-frame (Fig.2-2).

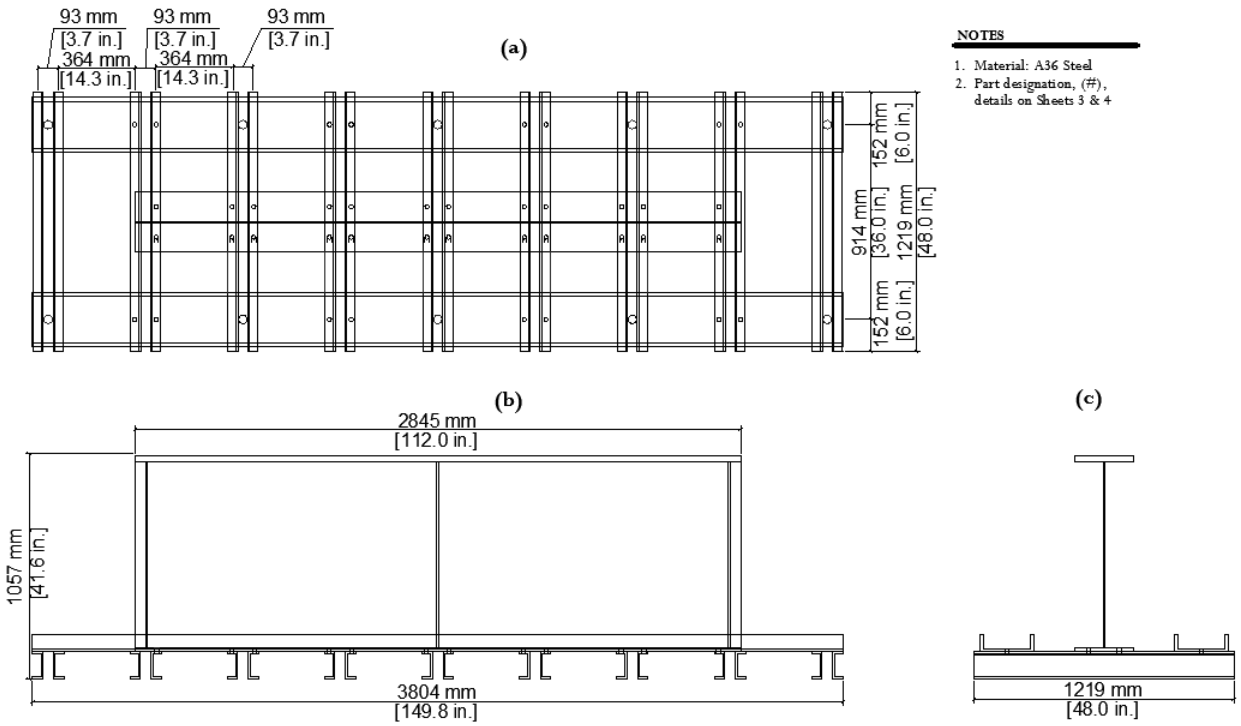

Figure 2-1 Girder Specimen: a) Plan view b) Elevation view c) Section view

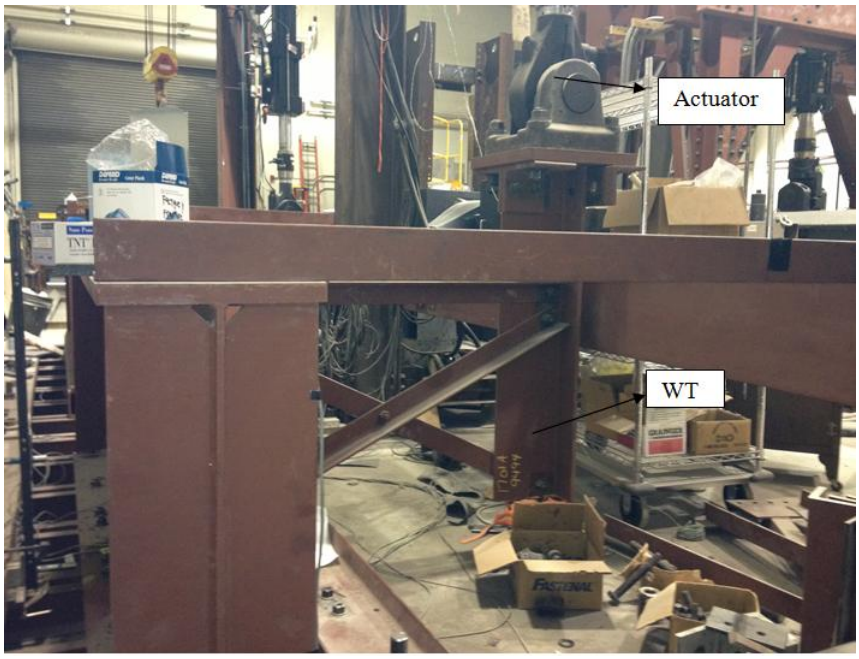

Figure 2-2 Cross-sectional view of the test girder subassembly

Specimen Dimensions and Material Properties

The built-up steel girder used in the experimental study was 2.7-m (9-ft) long and 918-mm (36-in) tall. The web had a cross-section dimension of 10 x 876-mm ($^{3}/_{8}$ x 34 ½-in). The bottom and top flanges had cross-sections of 279 x 25-mm (11 x $^{5}/_{8}$-in) and 279 x 25-mm (11 x 1-in), respectively. The web, bottom flange and top flange all had 345-Mpa (50-ksi) nominal yield strength. Full-depth stiffeners were provided at the girder ends to prevent from web instability at those regions. At each end of the girder, there were two stiffeners welded to the web and flanges. The four stiffeners were 876-mm (34 $^{1}/_{2}$-in) tall and 127-mm (5-in) wide. There was a connection plate welded to the web at the middle of the girder. The connection plate was 873-mm (34 $^{3}/_{8}$-in.) tall and 127-mm (5-in) wide. All stiffeners had a cropped end of 32-mm (1 ¼-in), and a thickness of 10-mm ($^{3}/_{8}$-in).

A cross-frame was connected to the connection plate; loads were applied to the assembly via the free end of the cross-frame, through an attached WT section. The cross-frame was made up of three L76x76x10-mm (L3x3x$^{3}/_{8}$-in) angles, of which two were in an X-configuration, and one horizontal member. This assembly had previously been subjected to fatigue testing over approximately 8 million cycles, under a load range from 2.2-kN (0.5-kip) to 25.4-kN (5.7-kip), which resulted in 267-mm (10½-in) deep cracks in the girder's web as shown in Fig.2-3.

Figure 2-3 Existing cracks on exterior face of the girder's web

Instrumentation

The girder subassembly was instrumented with three linear variable differential transformers (LVDTs) and nine strain gages (Fig. 2-4). Two strain gages were placed at the top and bottom web gaps where cracks commonly initiate under distortion-induced fatigue. The three LVDTs were used to measure the out-of-plane deflections of the girder at three different locations along the depth of the girder.

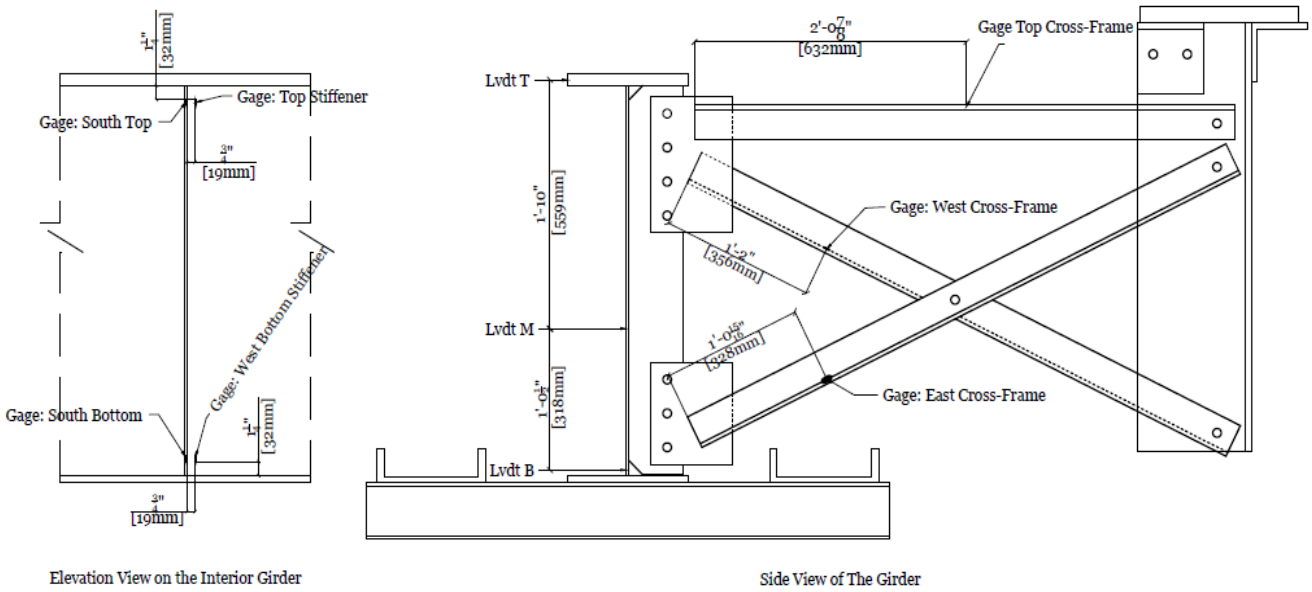

Figure 2-4 Instrumentation on the steel girder

Experimental Program

The girder subassembly was tested under a cyclic tensile force that ranged from 2.2-kN (0.5-kip) to 25.4-kN (5.7-kip), applied through the top of the WT member. The test was divided into two trials: Trial 1 was the test performed with steel retrofit (only angles-with-back-plate retrofit), followed by Trial 2 which also included a 1.6-mm ($^1/_{16}$-in) thick CFRP layer attached to the web and connection plate (Fig.2-5 and Fig.2-6), sandwiched under the angles-with-plate retrofit. In both Trials 1 and 2, the steel retrofit used was two double angles and a back plate. The angles were 483-mm (19-in.) long, 2L3x3x$^3/_8$ standard angle size, and the back plate was 113-mm (½-in) thick with the dimension of 457x457-mm (18x18-in) Each angle was placed on each side of the connection plate and bolted to the girder's web using A325 structural bolts. The back plate was placed on the exterior face of the girder's web where there was no connection plate.

In each trial, the girder subassembly was fatigue cycled for 1.2 million cycles. This targeted cycle number corresponds to the number of cycles on the AASHTO S-N curve (AASHTO 2010) for a fatigue Category A detail based on a stress demand of 193-Mpa (28-ksi)

at the bottom web gap of un-cracked specimen, as calculated by Alemdar (2010). The strain and deflection data were collected continuously throughout the tests. The steel girder was inspected at the end of each of the trials using UV light and dye penetrant.

Figure 2-5 View on the exterior face of the girder's web with a steel back plate

Figure 2-6 View on the interior face of the girder's web

CFRP Preparation Processes

The laminar CFRP materials were made by stacking two layers of graphite fibers and WEST epoxy. Each layer of the graphite fibers had a thickness of 0.8-mm ($^{1}/_{32}$-in) which provided the same thickness as the target thickness. The fabrication process is described in the following.

First, the graphite fiber sheets were cut to dimensions of 457 x 609-mm (18 x 24-in) and 152 x 483-mm (6 x 19-in). Two layers of graphite sheets with the dimensions of 457 x 609-mm (18 x 24-in) were used on the fascia side of the web where the steel back plate was attached. Four layers of the graphite sheets having dimensions of 152 x 483-mm (6 x 19-in) were applied on the interior surface of the girder, on both sides of the connection plate.

Second, 21-mm ($^{13}/_{16}$-in) diameter holes were drilled on all the six graphite sheets using a metal hole punch, and the graphite sheets were then stored in a refrigerator.

Before application of the graphite sheets, the steel surfaces were prepared by grinding off the paint and degreased using Isopropyl Alcohol. The steel-to-CFRP bond was considered to be

the most important factor influencing the effectiveness of this retrofit. Next, the CFRP laminates were applied to the girder's web. Then, a two-part epoxy was used to bond the CFRP laminates to the steel surfaces. The mixing ratio of the epoxy was five parts resin to one part hardener, as measured by volume. The epoxy was first applied on the steel surfaces by brushing, and then the graphite fibers were applied to the web and connection plate one layer at a time.

In the retrofit that included steel elements applied over the CFRP layers, an additional step of applying the steel elements was performed. The steel angles and back plate were attached over the graphite fibers by pre-tensioning the bolts (Fig.2-7 and Fig.2-8). The pressure applied from the pretension bolts activated the matrix material (epoxy) and caused the matrix to flow entirely around the fibers. The retrofit was left to cure for 48 hours before the test began.

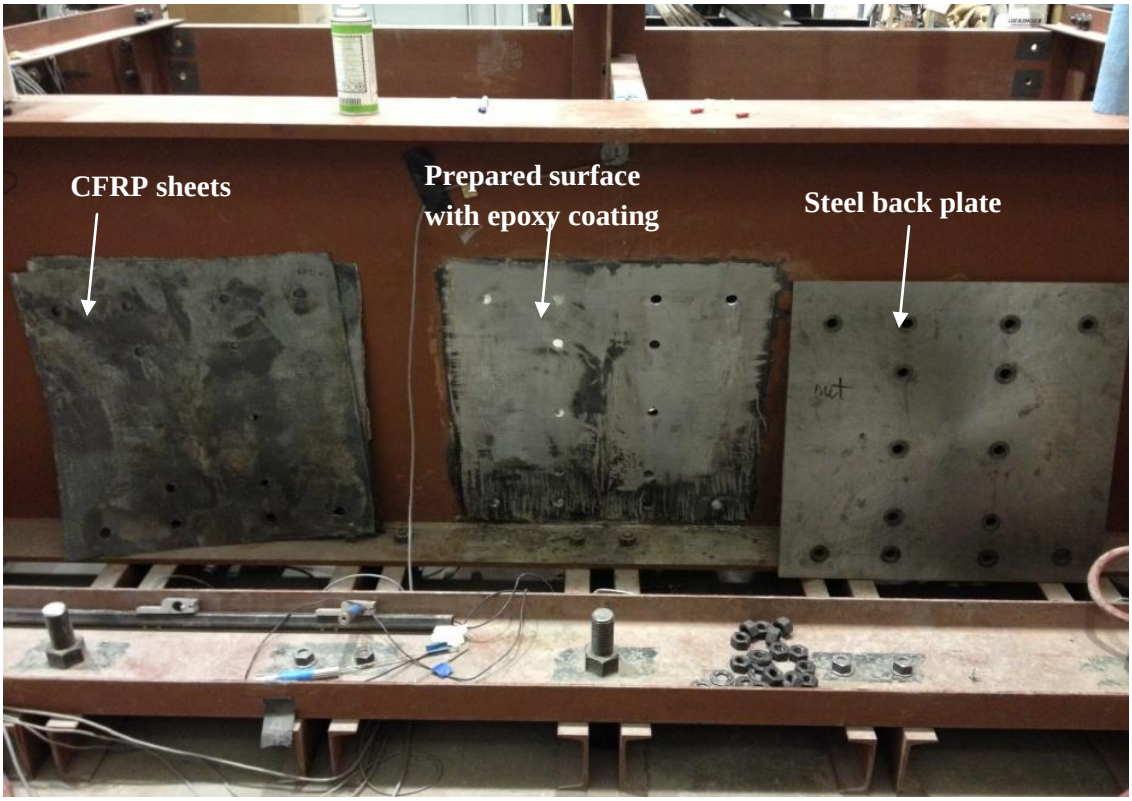

Figure 2-7: Test Trial 2- view of the exterior face of the girder's web

Figure 2-8: Test Trial 2-view of the interior face of the girder's web

Finite Element Analysis

A linear-elastic Finite Element Analysis (FEA) investigating the performance of the retrofits was carried out by Gangel (2011) using Abaqus v6.10 (Simulia 2010). Each FE model consisted of a single 3.0-m (120.0-in) wide by 1524-mm (60-in) deep steel girder section, as shown in Figures 2-9 and 2-10. At each end of the girder, a transverse stiffener was welded to web of the girder, and the top and bottom flanges. At the mid span of the girder, a connection plate was welded to the web and truncated 6-mm (1.4-in) from the face of each adjacent flange, producing a web gap region that was vulnerable to fatigue cracking. The model studied here was somewhat different from the girder used in the physical testing. While the results are not intended to be directly comparable, they can still provide a useful frame of reference.

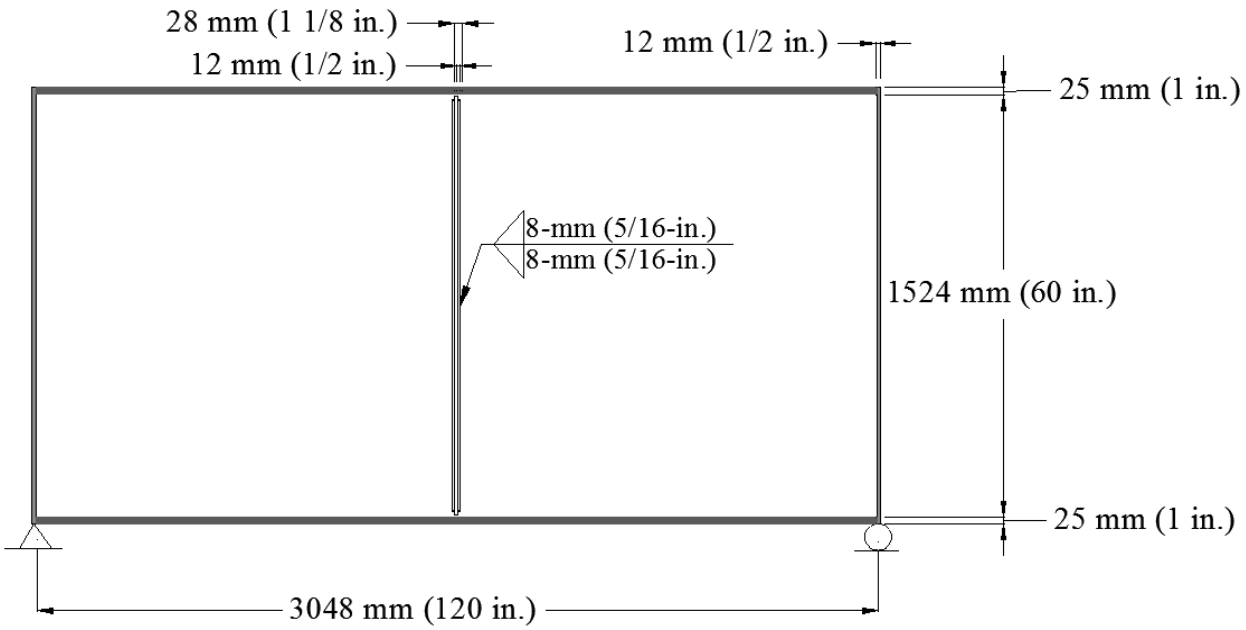

Figure 2-9 Plan view of the girder (Gangel 2011)

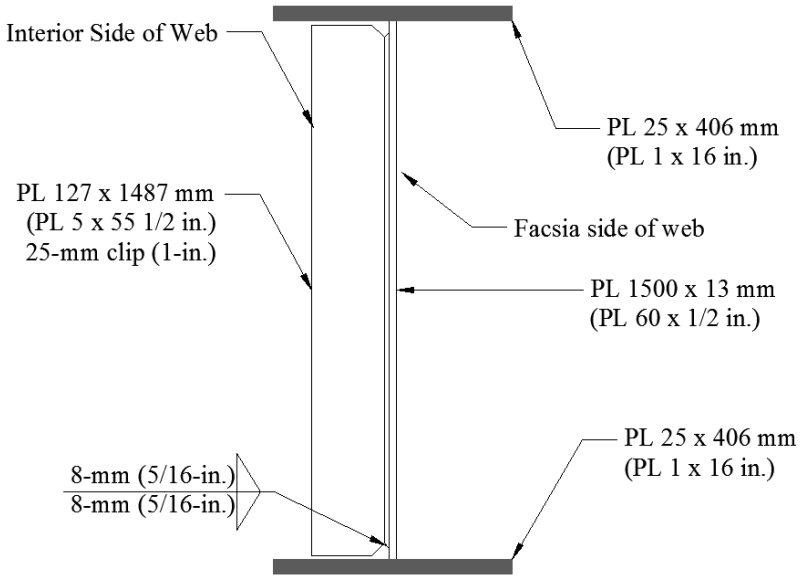

Figure 2-10 Girder cross sectional view (Gangel 2011)

All steel parts of the girder including the welds were assigned a modulus of elasticity of 200-GPa (29,000-ksi) and a Poisson's ratio of 0.3. A mesh size of 5-mm (0.2-in) was assigned to the welds, and a mesh size of 6-mm ($^1/_4$-in) was assigned for all others. All surfaces were attached using tie constraints. The girder was modeled as simply-supported. Translational

restraint was applied along the bottom edge of both transverse stiffeners to allow the stress demand to be transferred from web to flanges. The free edge of the transverse stiffeners was also restrained from out-of-plane movement. A gravity load was applied on top of the top flange to produce 35-Mpa (5-ksi) bending stress on the top flange. Out-of-plane 22-kN (5-kip) loads were applied at two locations near the top and bottom of the connection plate. The load near the top of connection plate was in tension, and the load near the bottom of connection plate was in compression. These loads were chosen based upon cross-frame forces calculated using full-scale bridge models created by Hassel (2011) and Roddis and Zhao (2003).

In the analyses performed in this study, a horseshoe-shaped crack was created in the model using XFEM modeling technique. The advantages of the XFEM method over explicitly modeling cracks is that the mesh is independent of the crack geometry, and the crack in an XFEM model is allowed to propagate and does not need to align with element boundaries. A crack length of 190-mm (7 $^{1}/_{2}$-in) was created around the web-to-connection-plate weld. Hot Spot Stress (HSS) was chosen for selecting representative values of maximum principal stress. Two HSS paths were defined to be a distance of 6-mm ($^{1}/_{4}$-in) from the crack. The first HSS path was designated as a horizontal path extending away from the tips of the curved crack, as shown in Fig. 2-11. The second HSS path was designated as a path taken around the crack curve. The maximum principal stress demands taken from the two paths were defined as HSS#3 and HSS#4 (Fig.2-11), respectively.

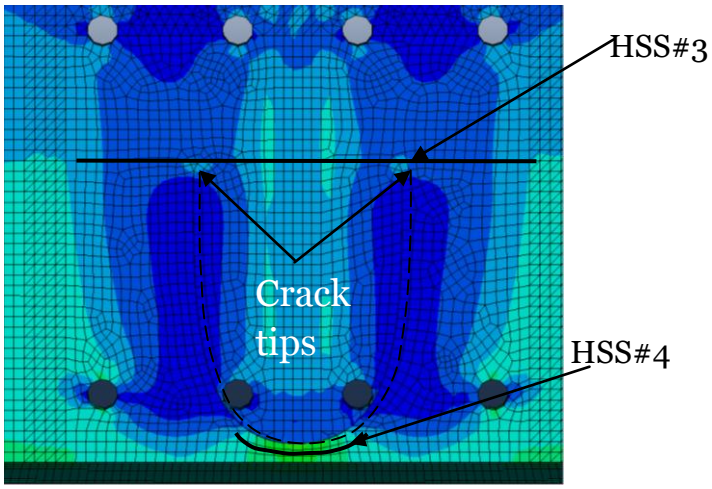

Figure 2-11 Hot Spot Stress paths used to select representative values of maximum principal stresses (Gangel 2011)

Gangel (2012) evaluated two retrofits in the finite element models. The first retrofit consisted of full depth steel plates applied on both the fascia and stiffener sides of the web. The second retrofit consisted of steel plates used in the first retrofit plus 6-mm (0.25-in) thick CFRP and 0.6-mm (25-mil) thick resin bond layers, as shown in Fig.2-12.

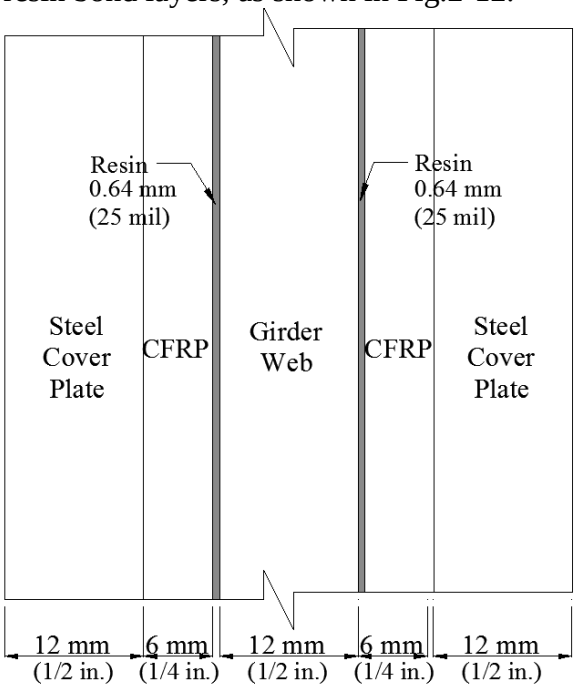

Figure 2-12 Cross section of CFRP repair (Gangel 2011)

Results

The finite element analyses performed (Gangel 2012) allowed for a comparison between the two retrofit techniques, and it was found that the CFRP-steel plate retrofit measure resulted in the greatest reductions in stress demand. In the non-retrofitted state, high stress (red regions in Fig. 2-13a represent stress values greater than 345-Mpa (50-ksi)) concentrated at three locations: below the horseshoe-shaped crack and at the tips of the crack (Fig.2-13(a)).

The model characterizing the steel girder retrofitted with full depth spice plates on both the interior and exterior faces of the girder's web showed that the high stress concentrations were reduced about 40% (from red to green (about 207-Mpa (30-ksi)) (Fig.2-13(b) and Fig.2-13(c)).

Finally, the model characterizing the steel girder retrofitted with the CFRP and the steel angles-with-plate technique indicated that there was 20% more stress reduction compared to the retrofit without the CFRP layer (Fig.2-13(d) and Fig.2-13(e)).

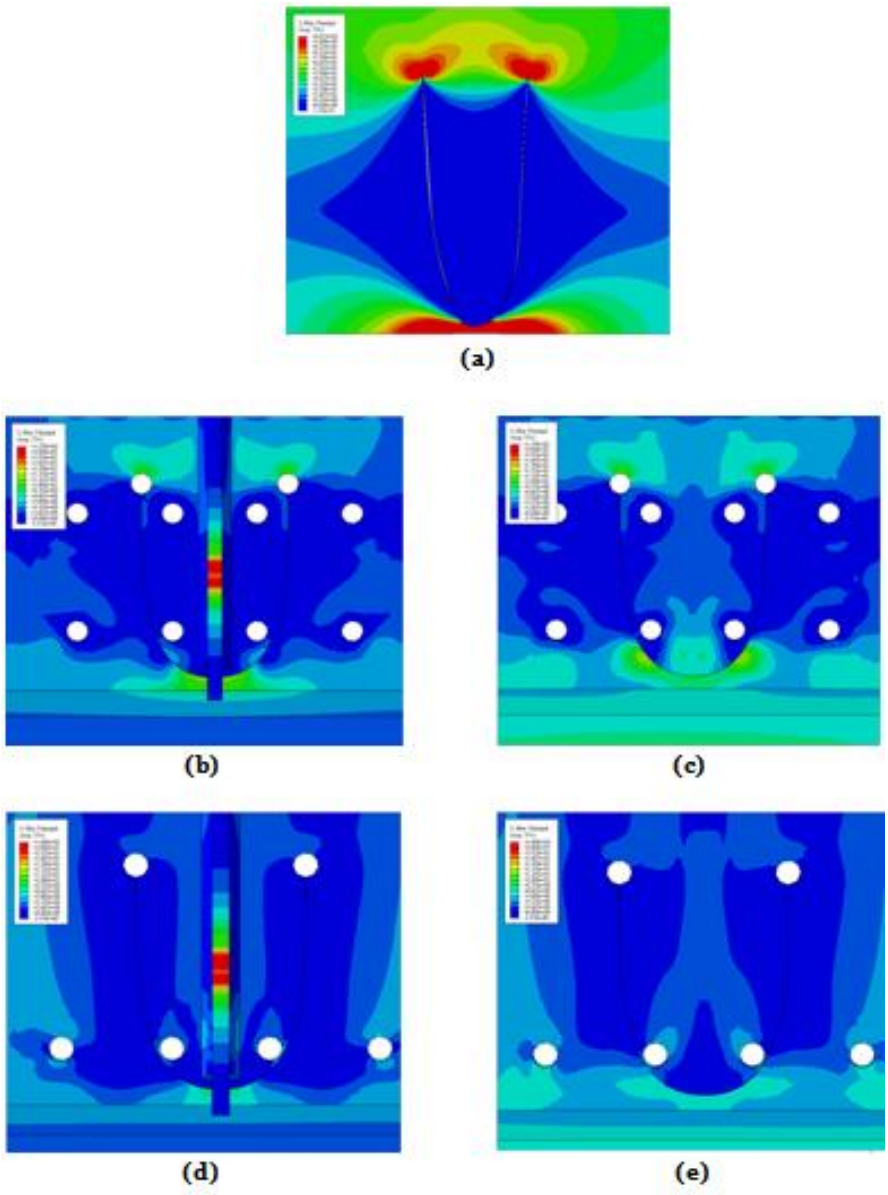

Figure 2-13: Maximum principal stress comparison (a) non-retrofitted (b) retrofitted with full depth spice plate – interior (c) retrofitted with full depth spice – fascia (d) retrofitted with CFRP system – interior (e) retrofitted with CFRP system – fascia (Gangel 2011)

From the results of the physical testing, the inspection at the end of both retrofitted trials (Trial 1 and Trial 2) indicated that the cracks did not propagate under the retrofit. However, by comparing strain data from a strain gag on a steel angle restraining the top flange of the girder , the result indicated that with the present of CFRP material, the percentage of stress reduction was higher than the retrofit without CFRP material by about 30% more (Table 2-1).

Table 2- 1 Stress and strain data obtained from physical testing

	Steel Retrofit	**CFRP Retrofit**
Strain, με	43	33
Stress, MPa (ksi)	8.96 (1.3)	6.2 (0.9)

Conclusion

From the results of the analytical study and experimental testing of the two retrofit systems, it was found that CFRP materials used in combination with the angles-with-plate retrofit worked better than the conventional steel retrofit system. Even though the FE model geometry was not identical to the physical test setup, the results still provided a useful reference. Further testing is recommended by varying the thickness of the CFRP materials in order to identify an optimal thickness.

References

Meier, U. (1996) "Carbon fibre-reinforced polymers: Modern materials in bridge engineering*." Struct. Engng. Int.* 1(92), 7-12.

AASHTO (2010). "AASHTO-LRFD Bridge Design Specifications: 5th." *American Association of State Highway and Transportation Officials* (AASHTO), Washington D.C.

Mallick, P. K. (1988). Fiber-*reinforced Composites: Materials, Manufacture, and Design*, 2nd Ed., Marcel Dekker, New York, NY.

Roddis, K, and Y Zhao (2003). "Finite Element analysis of steel bridge distortion induced fatigue" *Journal of Bridge Engineering, 8(5),* 259-266.

Hassel, H.L. (2011). "An Analytical Evaluation of Distortion-induced Fatigue in Steel Bridges." thesis, presented to The University of Kansas, at Lawrence, Kansas, in partial fulfillment of the requirements for the degree of Master of Science in Civil Engineering.

Colombi, P., Bassetti, A., and Nussbaumer, A. (2003) "*Crack Growth Induced Delamination on Steel Members Reinforced by Prestressed Composite Patch*." Fatigue Fract. Engng. Mater. Struct. 26, 429-437.

Alemdar, F. (2011). "Repair of bridge steel girders damaged by distortion-induced fatigue," thesis, presented to The University of Kansas, at Lawrence, KS, in partial fulfillment of the requirments for the degree of Doctor of Philosophy in Civil Engineering.

Gangel, R.E (2012) "Evaluation of Fatigue Damage Repair Measures in Welded Steel Plate Bridge Girders." thesis, presented to The University of Kansas, at Lawrence, KS, in partial fulfillment of the requirements for the degrees of Master of Science in Civil Engineering.

Simulia. (2010). ABAQUS FEA Version 6.10-2. Providence, RI. http://www.simulia.com.

Chapter Three:

Use of Crack-Arrest Holes as a Distortion–Induced Fatigue Mitigation Measure

Say Hak Bun
Caroline Bennett
Adolfo Matamoros
Ron Barrett-Gonzalez
Stan Rolfe

Abstract

Implementation of crack-arrest holes to control fatigue crack propagation under distortion-induced fatigue loading is a commonly applied measure. However, little research has been performed regarding the effectiveness of crack-arrest holes under distortion-induced fatigue (as opposed to in-plane fatigue). This paper presents a use of 51-mm (2-in) crack-arrest holes on a 3-m (9-ft) steel girder subjected to out-of-plane distortion. Results of the study have shown implementation of these crack-arrest holes as having improved the fatigue life steel girder under distortion-induced fatigue.

Introduction and Background

Multi-girder bridges built prior to the mid 1980s are often susceptible to fatigue damage at the connections between girders and cross-frames or diaphragms. Cross-frames and diaphragms between girders are generally used to provide stability during construction and deck placement, and to distribute live load between girders. Rotation of the cross-frames or diaphragms due to differential vertical deflection between girders can produce fatigue cracking in the girder webs at connection plate-to-web welds when the connection plate is not attached to the adjacent girder flange.

Many retrofit techniques have been used to stop distortion-induced fatigue cracks. Arguably the most commonly-used technique by bridge engineers is the use of crack-arrest holes. Drilling holes at the tips of cracks eliminates the sharp termination of the crack and replaces it

with a smooth radius. It has been well-shown that for planar fatigue that crack-arrest holes can become effective depending on the size of the hole, the location of the hole, and the fatigue stress range to which the web is subjected. Equation 3-1 below was proposed by Barsom and Rolfe (2006) for calculating the size of the holes:.

$$\frac{\Delta K}{\sqrt{\rho}} < 10\sqrt{\sigma_y} \qquad \text{Eq. } 3-1$$

where ρ : hole radius

K : stress intensity factor

σ_y : yield strength of material

Fisher (1990) stated that the hole diameter could be varied from 19-mm ($^3/_4$-in) to 76-mm (3-in). Crack-arrest hole sizes used by Kansas Department of Transportation engineers are generally sized from 19-mm ($^3/_4$-in) to 38-mm ($1\ ^1/_2$-in). Many fatigue cracks have been reported to have propagated through the holes, and it is not clear if this behavior could have been avoided by using a larger crack-arrest hole, or if crack-arrest holes are simply not very effective under the action of distortion-induced fatigue.

Field tests conducted by Cousins, Stallings, Lower and Stafford (1998) on six different multi-girder bridges in the Birmingham, Ala. area examined crack-arrest holes as a technique to stop crack propagation under distortion-induced fatigue. Results of the study indicated that cracks propagated beyond the holes at approximately 5% of the connections where holes were drilled. The fatigue stress ranges were reported to be above 105-Mpa (15-ksi) at the holes that experienced crack re-initiation.

Objective

The objective of this research was to investigate the effectiveness of drilling 51-mm (2-in) crack-arrest holes in a steel girder web subjected to distortion-induced fatigue damage for

mitigating crack propagation. This involved gaining a clearer understanding of the stress field around the crack-arrest hole and the effects of the 51-mm (2-in) diameter holes on the crack growth rate of a crack around the connection plate-to-web weld.

Research Approach

This study included both physical testing and an analytical investigation. The analytical part was performing through a Finite Element Analysis application, ABAQUS v6.10-2 (Simulia 2010). The experimental component was carried out in a laboratory at the University of Kansas on a 3-m (9-ft) length of a steel girder.

Experimental Test Set-Up

The physical test setup was comprised of a built-up steel girder connected to the concrete laboratory floor through a series of C5x9 channels post-tensioned to floor as shown in Figure 3-1. The girder subassembly was tested upside-down so that laboratory concrete floor simulated the lateral stiffness of a concrete deck on the bridge. The top flange in the laboratory was restrained from in-plane lateral moment by a L3x3x$^{3}/_{8}$ angle at each end of the girder. These constraints allowed only for out-of-plane bending (no strong-axis bending of the girder was possible). The subassembly was tested under a dynamic tensile load that varied from 2-kN (0.5-kip) to 25-kN (5.7-kip), applied through a WT section that connected to the cross-frame (Fig. 3-2).

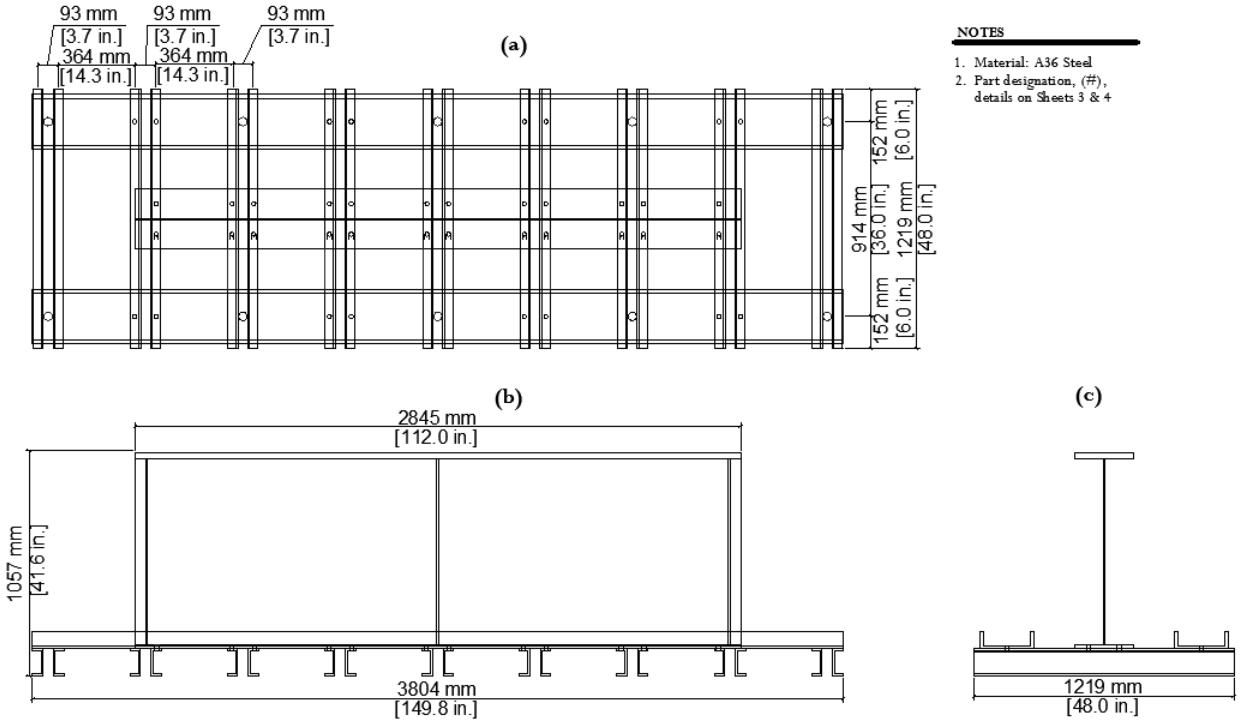

Figure 3-1 Girder Specimen: a) Plan view b) Elevation view c) Section view

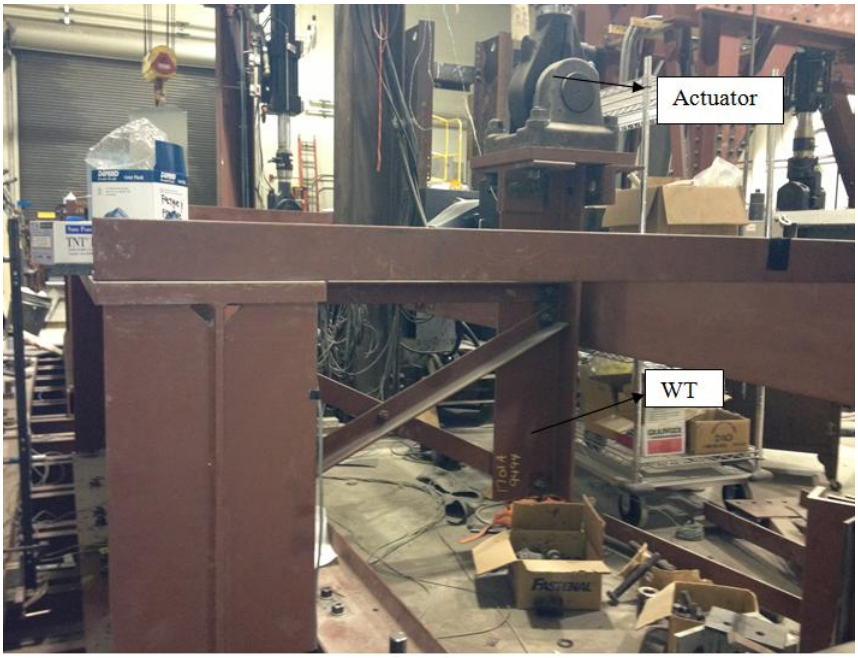

Figure 3-2 Cross-sectional view of the assembly

Specimen Dimensions and Material Properties

The built-up steel girder used in the experimental study was 3-m (9-ft) long and 918-mm (36-in) tall. The web had cross-section dimensions of 10x876-mm ($^{3}/_{8}$x34 ½-in). The bottom and top flanges had cross-sections of 279x25-mm (11x$^{5}/_{8}$-in) and 279x25-mm (11x1-in), respectively. The web, bottom flange, and top flange all had 345-Mpa (50-ksi) nominal yield strength. Four full-depth stiffeners were provided at the girder ends to prevent web instability from occurring at those regions. At each end of the girder, there were two stiffeners welded to the web and flanges. The four stiffeners were 876-mm (34 ½-in) tall and 127-mm (5-in) wide. There was a connection plate welded to the web at the middle of the girder. The connection plate was 873-mm (34 $^{3}/_{8}$-in.) tall and 127-mm (5-in) wide. All stiffeners had a cropped end of 32-mm (1 ¼-in), and the thickness of 10-mm ($^{3}/_{8}$-in). A cross-frame was attached at the center of the girder specimen. The cross-frame was made up of three L76x76x10-mm (L3x3x$^{3}/_{8}$-in) angles of which two were in an X-configuration, and one was horizontal.

Instrumentation

The girder of the subassembly was instrumented with three linear variable differential transformers (LVDTs) and seven strain gages (Fig. 3-3). Two strain gages were placed at the top and bottom web-gaps where the cracks were expected to initiate. The three LVDTs were used to capture the out-of-plane deflection at three different locations.

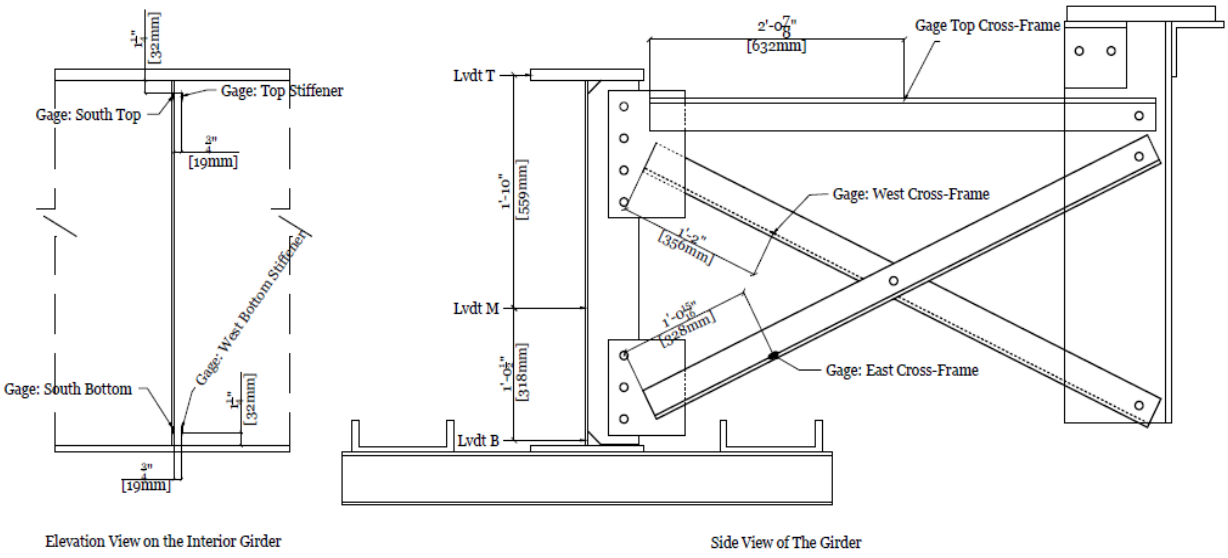

Figure 3-3 Instrumentation on 9ft-steel girder

Experimental Program

The 3-m (9-ft) girder subassembly was tested under the action of a dynamic tensile force ranging from 2-kN (0.5-kip) to 25-kN (5.7-kip) applied through the top of the WT member. The test was divided into three segments; Segment 1 was the initial test that allowed a horseshoe-shaped crack to initiate and propagate to 38-mm (1½-in) long around the connection plate-to-web weld. The girder was inspected often using UV light and dye penetrant to determine crack growth rate, and the data was collected continuously while being cycled. In Segment 2 of the test, a pair of crack-arrest holes were drilled at the tips of the cracks, one on each side of the connection plate. The diameter of the holes was 50.8-mm (2-in). Since the crack was too close to the connection plate, there was not enough room to drill the holes such that the tips of the cracks were located right at the center of the holes. Therefore, the holes were drilled about 3-mm ($^1/_8$-in) over the weld instead of placing the holes' circumference right at the edge of the weld. Around the holes, strain gages were installed to capture the deformation. The specimen was then fatigue cycled at the same load range as in Segment 1 of the test. The inspection procedures were carried out the same ways as mentioned in Segment 1. The specimen was tested until new cracks appeared and propagated to 76-mm (3-in) long. Finally, another pair of holes was drilled at the tips of the cracks. The location of the hole placement and the testing procedures were carried in

the same way as in Segment 2. The locations of the crack-arrest holes and strain gages are shown in Fig.3-4 and Fig.3-5.

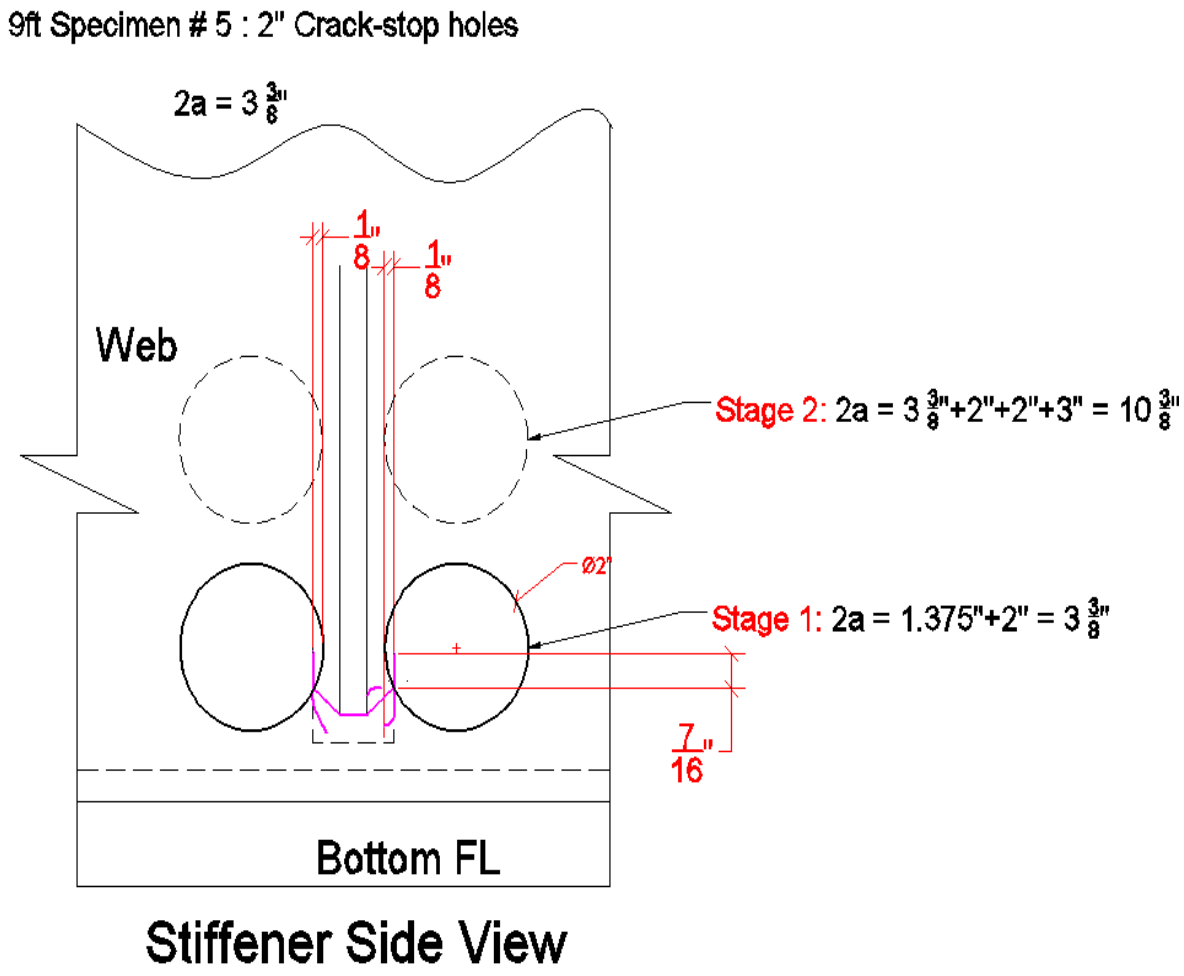

Figure 3-4 Interior girder view where holes were drilled

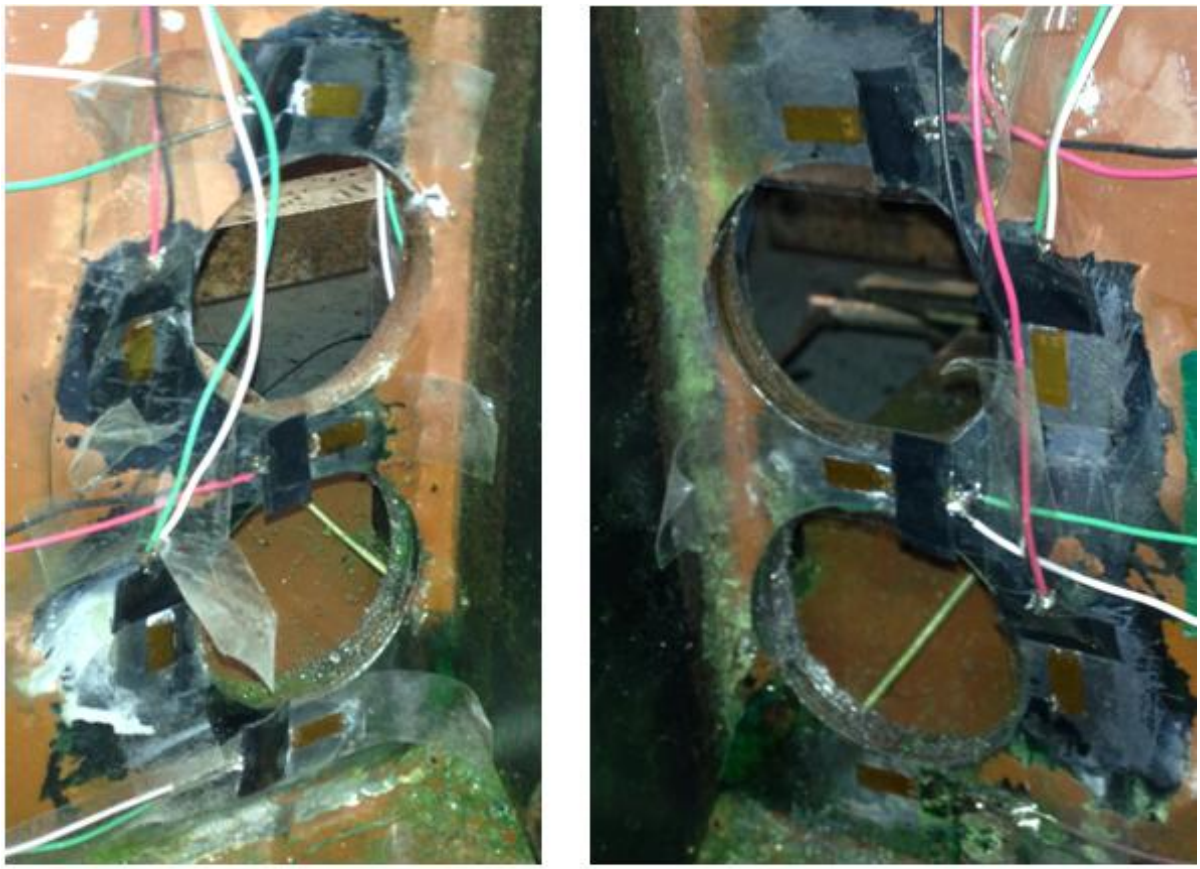

Figure 3-5 Strain gage locations around the holes (a) Left side of connection plate (b) Right side of connection stiffener.

Finite Element Analysis

A linear-elastic Finite Element Analysis (FEA) of the retrofits was carried out using Abaqus v6.10 (Simulia 2012). The model consisted of a single 3-m (120-in) wide by 1524-mm (60-in) deep steel girder section, as shown in Fig.3-6 and 3-7. At each end of the girder, a transverse stiffener was welded to web of the girder, and the top and bottom flanges. At the mid span of the girder, a connection stiffener was welded to the web and then truncated 6-mm (1.4-in) long from the face of each adjacent flange produced a web gap region that was vulnerable to fatigue cracking. The model generated for this investigation was not identical to that used in the physical testing, but the crack configurations and the application of the crack-arrest holes were identical.

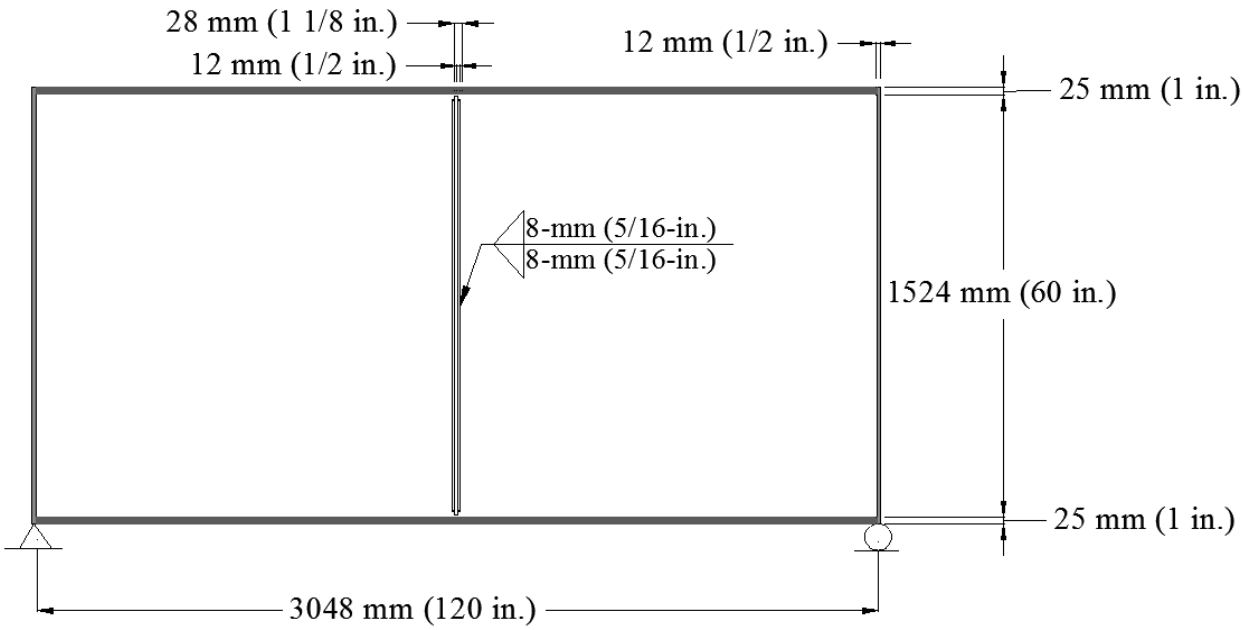

Figure 3-6 Plan view of the girder used within the FEA

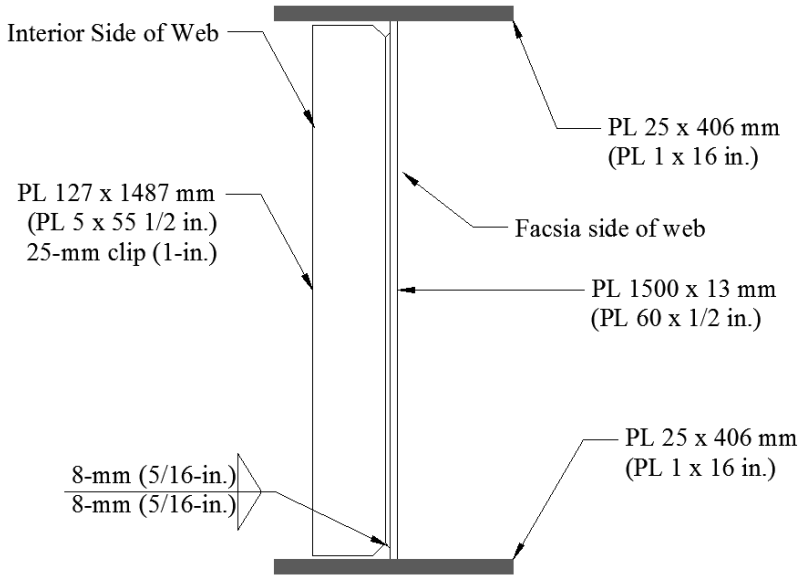

Figure 3-7 Cross-section view of the girder used within the FEA

All steel parts of the girder, including the welds, were assigned a modulus of elasticity of 200-Gpa (29,000-ksi) and a Poisson's ratio of 0.3. A mesh size of 5-mm (0.2-in) was assigned to the welds, and a mesh size of 6-mm ($^1/_4$-in) was assigned for all others. All surfaces were attached using tie constraints. The girder was modeled as simply-supported. Along the bottom

edge of both transverse stiffeners, translational restraint was assigned to allow the stress demand to be transferred to the bottom flange. The outermost side of the transverse stiffeners was also restrained from out-of-plane movement. A gravity load was applied on the top flange to produce 35-Mpa (5-ksi) bending stress in the top flange. A 22-kN (5-kip) out-of-plane load was applied at two locations near the top and bottom of the connection stiffener. The load near the top was in tension, and the load in the bottom was in compression. These loads were selected after examination of forces induced by cross-frames in full-scale bridge models created by Hassel (2011) and Roddis and Zhao (2003).

In these analyses, a horseshoe-shaped crack was modeled explicitly along the connection-plate-to-web weld. The initial length of the crack was 38-mm (1 ½-in). Two models were analyzed: one model included a pair of 51-mm (2-in) crack-arrest holes, and the other included two pairs of 51-mm (2-in) crack-arrest holes. The first pair of crack-arrest holes was created at the tips of the horseshoe-shaped crack around the connection plate-to-web weld in such a way that each hole also removed a 3-mm ($^1/_8$-in) deep portion of the connection-plate-to-web weld. In the second model, the original crack was extended to a greater length, starting from the edges of the first pair of crack-arrest holes moving along the welds. The length of the additional crack was 76-mm (3-in). A second pair of crack-arrest holes was created at the tips of the new crack in this new model.

Results

One pair of crack-arrest holes

The results from the FE model concluded that drilling the first pair of 51-mm (2-in) diameter crack-arrest holes at the tips of the horseshoe-shaped crack eliminated the high stress demand at the tips of the crack. However, the stress concentrated at new locations along the stiffener-to-web weld at a small distance from the edge of the holes. The magnitude of stress was above 345-Mpa (50-ksi), which could have easily resulted in cracking at those locations (Fig.3-8). However, since the highest stress demand did not start at the edge of the holes, the FEA results indicated that cracking would re-initiate a short distance away from the first pair of

crack-arrest holes, again along the connection plate-to-web weld. These findings were in agreement with results from the experimental testing. In the physical testing, it was found that new cracks did not initiate from the first pair of crack-arrest holes until the cycle count reached about 420,000. Then, new cracking initiated located along the connection plate-to-web weld at a distance approximately 13-mm ($^1/_2$-in) away from the edge of the holes (Fig.3-11). There was no sign of cracks re-initiating from the edge of the holes.

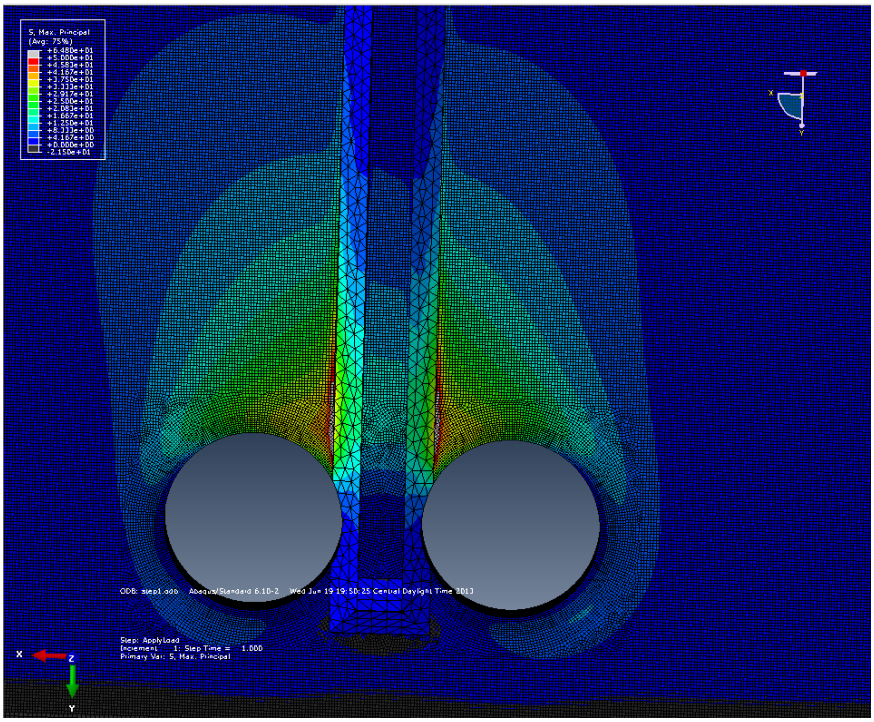

Figure 3-8 Finite Element Model for the girder including one pair crack-arrest holes

Figure 3-9 Crack-arrest hole on the left side of the connection plate (Segment 2)

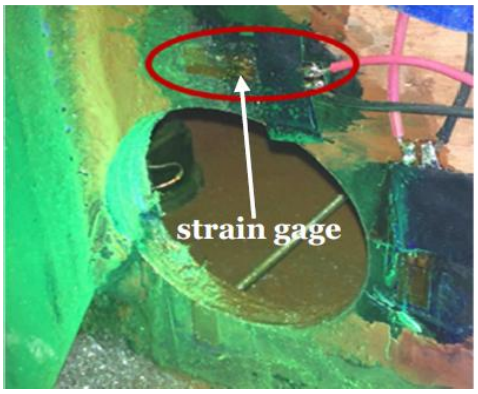

Figure 3-10 Crack-arrest hole on the right side of the connection plate (Segment 2)

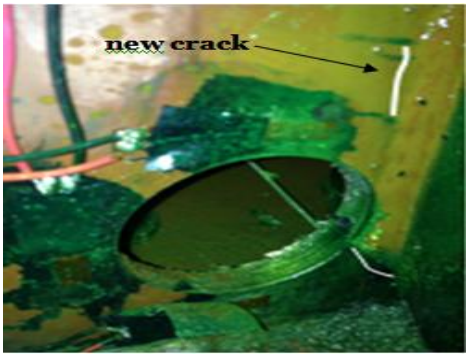

Figure 3-11 Cracking forming after the first pair of crack-arrest holes had been drilled and tested (Segment 2)

Strain gages were installed around the holes at 90 degree apart to measure the deformation around the holes. The data from two strain gages were presented in this paper. The gages were named as Left CSH and Right CSH, both located on the top of the holes next to the connection plate-web weld (Fig.3-9 and Fig.3-10). Left CSH was the gage on the left side of the connection plate, and Right CSH was on the right side. Strain data collected from these two strain gages indicated that the magnitude of strain was closed to the strain at yield (Fig.3-12). Also, the strain on the left crack-arrest hole was higher than the strain value obtained on the right crack-arrest hole, which was corroborated by the fact that a crack was first seen on the left side of the connection plate before it was found to have initiated on the right side of the connection plate (Fig.3-11).

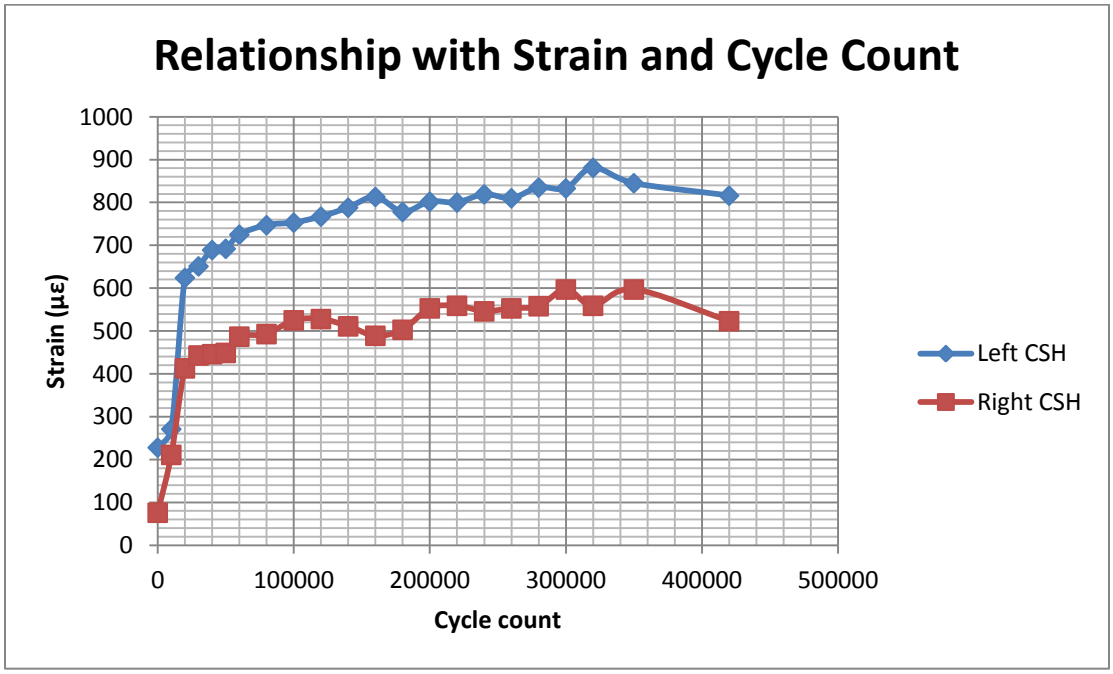

Figure 3-12 Strain data from Left CSH and Right CSH gages both measured at 10-mm ($^3/_8$-in) from the edge of the hole (Segment 2)

The lateral deflection along the height of the girder clearly indicated that the deflection of the girder was increased significantly resulting from the web becoming more flexible due to the presence of the holes (Fig.3-13).

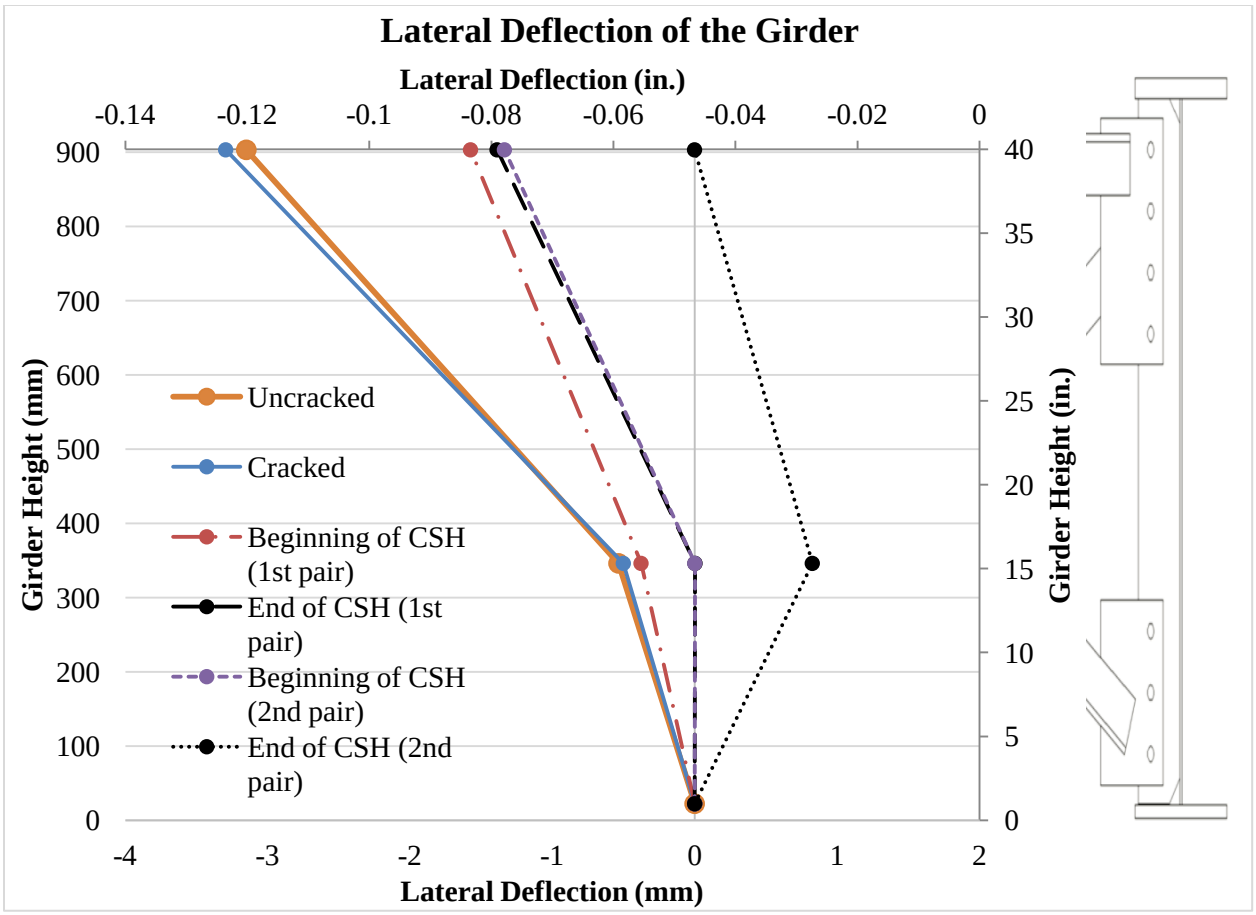

Figure 3-13 Lateral deflection along the height of the girder

Two pairs of crack-arrest holes

The FE model results for the model including the second pair of crack-arrest holes showed that new locations of high stress demand were induced along the connection plate-to-web weld at a distance approximately 38-mm ($1^1/_2$-in) from the edge of the holes as shown in Fig.3-14. These results were comparable to the results from the physical testing, which showed that new cracks first initiated at a distance approximately 19-mm (¾-in) away from the edge of the holes at 980,000 cycles, and then propagated towards the edge of the holes. The lateral deflection along the height of the girder was once again increase greatly as shown in Fig.3-13, and the web became more and more flexible.

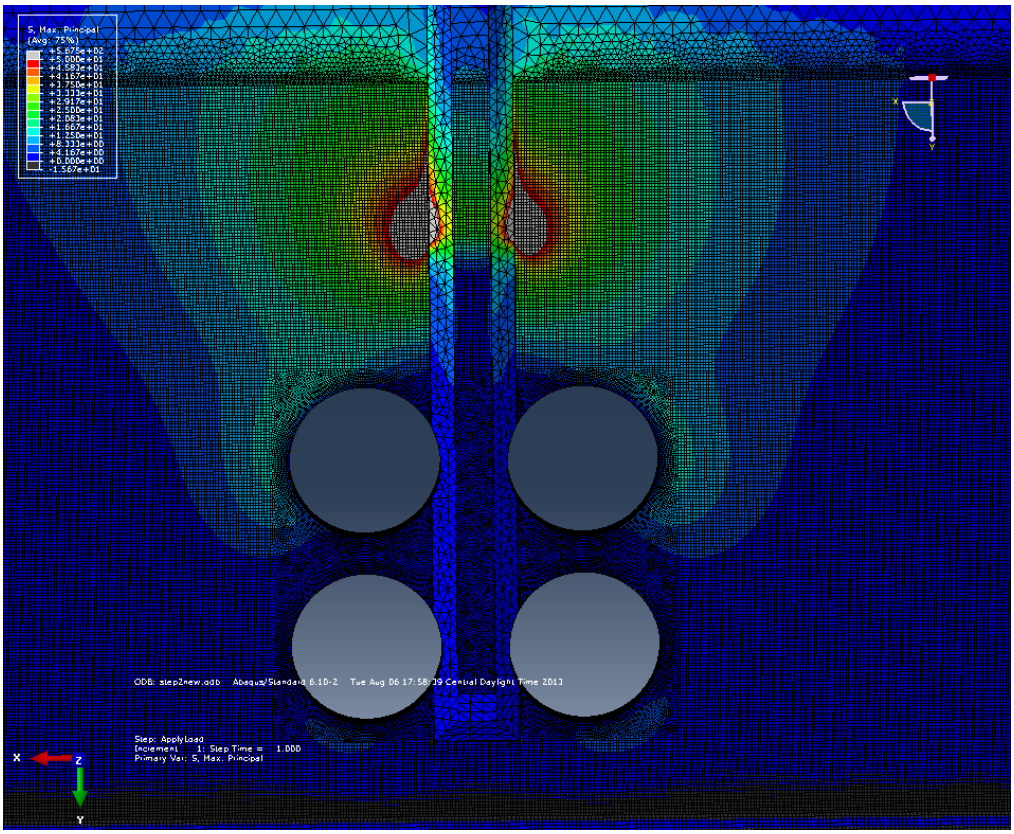

Figure 3-14 Finite element model showing two pairs of crack-arrest holes (cracking modeled explicitly)

There were two strain gages installed on the top of the second pair crack-arrest holes at a distance of 10-mm ($^{3}/_{8}$-in) from the edge of the holes (Fig.3-15). Both gages were denoted as Left CSH and Right CSH. The Left CSH was the strain gage on left side of the connection plate at a distance of 25.4-mm (1-in) from the connection plate-to-web weld (Fig. 3-15(a)), and Right CSH was the strain gage on right side of the connection plate A (Fig. 3-15(b)). The data indicated that the highest strains were located on the right side of the connection plate (Fig.3-16).

Figure 3-15 Strain gage placement around two pairs of crack-arrest holes in the physical testing. (a) Left side of the connection plate (b) Right side of the connection plate

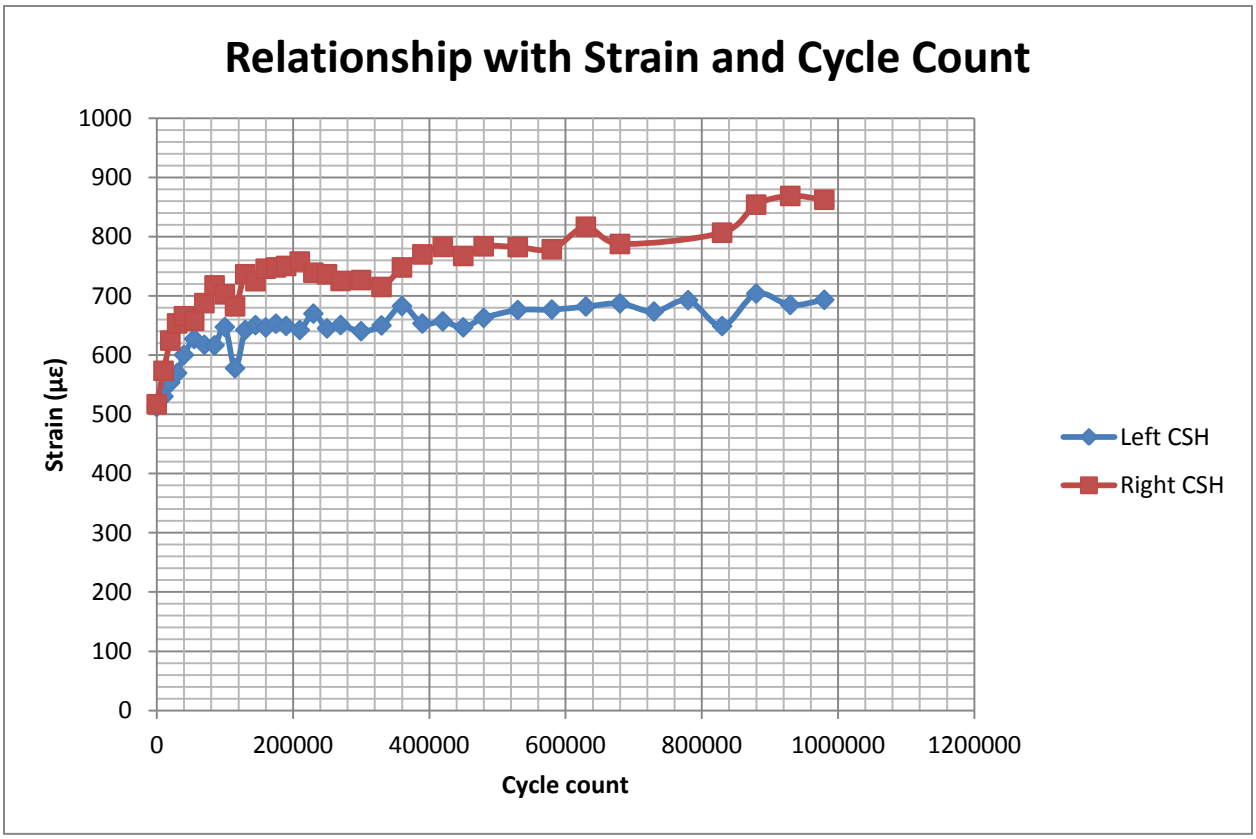

Figure 3-16 Strain data from Left CSH and Right CSH gages both measured at 10-mm ($^{3}/_{8}$-in) from the edge of the hole (Segment 3)

Conclusion

Crack-arrest holes with a diameter of 51-mm (2-in) were evaluated analytically and experimentally. It was found that after drilling relatively large crack-arrest holes at the tips of the cracks around the connection plate weld, the web became more flexible. From the results of inspection, the existing cracks never reinitiated from the holes. However, new cracks tended to form along the connection plate-to-web weld downstream from the holes. The holes provided a wider area in the web for stresses to be distributed away from the stiffener. These studies concluded that the 51-mm (2-in) crack-arrest holes did stop the horseshoe-shaped crack from undergoing additional propagation. However, due to the high stress demand at the connection-plate-to-web weld, new cracks initiated along the same weld at a small distance away from the edge of drilled holes, greatly limiting the overall effectiveness of this technique.

References

Barson, J.M. & Rolfe, S. T. (2006). Fracture and Fatigue Control in Structures: Application of Fracture Mechanics Third Edition. ASTM, West Conshohocken, PA.

Fisher, J. W., Jian, J., Wagner, D. C. and Yen, B. T. (1988). "Distortion-induced fatigue cracking in steel bridges." National Coorperative Highway Research Program Report #336, Transportation Research Board, National Research Council, Washington, D.C.

Roddis, K, and Y Zhao (2003). "Finite Element analysis of steel bridge distortion induced fatigue" *Journal of Bridge Engineering, 8(5),* 259-266.

Hassel, H.L. (2011). "An Analytical Evaluation of Distortion-induced Fatigue in Steel Bridges." thesis, presented to The University of Kansas, at Lawrence, KS, in partial fulfillment of the requirements for the degree of Master of Science in Civil Engineering.

Cousins, T.E., Stallings, J. M., Lower, D. A., Stafford, T. E. (1998) "Field evaluation of fatigue cracking in diaphragm-girder connections." J. Perform. Constr. Facil. 1998.12:25-32.

Alemdar, F. (2011) "Repair of bridge steel girders damage by distortin-induced fatigue," thesis, presented to The University of Kansas, at Lawrence, KS, in partial fulfillment of the requirements for the degree of Doctor of Philosophy in Civil Engineering.

Gangel, R.E (2012) "Evaluation of Fatigue Damage Repair Measures in Welded Steel Plate Bridge Girders." thesis, presented to The University of Kansas, at Lawrence, KS, in partial fulfillment of the requirements for the degree of Master of Science in Civil Engineering.

Simulia. (2010). ABAQUS FEA Version 6.10-2. Providence, RI. http://www.simulia.com.

Chapter Four:

Repairing Distortion–Induced Fatigue Damage at Floorbeam-Stringer Connections in Steel Bridge Girders

Say Hak Bun
Caroline Bennett
Adolfo Matamoros
Ron Barrett-Gonzalez
Stan Rolfe

Abstract

Distortion-induced fatigue cracking has been detected in numerous floorbeam-stringer bridges resulting from restraining the rotation of the stringers at the connection. Two floorbeam-stringer connection details include: the case in which the stringer web is bolted to the floorbeam via a connection plate, and the case in which double angles are bolted or riveted to the webs of the floorbeam and the stringer. Cracks have been reported to occur at the double angles in the web of the floorbeam and at the cope of the stringer. Damage Limitation Methods (DLMs) have been used by bridge engineers to stop crack growth at the cope. However, the DLMs were proved by some researchers to be ineffective under fatigue loading. Therefore, the objective of this research was to investigate the effectiveness of a retrofit technique in reducing high local stress at the cope as well as stopping the crack from further propagation. The retrofit investigated is a combination of a steel back plate and double bent plates. The retrofit will be studied and investigated analytically and experimentally.

Introduction

Floorbeam-stringer deck framing systems have been historically used in interstate highway and railway bridge systems with heavy truck traffic. There are two types of floorbeam-stringer connection details typically seen on those existing bridges. For Type I connection details, the web of the stringer was bolted or riveted directly to the connection stiffener of the floorbeam.

Type II connection details were constructed by using double angles to connect the webs of the stringer and the floorbeam.

These connections were initially designed as simple shear connections. However, field measurements conducted by Roeder (1998) showed that significant rotational connection stiffness can occur at end connection of floorbeam-stringer connections. This stiffness multiplied by the angle of rotation of the stringer denotes the end moment, which was not accounted for in the initial assumption of the design. The rotation, θ, at each end of the stringer can be viewed as the combination of rotation due to stringer curvature, θ_{str}, rotation due to the floorbeam twisting, $\theta_{fb\text{-}twist}$, and rotation from floorbeam differential vertical displacement, $\theta_{vertical}$, as shown in Fig.4-1 (Roeder 1998). Because of the end moment, fatigue cracks have been found to develop at either the cope of the stringers or at the double angles used in the connection. Effective retrofit techniques must be carefully studied and chosen to permanently stop crack growth.

This paper explores the application of a retrofit technique tested on two girder subassemblies conducted in a laboratory at the University of Kansas and in computation simulations using the commercially-available software Abaqus.

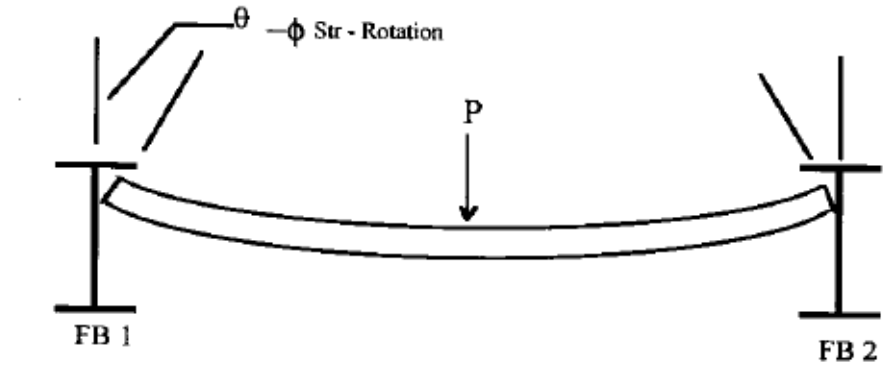

(a) Rotation due to stringer curvature force P.

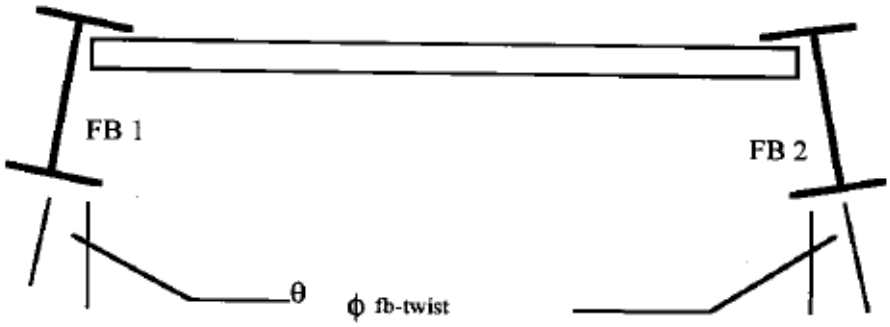

(b) Rotation due to the Floorbeam twisting which is caused by the stringer curvature.

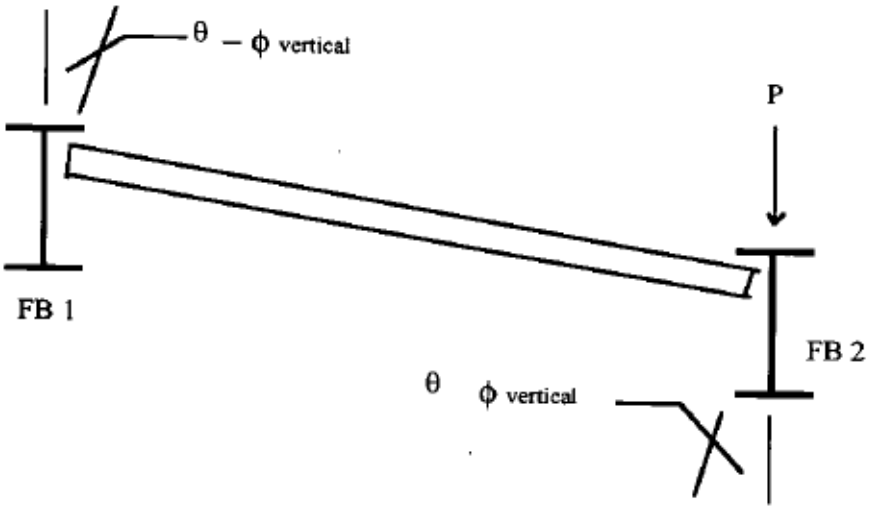

(c) Rotation due to the floorbeam vertical-differential-displacement.

Figure 4-1 Description of three different rotations (Roeder, 1998)

Bacground

Fatigue Crack Locations in Floorbeam-Stringer Connections

A common crack pattern seen in stringer-floorbeam bridge systems occurs at the cope of the stringers' web, as shown in Figure 4-2. Flame cutting to create the cope or physical notches from other sources leads to a fatigue-susceptible detail (Fisher, 1990). Research conducted by Yam and Cheng (1997) showed that crack initiation in the cope depends upon the stress level, number of cycles, roughness, and cope geometry. The smaller the radius of the cope, the faster the crack initiates.

Another location in floorbeam-stringer connections that has been shown to be susceptible to fatigue damage is at the connection angles. Al-Emrani (2002) reported a number of case studies in which fatigue cracks were detected in the connection angles. These cases have involved both cracking in the outstanding legs of the connection angles or crack development in rivets connecting the outstanding legs to the floorbeam web, eventually resulting in failure of the rivets.

Al-Emrani (2005) investigated the behavior of riveted double-angle stringer-to-floorbeam connections experimentally on three full-scale bridge parts taken from an old riveted railway bridge. The results concluded that fatigue damage initiated in the upper regions of the connections where the maximum distortion-induced fatigue stress concentrated. The propagation rates were typically very slow and decreased gradually, and the fatigue cracking in riveted double-angle stringer-to-floorbeam connections was not found to immediately reduce the load-carrying capacity. Therefore, work done by Al-Emrani (2005) focused on retrofitting the cracking at the cope of the stringer.

Figure 4-2 Fatigue cracking at the coped stringer near a floorbeam-to-stringer connection (Source: KDOT)

Common Repair Techniques for Fatigue Cracking at Floorbeam-Stringer Connections

Roeder (2005) described three Damage Limitation Methods (DLMs) used by engineers to control growth at a coped stringer near a Floorbeam-Stringer connection. One of the DLMs described a crack-arrest hole drilled at the tip of the crack. In theory, smoothing out a crack tip by drilling a hole can slow or permanently stop crack growth. Another DLM described was to install a high-strength bolt in the drilled crack-arrest hole. By installing a tightened bolt, the bolt pretension develops triaxial compressive stresses in the stringer web, which acts to slow crack growth propagation rate. The last DLM described was to remove some of the rivets or bolts at the connection in order to reduce stiffness of the connection, reducing the tensile bending stress at the cope.

Roeder (2005) experimentally evaluated the effectiveness of the described DLMs under fatigue loading. The scaled test setup was comprised of a W21x62 specimen connected to a reaction wall at one end by a single angle, and connected to the floor at the other end with a pinned support. This configuration simulated the end span member of the bridge. Sixteen specimens were tested with different cope geometries. Roeder concluded that the drilled hole DLM provided a short-term extension of fatigue life, but that it was a relatively ineffective technique in stopping crack growth. The DLM including a tightened bolt in the crack-arrest hole

was found to be very effective in controlling crack growth, but new cracks were found to then occur at other less critical locations. Finally, it was found that removing connectors was effective at stopping crack growth if the connection stiffness was reduced sufficiently. If this is not achieved, continued crack growth should be expected.

Research Approach

Two floorbeam-stringer subassemblies utilizing different connection geometry were tested in the Structures Laboratory at the University of Kansas. A sub-assembly utilizing a Type I detail (stringer connected directly to a connection plate on the web of a floorbeam by bolting) was tested, and a sub-assembly utilizing a Type II detail (stringer was connected to the web of a floorbeam via bolted double angles) was tested. Additionally, the two details and repair methodologies were analyzed using finite element analyses performed using Abaqus v.6.10.2 (Simulia 2010).

Test Set-Up

Both of the two test set-ups consisted of a 3-m (9-ft) built-up steel floorbeam-stringer assembly, as pictured in Figures 4-4a and Figure 4-4b. The floorbeam was connected to the concrete laboratory floor through a pair of HSS6x6x$^{1}/_{2}$ and a series of C5x9 channels post-tensioned to the 914-mm (3-ft) thick concrete floor, as shown in Fig.4-3. The assembly was tested upside-down so that laboratory concrete floor simulated the lateral stiffness of a concrete deck on a bridge. The top flange of the floorbeam was restrained from lateral movement through use of an L3x3x$^{3}/_{8}$ angle on each end of the floorbeam. The specimen is entirely allowed only for out-of-plane bending. Four full-depth stiffeners were provided at the floorbeam ends to prevent from web instability at those regions. A WT member was connected to one end of the stringer and attached to an actuator (Fig.4-4a and 4b). Two specimens are being cycled simultaneously with two connections CXN#1 and CXN#2.

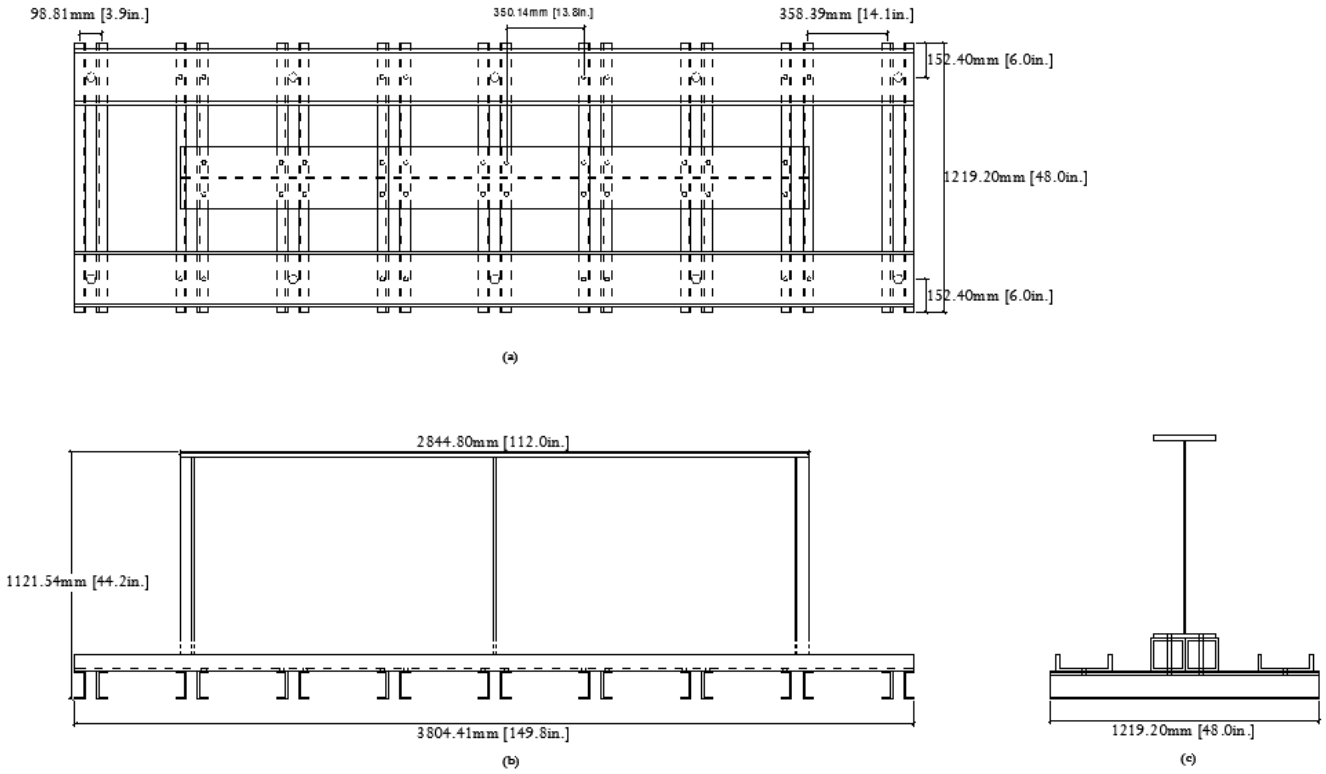

Figure 4-3 Floorbeam tie down system : a) Plan view b) Elevation view c) Section view

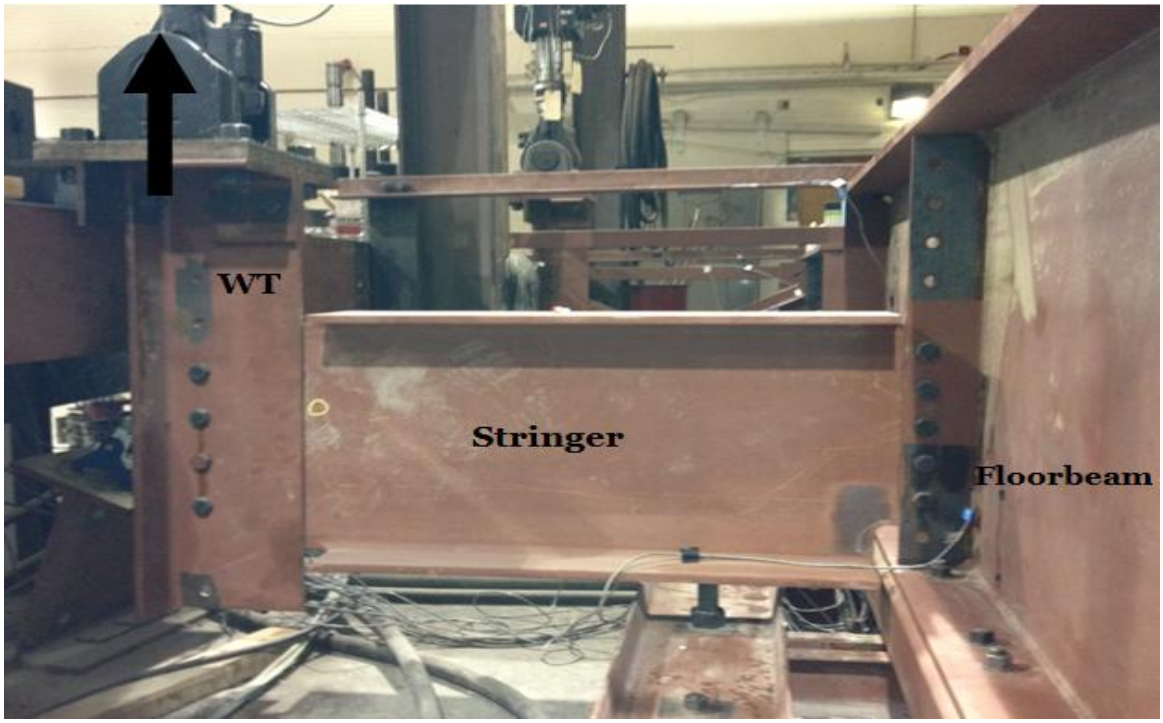

Figure 4-4a Stringer's physical end connections (CXN1)

Figure 4-4b Stringer's physical end connection (CXN2)

Specimen Dimensions and Material Properties

The built-up floorbeam used in the experimental study was 3-m (9-ft) long and 918-mm (36-in) tall. The web had cross-section dimensions of 10x876-mm ($^{3}/_{8}$x34 ½-in). The bottom and top flanges had cross-sections that measured 279x25-mm (11x$^{5}/_{8}$-in) and 279x25-mm (11x1-in), respectively. The web, bottom flange and top flange were comprised of steel having 345-MPa (50-ksi) nominal yield strength. At each end of the floorbeam, two 10-mm ($^{3}/_{8}$-in) thick stiffeners were welded to the web and flanges. A connection plate was welded to the web at the middle of the floorbeam used in Connection Type I to connect a coped stringer. However, this connection plate was not present in the second test setup where the coped stringer and floorbeam were connected through double angles.

The connection plate used in the Type I Connection test setup was 873-mm (34 $^{3}/_{8}$-in.) tall, 127-mm (5-in) wide, and 10-mm ($^{3}/_{8}$-in) thick. All stiffeners had a cropped end of 32-mm (1 ¼-in), and the weld dimension used was 10-mm ($^{3}/_{8}$-in). The coped stringers used in the tests were W21x73 with a length of 997-mm (39 $^{1}/_{2}$-in) and 1124-mm (44 $^{1}/_{4}$-in), respectively (Fig.4-5). The built-up floorbeam was attached to a pair of HSS 6x6x$^{1}/_{2}$ and then to the laboratory concrete floor through a series of C5x9 channels.

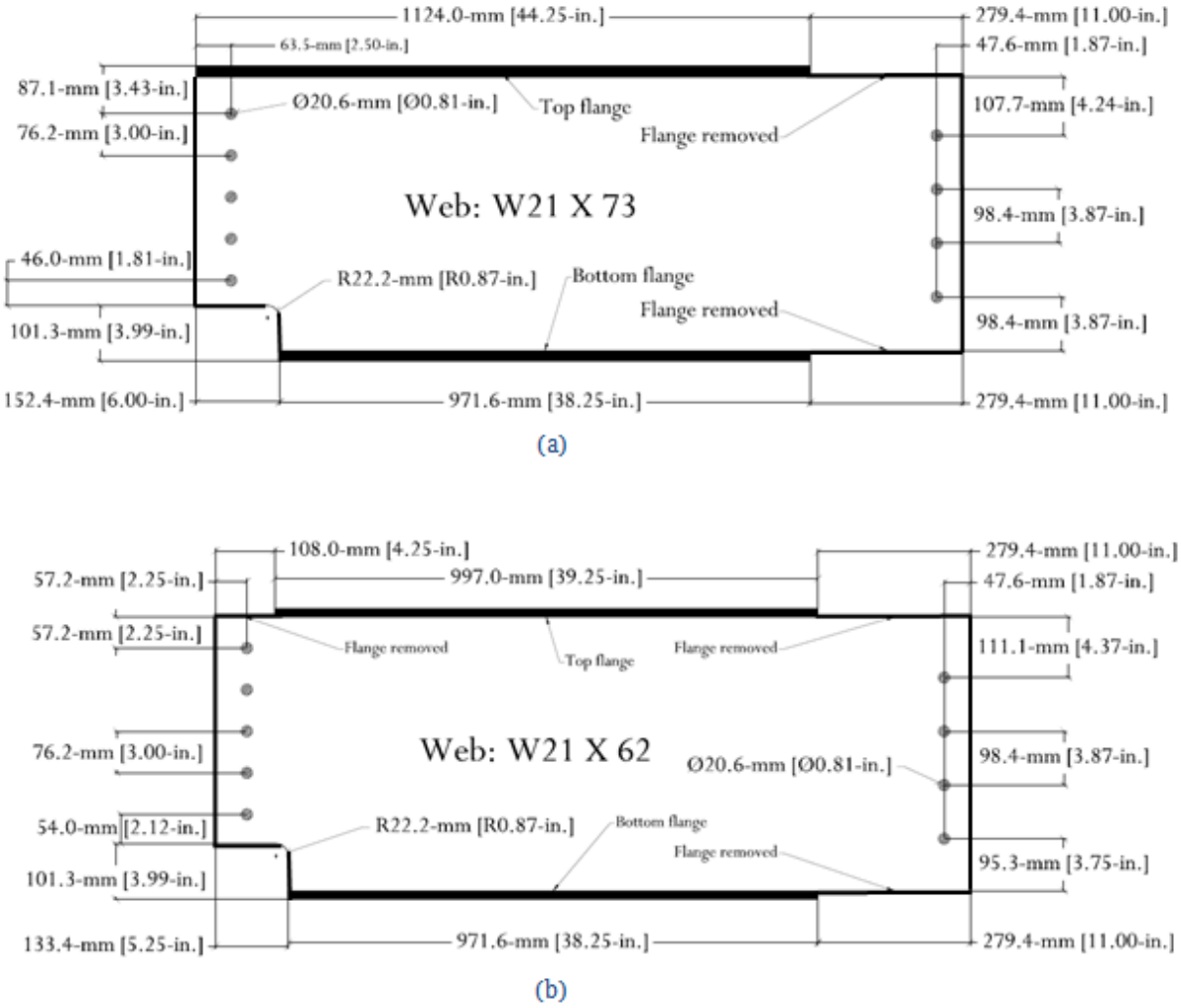

Figure 4-5 a) Stringer detailing used with Connection Type I b) Stringer detailing used with Connection Type II

Instrumentation

The web of floorbeam was instrumented with three linear variable differential transformers (LVDTs) and nine strain gages. The three LVDTs were used to capture the out-of-plane deflection at three different locations along the height of the floorbeam as shown in figure 4-6. The strain gages used were Micro-Measurements WK-06-250BG-350. The location of each strain gage was shown in figure 4-7 to 4-9.

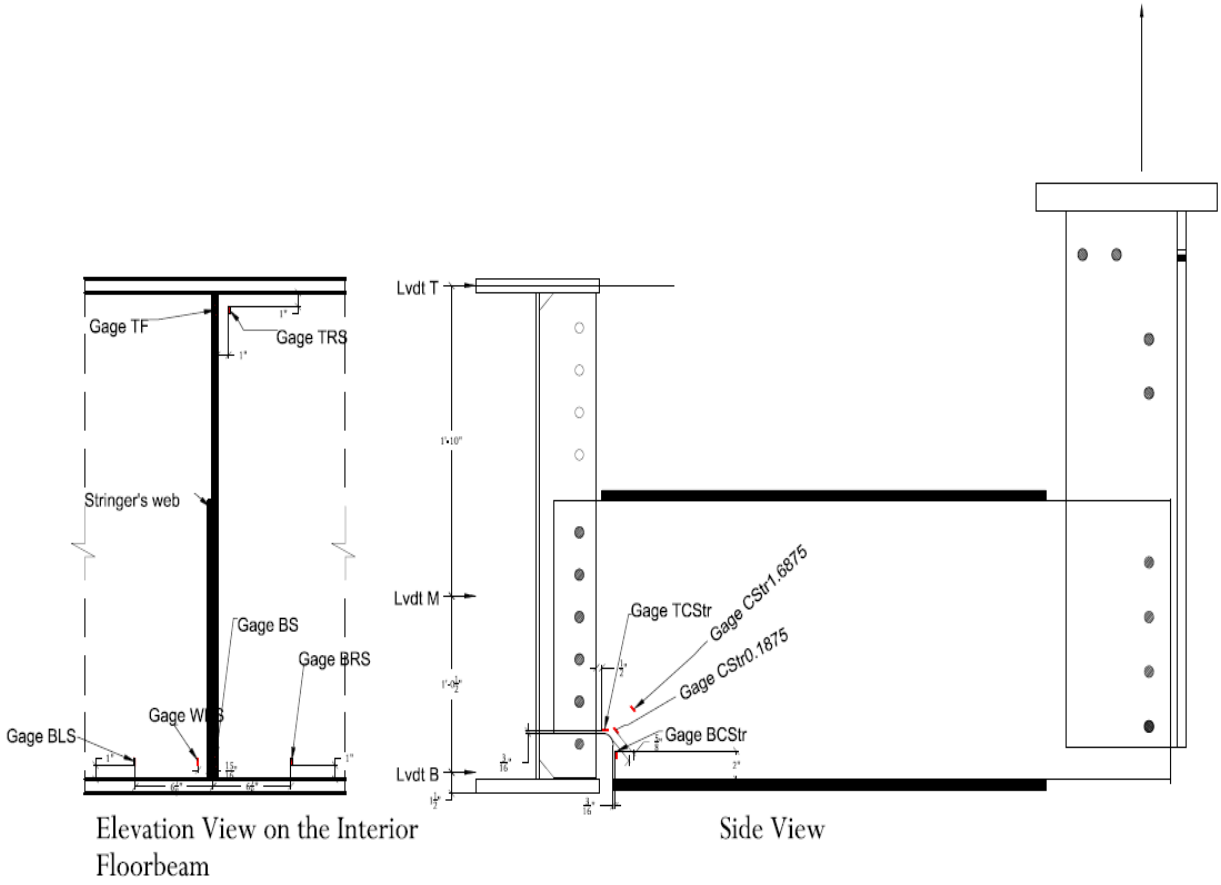

Figure 4-6 Instrumentation used on the floorbeam-stringer test set-up

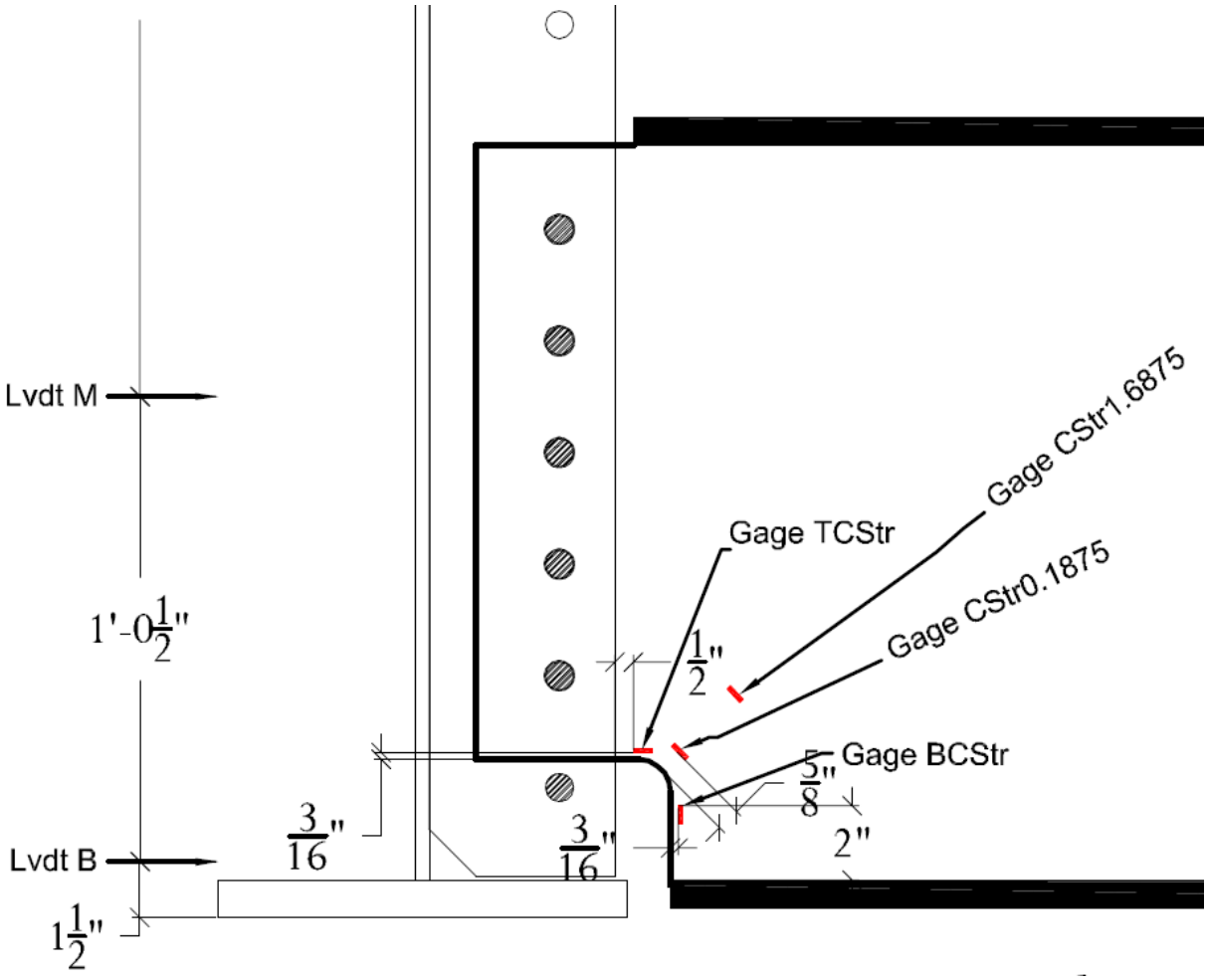

Figure 4-7 A closer view of the strain gages around the cope of stringer (schematic)

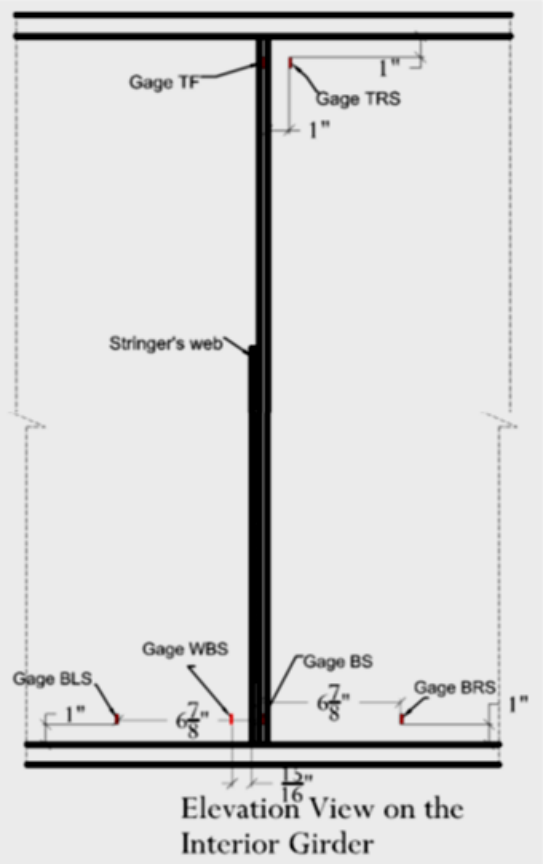

Figure 4-8 A closer view of strain gages on the web of floorbeam (schematic)

Figure 4-9 Closer view of the strain gaging layout at the stringer cope (actual specimen)

Finite Element Analysis

The two floorbeam-stringer subassemblies were modeled using the finite element software Abaqus v.6.10 to analyze the variation of stress due to the out-of-plane distortion effect. Two models were created and analyzed separately. The two models differed in the connection between the stringer and the floorbeam, as also differentiated the two physical tests. The Type I and Type II connections that were modeled are shown in Fig.4-10.

Test set-up details were modeled as faithfully as possible. A WT section was modeled and attached to one end of the stringer with a steel plate on the top simulating the location of load applied. The steel plate was restrained from moving in both longitudinal and lateral directions. The concrete floor was assigned as a fully fixed support that eliminated the girder in-plane bending. To prevent surfaces from intersecting, a hard contact interaction was assigned for all potential contact surfaces. All welds were modeled as right triangles, and were assigned as "tie constraint" for the contact surfaces between web and flange, and between web and stiffener. Bolts were modeled explicitly as a clamping mechanism between interactive surfaces. The bolts were 19-mm (¾-in) diameter and consisted of three parts merged together. In the center of each bolt shank, a 125-kN (28-kip) bolt load was applied based on the AISC specification for Gr. A325 high-strength structural bolts.

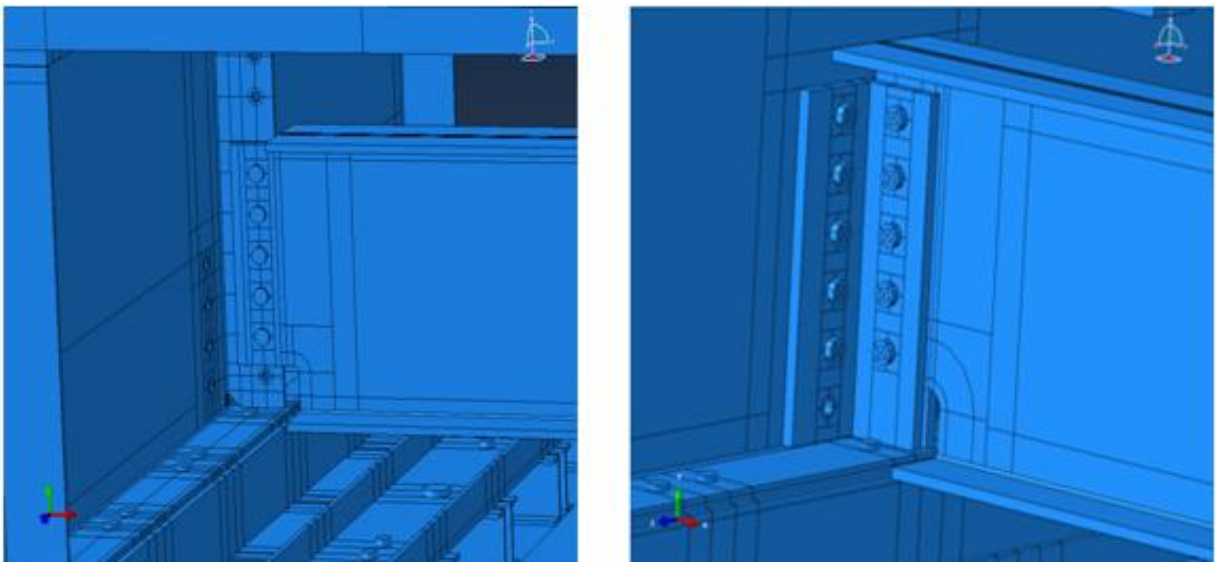

Figure 4-10 stringer-floorbeam connections: a) Type I b) Type II

Tetrahedral and brick elements (C3D8R) were used throughout the model mesh. Tetrahedral elements were used to transition between different brick mesh densities, and brick elements comprised the majority of the mesh. A mesh size of 3-mm (0.1-in) was used at the locations of critical stress. A mesh size of 25-mm (1.0-in) was assigned at non-critical locations, and a mesh size of 13-mm (0.5-in) was assigned at the transition element locations. The number of degrees of freedom in each model ranged from 1 to 2.5 million, depending on the particular model geometry and retrofit inclusion.

Cracks were modeled using an explicit crack modeling technique employed by removing elements from the web along the length of the crack. The width of the cracks was 0.25-mm (0.01-in). A Hot Spot Stress (HSS) technique was used to compute the stress near welds and geometric discontinuities. Three HSS paths were defined to perform this computation, and each path was located a distance of half the web thickness away from the welds or geometric discontinuities. Maximum principal stresses were extracted along those paths. HSS#1 was the maximum principal stress taken from a path along the connection plate-to-web weld at a distance of 4.8-mm ($^3/_{16}$in) from the weld toe / modeled crack. HSS#2 was the maximum principal stresses extracted along the path paralleling the crack at the toe of the flange-to-web weld. HSS#3 was the maximum principal stresses extracted at a distance of 4.8-mm ($^3/_{16}$-in) from the cope of the stringer (Fig.4-11).

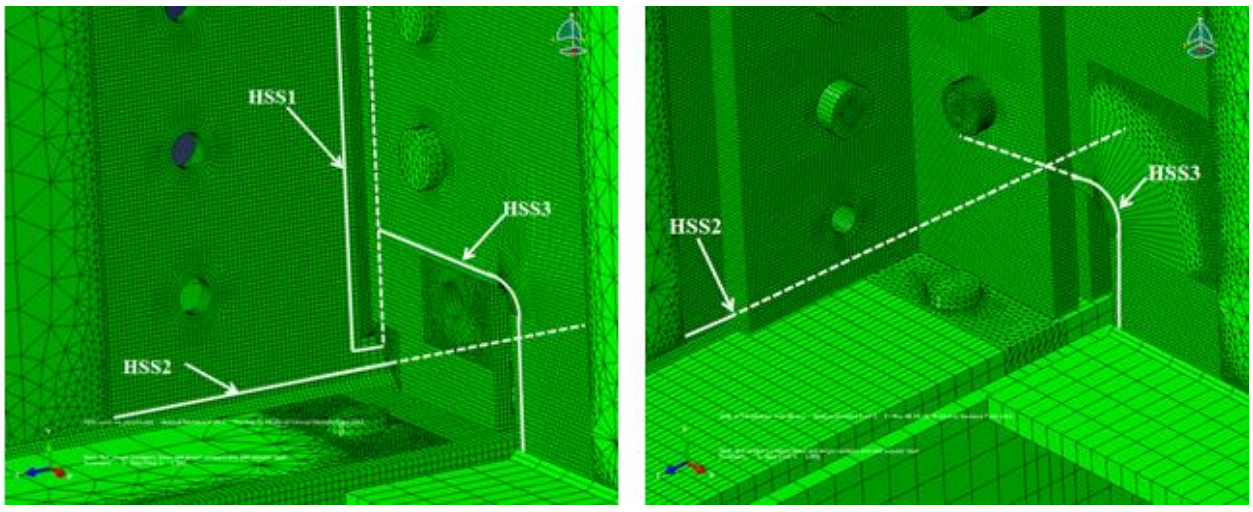

Figure 4-11 Hot Spot Stress paths a) Type I connection b) Type II connection

Three steps were used to execute the analyses: Initial, Pretension, and Bolt Length Constant. Contact interactions were initiated in the Initial step, bolt loads were applied in the Pretension step, and finally in Bolt Length Constant step, a static load of 22-kN (5-kip) was applied on the top of the WT member in the form of a pressure.

Stringer-to-Floorbeam Connection Type I

The Type I connection detail involved a bolted connection made through the stringer's web and the connection plate welded to the web of the floorbeam. Three locations exhibited high stresses: the connection plate-to-web weld, the web-to-flange weld in the floorbeam, and the cope of stringer. These three locations have been labeled as *Horseshoe*, *Horizontal*, and *Coped* in Fig. 4-12, which shows the distribution of maximum principal stresses in the un-cracked model.

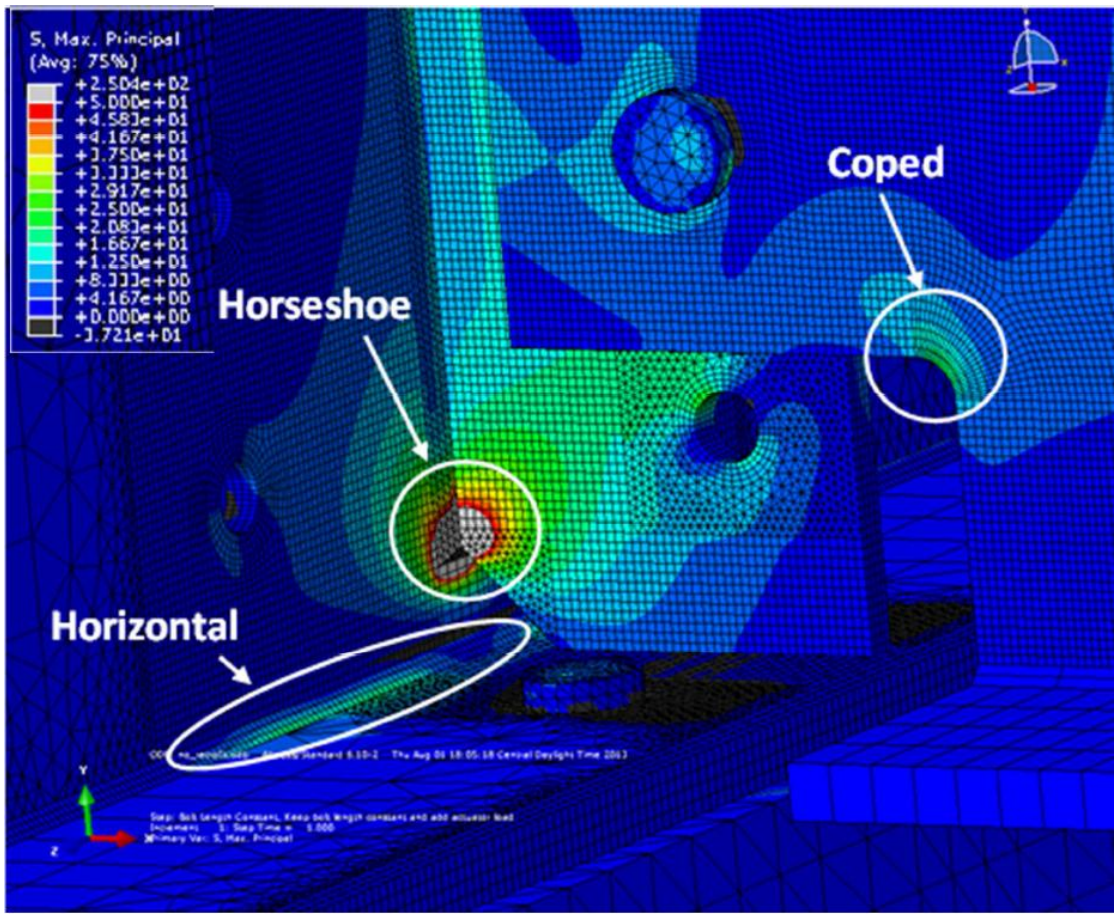

Figure 4-12 Distribution of maximum principal stresses in Type I connection (un-cracked)

The magnitude of principal stresses from highest to lowest was: Horseshoe, Coped and Horizontal. Three successive approaches were taken to eliminate high stress demand at these three locations, as described in the following.

The first approach examined was to repair the location around the connection plate-to-web weld that had the highest maximum principal stress (labeled as *horseshoe*). A model was generated that included a crack length of 38-mm ($1^1/_2$-in) around the stiffener-to-web weld (Fig.4-13a). The crack was modeled explicitly. Then, a retrofit was applied using steel angles and a back plate (Fig.4-14a). This retrofit significantly reduced the high stress demand at the connection plate-to-web weld toe, but stress demands increased at the cope of the stringer.

The second approach examined was to repair the coped location that had exhibited the second highest maximum principal stress demands. An additional 51-mm (2.0-in) long crack was modeled as radiating outwards from the cope at a 45 degree angle (Fig.4-13b). The model

now contained two cracks: a crack around the connection-plate-to-web weld and a crack at the cope. Two L-shaped plates were replaced the double angles that had been previously used as a retrofit on each side of the stiffener (Fig.4-15). Once this retrofit was applied, the high stress demand at the cope was greatly reduced, leaving only high stress demands at web-to-flange weld.

It is recommended that an additional retrofit be analyzed in which the L-shaped plates are replaced with steel bent plates (Fig.4-16).

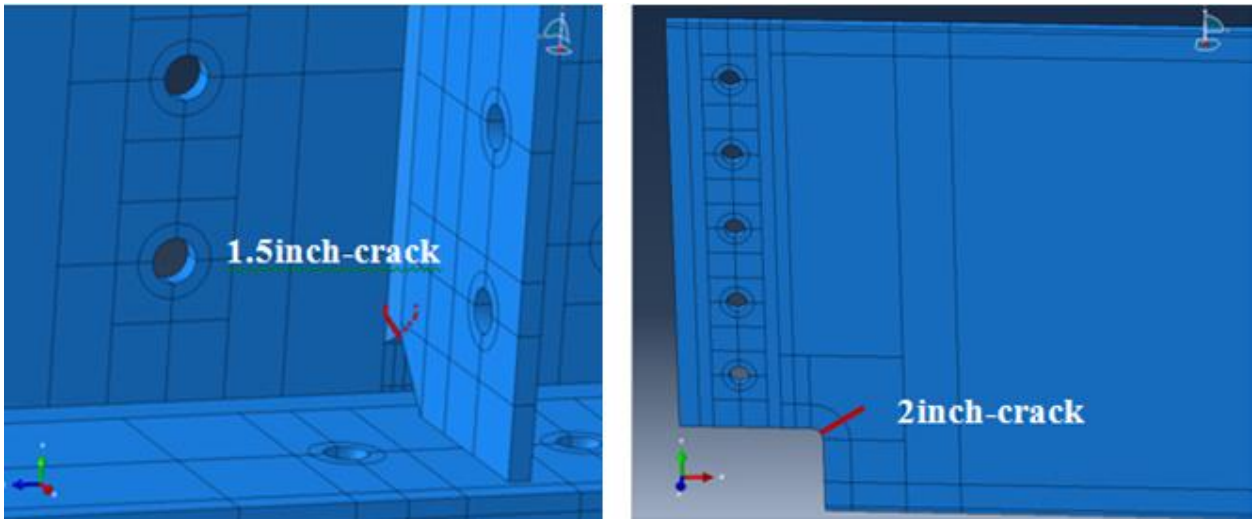

Figure 4-13 Cracks created in the 3D model. a) Horseshoe b) Coped

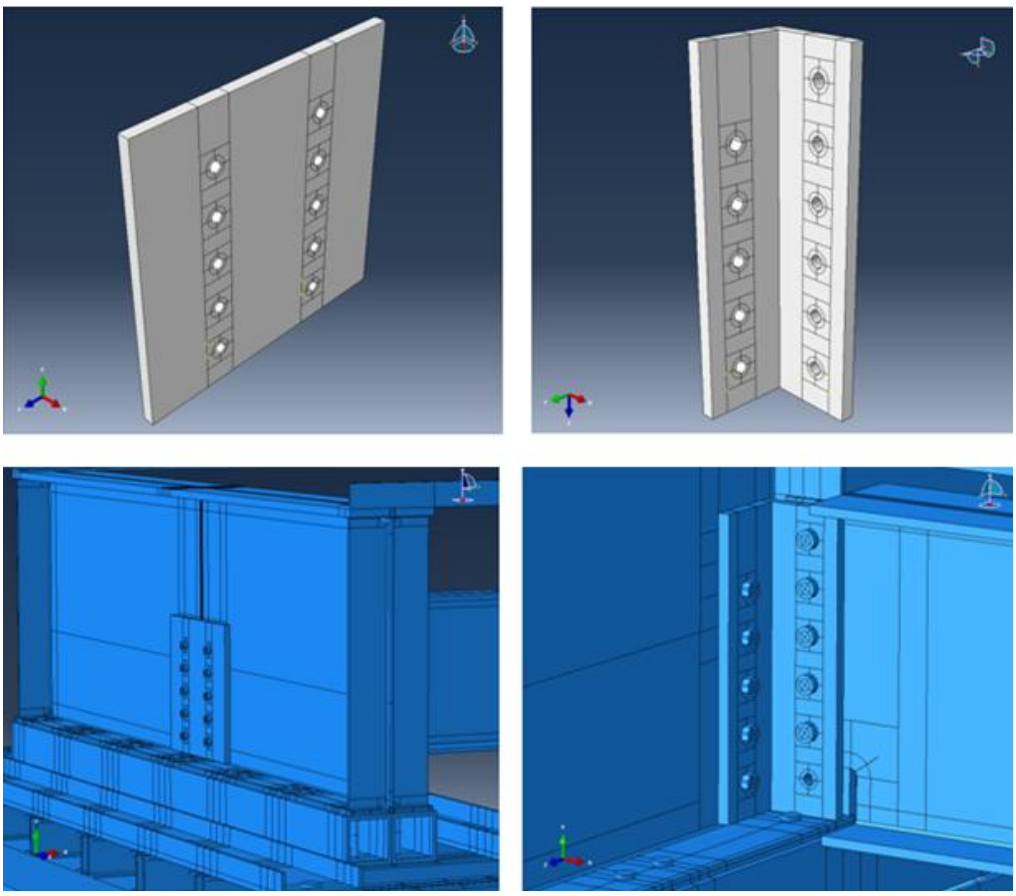

Figure 4-14 steel angle and back plate to repair Horseshoe crack

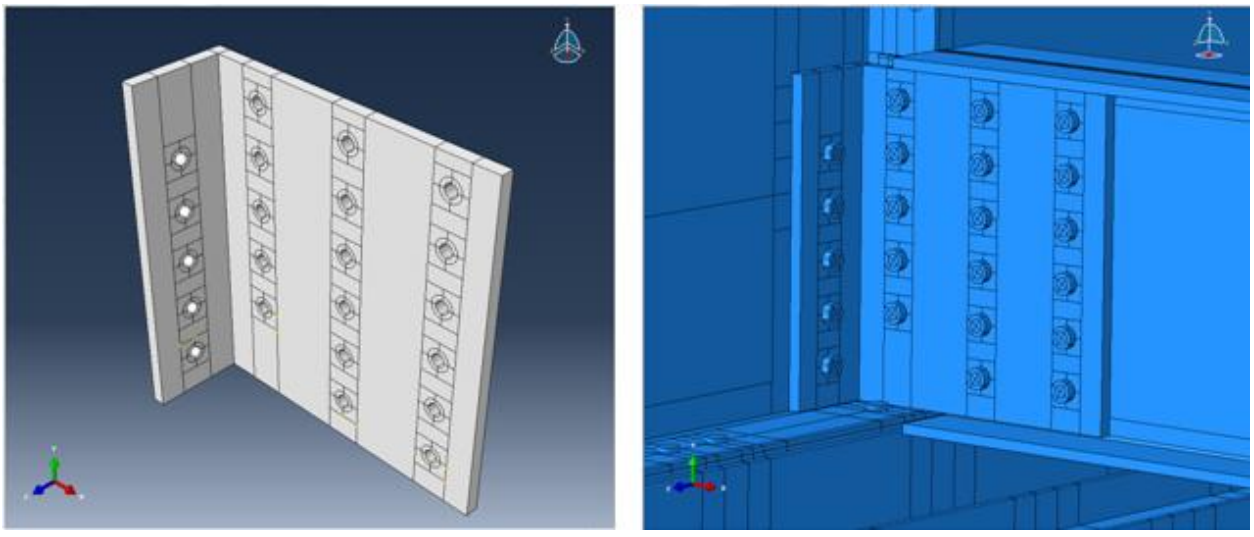

Figure 4-15 The application of L-shaped retrofit to repair the Coped

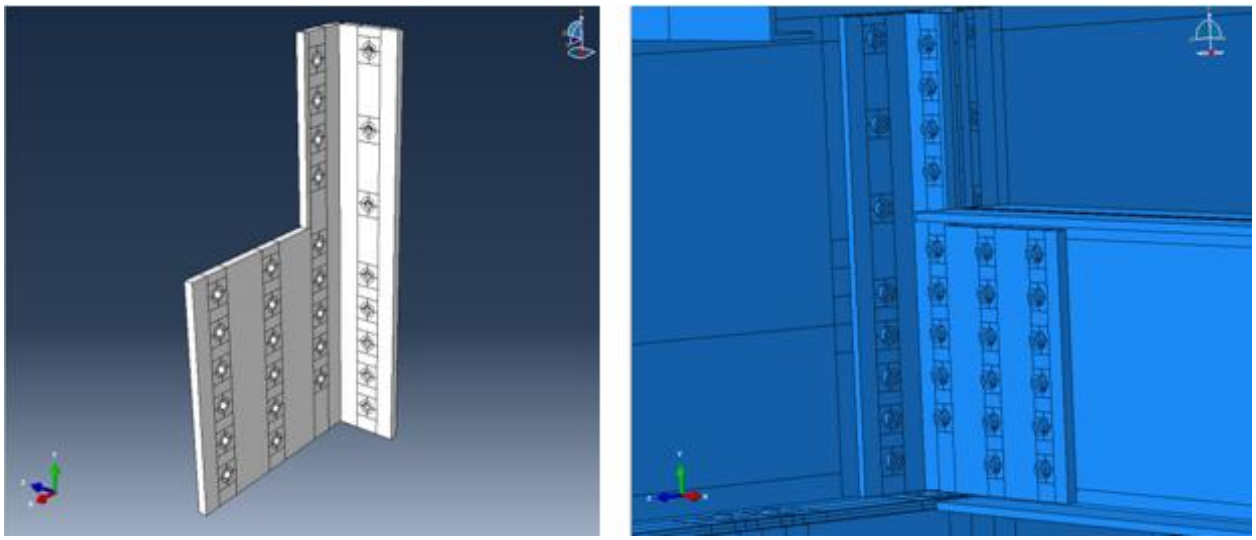

Figure 4-16 Bent plate retrofit intended to repair Horseshoe, Coped and Horizontal peak stresses

Stringer-to-Floorbeam Connection Type II

The second detail studied in this investigation, Type II Connection, was the stringer-to-floorbeam connection type made by using double angles bolted to the web of the doubly-coped stringer and the web of the floorbeam (Fig.4-17). The FEA showed that there were two critical locations with high stress concentration: the floorbeam web-to-flange weld and the cope of the stringer. The magnitude of stress demand along the web-to-flange weld was found to be higher than the stress at the cope (Fig.4-18).

The first approach taken to reduce the stress demands along the web-to-flange weld was to replace the double angles used in the original Type II connection with longer angles that were the same height as the web. The longer angles could diverge the stress concentration from the web-to-flange weld area to the wider web area of the floorbeam. The FE results showed great reduction of stresses along the web-to-flange weld (Fig.4-19 and Fig.4-20).

Future analyses should be performed to address the high stress demand at the stringer cope.

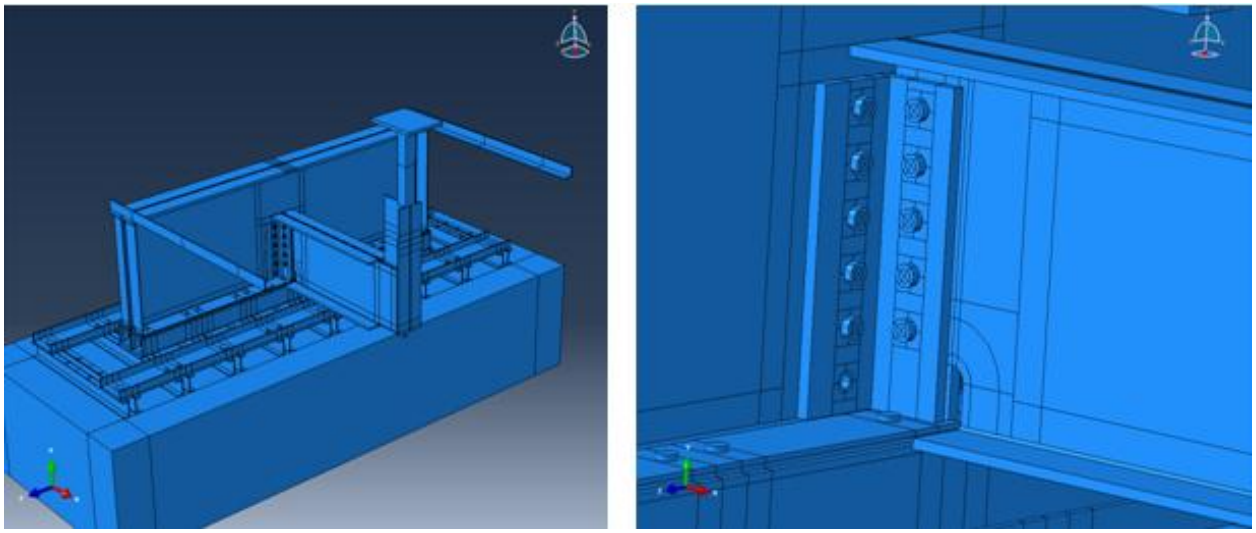

Figure 4-17 Stringer-to-floorbeam connection with CXN#2 (No Retrofit)

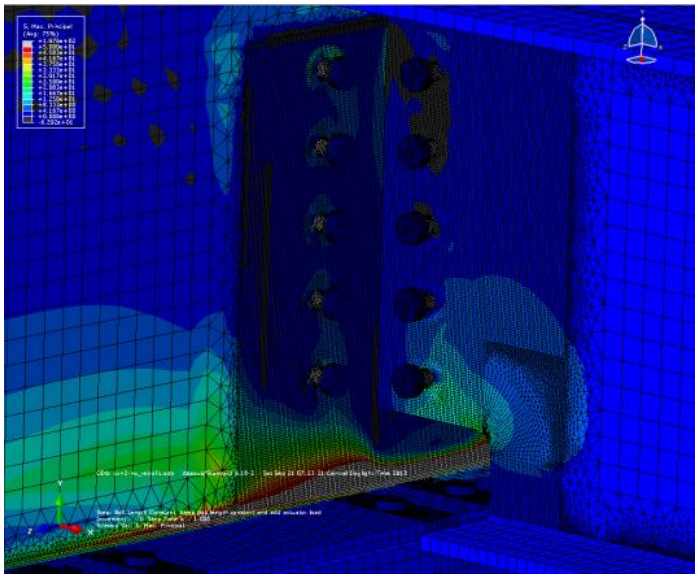

Figure 4-18 CXN#2 stress field on the interior floorbeam (No Retrofit)

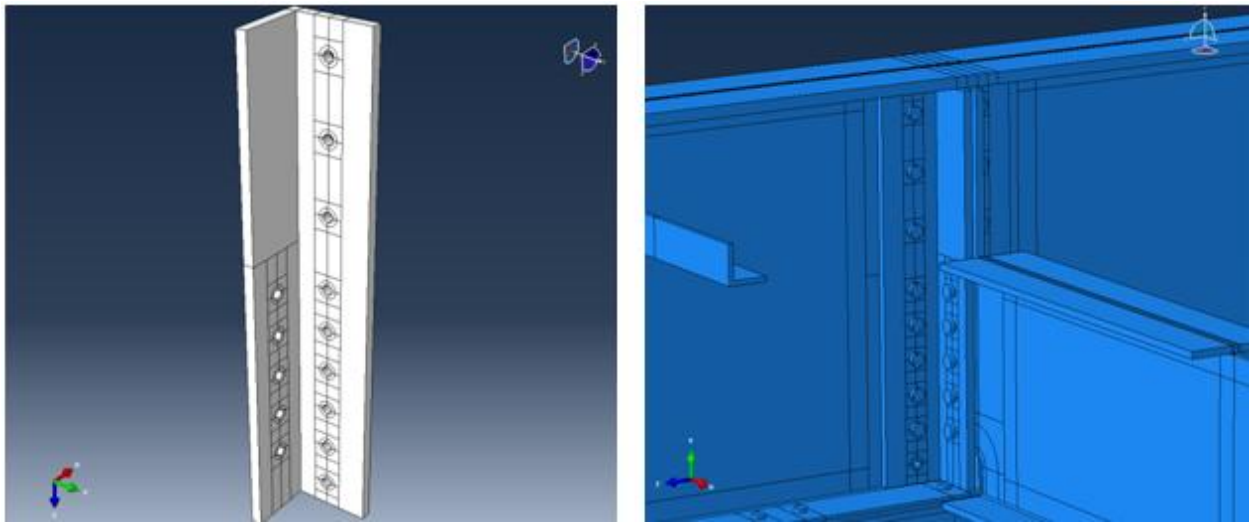

Figure 4-19 Longer angles used for repairing Horizontal crack (Retrofitted)

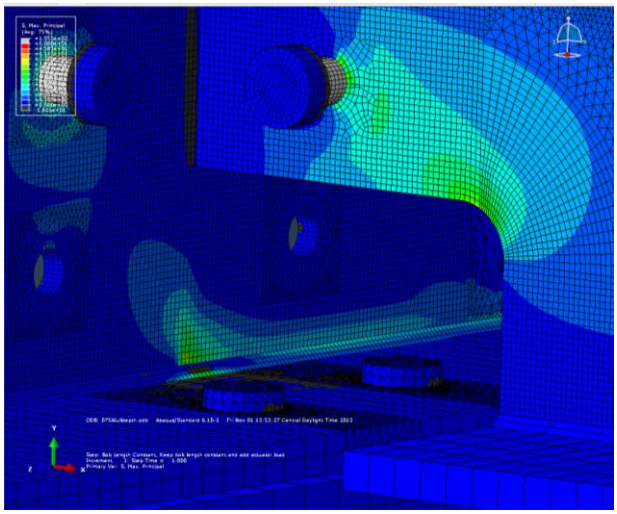

Figure 4-20 CXN#2 stress field on interior floorbeam (Retrofitted)

Experimental Program

The Type I connection subassembly was cycled under a dynamic tensile force that ranged from 4-kN (1.0-kip) to 22-kN (5.0-kip) that applied by 245-kN (55-kip) actuator at the top of the WT member. The connection plate-to-web weld crack was allowed to initiate and propagate to a length of 57-mm (1 ½ in-) before the retrofit was applied. The crack was inspected at every 5,000 cycles while the specimen was subjecting to cyclic loading. The inspection technique was performed using Zyglo Penetrant (ZL-27A) by Magnaflux and UV flashlight to see crack

openings. Data was recorded after each inspection under static load application. The static loading was done by applying a constant load progressing from 0-kN (0-kip) to 27-kN (6-kip). The data was recorded continuously using a data acquisition system manufactured by National Instruments. A protocol was written in Labview 2011 to read and record data at a rate of 20 samples/second. Once the horseshoe-crack length grew to about 38-mm (1½-in), the angles-with-back-plate retrofit was installed on the floorbeam engaging both sides of the connection plate and the fascia side of the floorbeam (Fig.4-21). The experimental testing was still ongoing at the time of writing. It is anticipated that cracking will next present at the cope of the stringer due to the high stress demand seen in FE model.

Figure 4-21 1st retrofit to repair horseshoe crack a) steel back plate b) steel angles

At the time of writing, the Type II connection subassembly was currently also being tested under the same load range as used for the Type I connection subassembly. A retrofit will be applied when cracking appears in the specimen.

Results

Type I Connection

In the un-retrofitted stage, the FE results showed high stress concentrations located at three different regions, of which the connection plate-to-web weld toe experienced the highest local stress demands (Fig.4-22). This result was also in agreement with the result from physical testing in which it was observed that cracks first initiated at the connection plate-to-web weld toe (Fig. 4-23). Three strain gages at three different locations were chosen to observe the variation in deformation as the number of cycles increased. Those strain gages were labeled as Gage WBS (*Horizontal)*, Gage BS (*Horseshoe)*, and Gage CStr0.1875 (*Coped)*, and the locations were shown in figure 4-7 and figure 4-8. The data recorded indicated to have the highest magnitudes at the connection plate-to-web weld toe with a maximum of 1450με. As more and more cycles were applied, the strains at the cope gradually increased whereas the strains at the flange-to-web weld decreased (Fig.4-24).

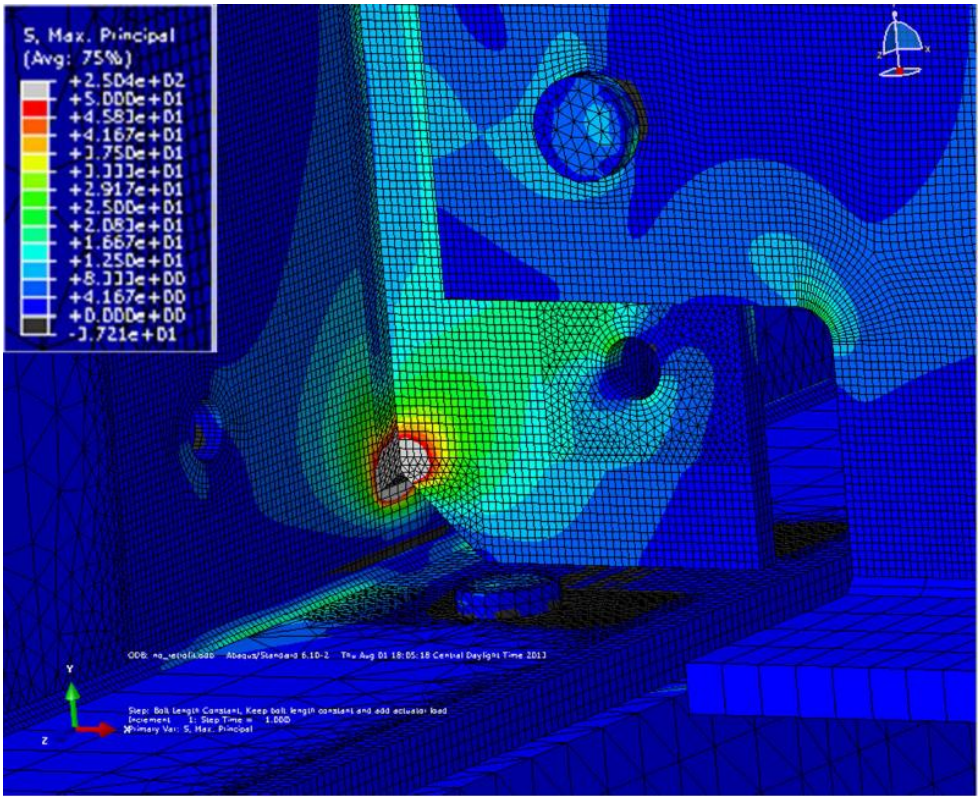

Figure 4-22 High stress demand in un-retrofitted model (un-cracked) (Type 1 Connection)

Figure 4-23 Cracks initiated from the connection plate-to-web weld in un-retrofitted model (Type I connection)

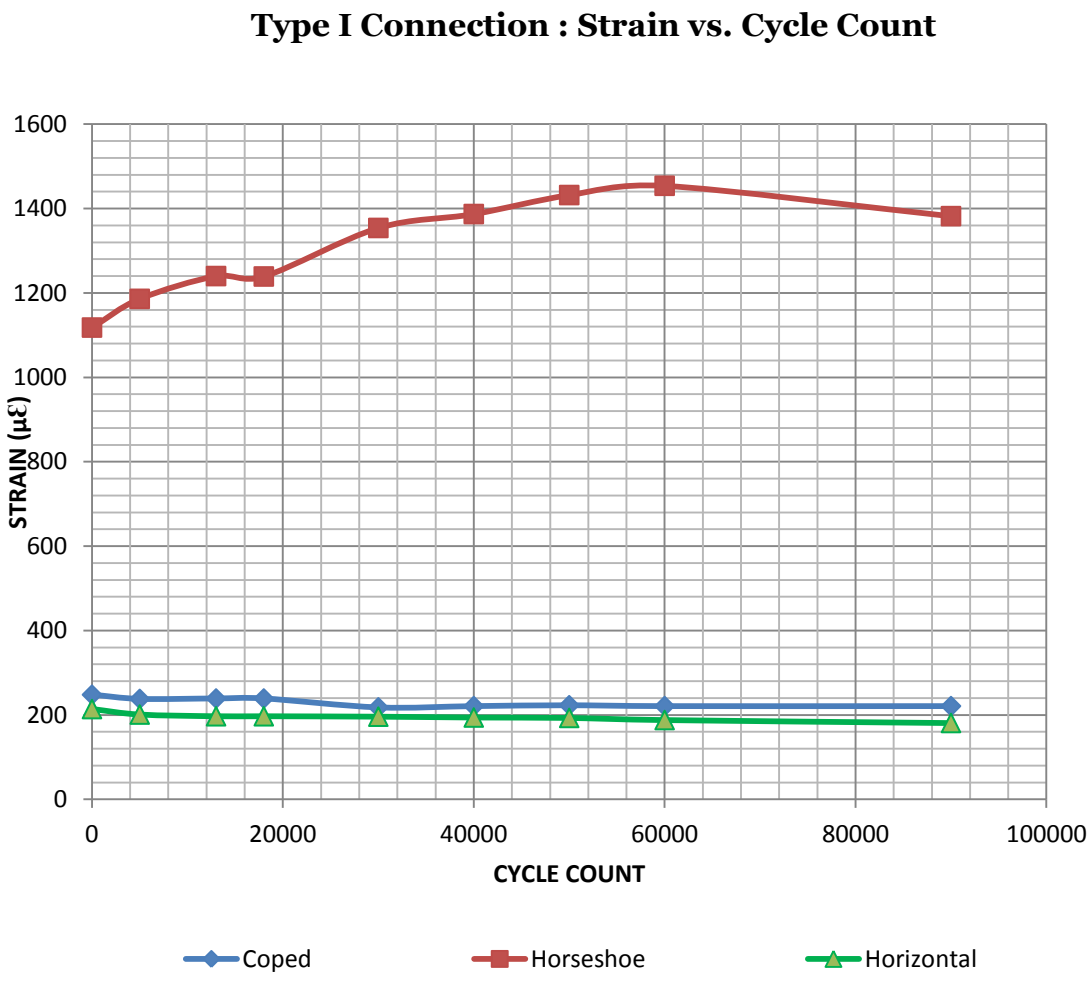

Figure 4-24 Relationship between cycle count and strain at three critical locations

The specimen was then retrofitted with steel angles and a back plate as shown in Fig.4-14. At the time of writing, physical testing is still ongoing.

Results from the retrofitted simulation showed that the maximum principal stress demand at the connection plate-to-web weld toe was reduced by 74.3%. However, maximum principal stresses at the cope of the stringer and at the flange-to-web weld were shown to increase after the retrofit by 40.9% and 322.4%, respectively (Fig.4-25 & Table 4-1). Since the maximum principal stress demand at the cope was slightly greater than at the flange-to-web weld, it was surmised that cracking might first initiate at the stringer cope. Thus, the L-shape retrofit was next applied, replacing the angles.

The model including the L-shape retrofit showed that the controlling maximum principal stress at the cope was reduced by 97.2%. The magnitude of principal stress at the flange-to-web weld was increased from 33.8-MPa (4.9-ksi) to 145.5-MPa (21.1-ksi) (Fig.4-26 & Table 4-1).

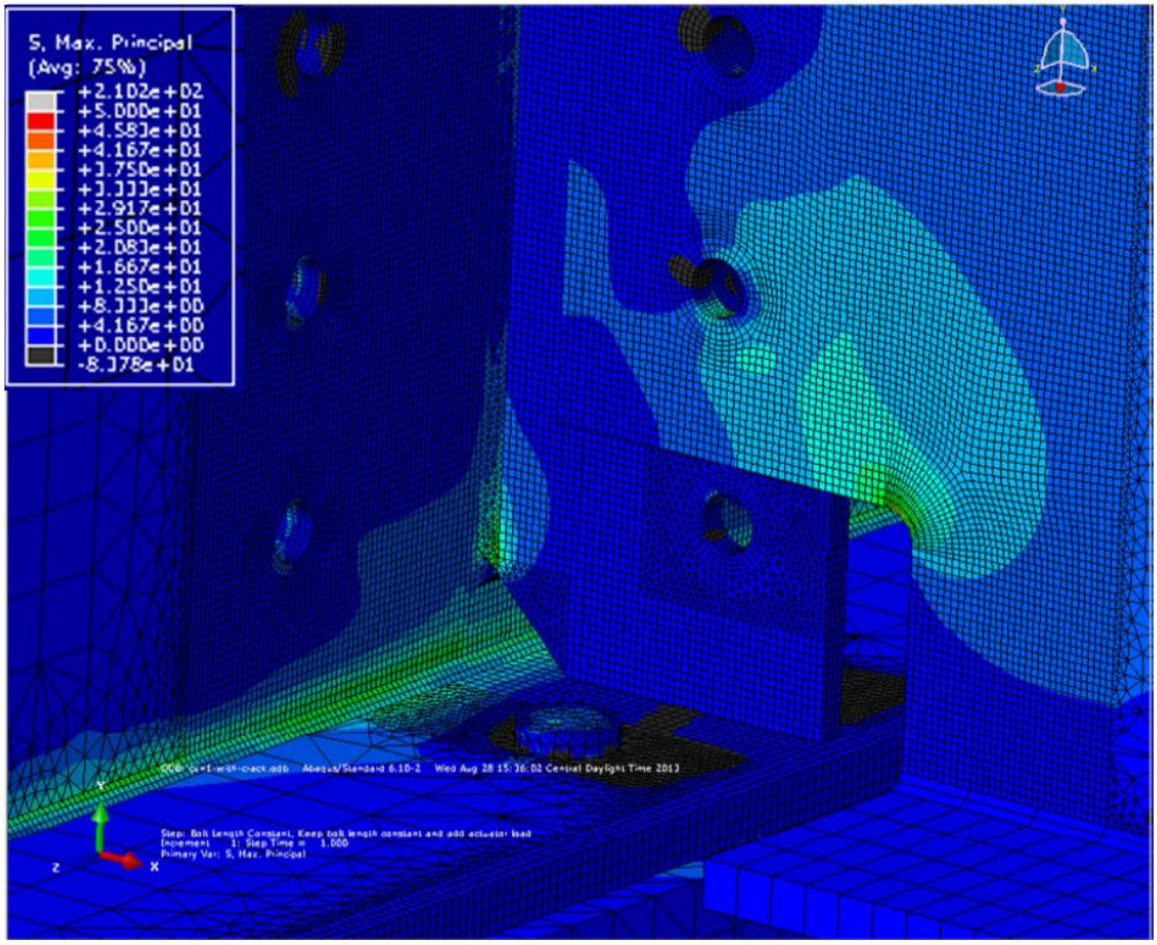

Figure 4-25 Stress field in Type I connection with angles-and-back-plate retrofit

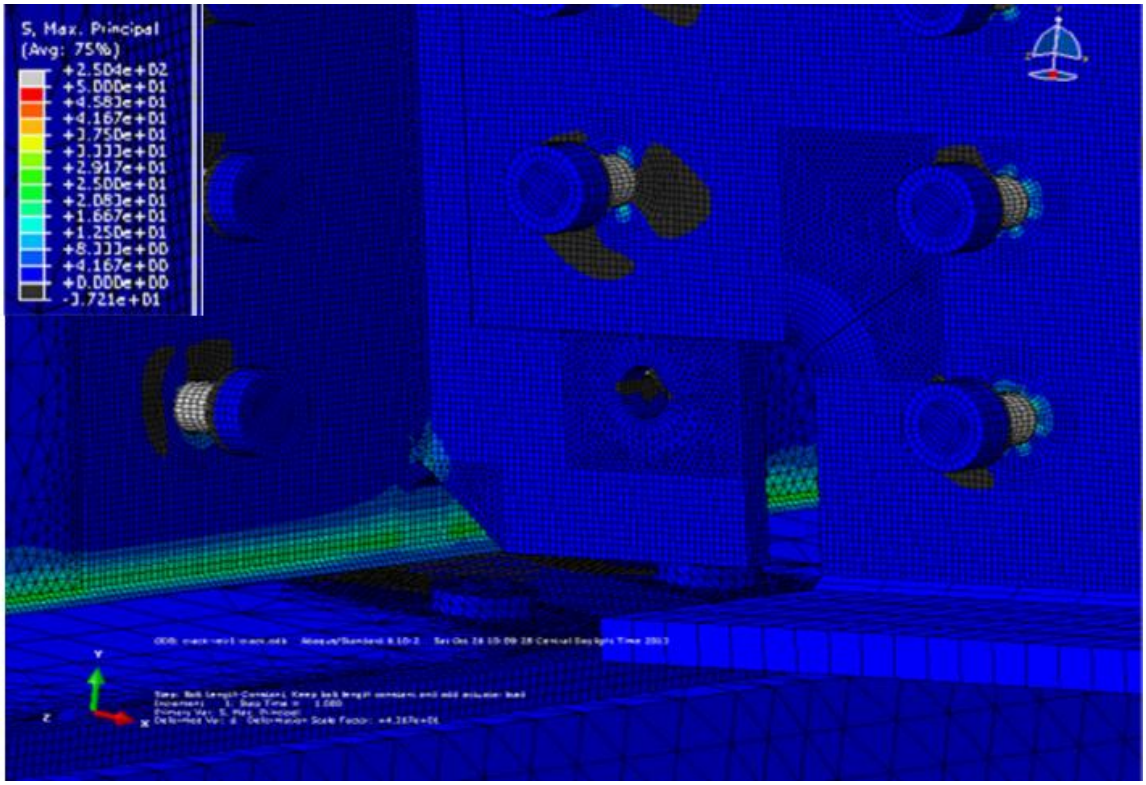

Figure 4-26 Stress field in Type I connection after applying L-shaped retrofit

Table 4-1 Maximum principal stress extracted from FE models

HSS path	Max. principal stress (non-retrofitted), MPa (ksi)	Max. principal stress (retrofitted), MPa (ksi)	
		Angles-with-back-plate Retrofit	L-shaped Retrofit
HSS1	271 (39.3)	69.6 (10.1)	51.7 (7.5)
HSS2	33.8 (4.9)	142.7 (20.7)	145.5 (21.1)
HSS3	106.2 (15.4)	149.6 (21.7)	4.1 (0.6)

Conclusion

The research presented in this paper was carried out to develop retrofits that may prolong the fatigue life of stringer-floobeam bridge systems. For Type I connection details, three locations susceptible to fatigue cracking were detected in the initial FE model. Those were the connection plate-to-web weld, the flange-to-web weld, and the stringer cope. Double angles and a back plate were applied as an initial retrofit to reduce the stress demand at the connection plate-to-web weld. The maximum principal stress at that weld was reduced by 74.3%, but at the same time, the maximum principal stresses at the cope and at the web-to-flange weld were increased by 40.9% and 322.4%, respectively. L-shaped plates were then applied as a retrofit in the model, replacing the double angles. The maximum principal stress at the cope was reduced by about 97.2% compared to the un-retrofitted stress demand. It is recommended that future research be performed to determine whether a set of bent L-shaped plates would be more effective, and able to reduce stress demands at the web-to-flange weld as well.

References

Roeder, C. W., MacRae, G. A., Arima, K., Crocker, P. N., Wong, S. D. (1998) "Fatigue cracking of riveted steel tied arch and truss bridges." *Rep. No WA-RD 447.1*, Washington Department of Transportation, Olympia, Washington.

Fisher, J. W., Yen, B. T., Wang, D. (1990). "Fatigue strength of riveted bridge members." *J. Struct. Eng.* 1990. 116:2968-2981.

Yam, M. C. H., and Cheng, J. J. R. (1990). "Fatigue strength of coped steel beams." *J. Struct. Eng.* 116(9), 2447-2463.

Al-Emrani, M. (2000). "Fatigue in riveted railway bridges – A study of the fatigue performance of stringers and stringer-to-floorbeam connections." Goteborg, Sweden.

Al-Emrani, M. (2005). "Fatigue performance of stringer-to-floor-beam connections in riveted railway bridges." *J. Bridge Eng*. 2005.010:179-185.

Roeder, C. W. MacRae, G., Leland A. Rospo, A. (2005) "Extending the fatigue life of riveted coped stringer connections." J. Bridge Eng. 2005.

Simulia. (2010). ABAQUS FEA Version 6.10-2. Providence, RI. http://www.simulia.com.

Appendix A-1: Lab Notes Recorded During Testing the Composite Block Retrofit

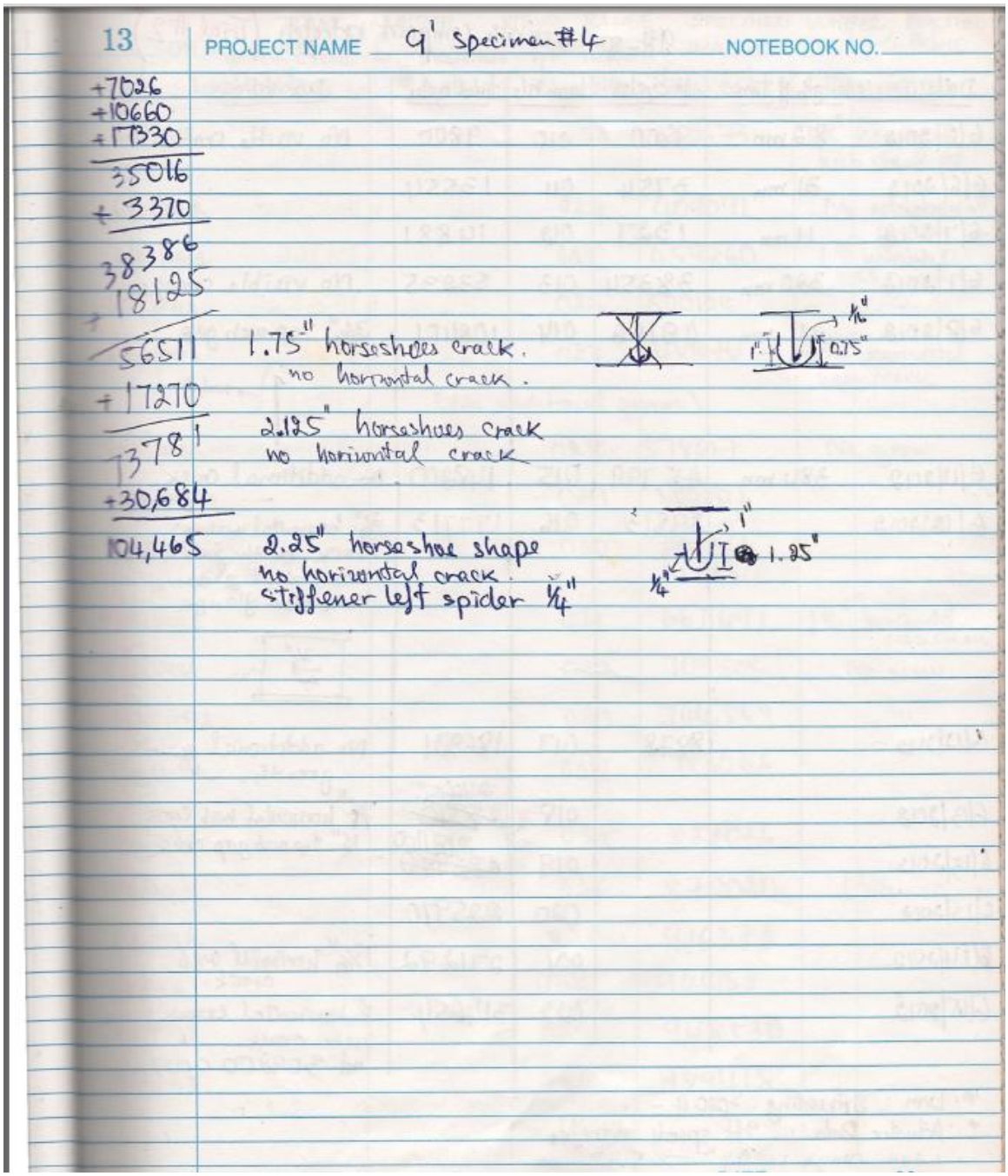

14 PROJECT NAME 9ft-spec4 with composit retrofits (Trial #2) NOTEBOOK NO.

Date	length of time	#cycles	Lvm File	total cycles	Description
6/6/2012	82 mn	9800	010	9800	No visible cracks
6/6/2012	31 mn	3754	011	13554	
6/7/2012	11 mn	1327	012	14881	
6/7/2012	380 mn	38354	013	53235	No visible cracks
6/8/2012	411 mn	49166	014	102401	3/16" top web gap 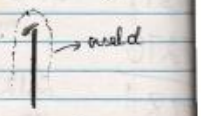
6/11/2012	384 mn	45,799	015	148200	No additional crack growth
6/12/2012		29513	016	177713	3/4" horizontal web crack on the facia side about 2" above the bottom flange. 
6/12/2012		8878	017	186591	No additional ~~grow~~ growth.
6/13/2012			018	~~218140~~ 214658	7/8" horizontal web crack 1/4" top web gap crack
6/13/2012			019	~~225970~~ 218160	
6/13/2012			020	225970	
6/14/2012			021	271292	13/16" horizontal web crack
6/15/2012			022	314654	1" horizontal ~~crack~~ web crack at 309200 cycles

*: Lvm : 9ftreading - 3pec 4 - ....
*. Actuator Data : 9ft spec4 retrofit

15 TRIAL NUMBER, STRESS RANGE, SPECIMEN NUMBER, REACTION FRAME

PROJECT NAME # OF CYCLE AT BEGINING OF TRIAL LOAD NOTEBOOK NO.

Date	Length of time	# cycles	Lvm File	total cycles	Description
6/18/2012			023	362673	1 1/16" horizontal web crack
6/19/2012			024	409091	No additional growth.
6/20/2012			025	459860	1 1/8" horizontal web crack.
6/21/2012			026	500104	
6/22/2012			027	540470	1 3/16" horizontal web crack
		(No additional growth).			
6/25/2012			028	578617	No grow
6/26/2012			029	600001	
6/26/2012			030	~~619930~~ 619930	
6/27/2012			031	667,497	1 1/4" horizontal web crack.
6/28/2012			032	709,505	No grow
6/29/2012			033	744,569	
7/2/2012			034	783062	
7/3/2012			035	827026	
7/5/2012			036	872020	1 5/16"
7/6/2012			037	916373	
7/9/2012			038	940158	
7/11/2012			039	948538	
7/12/2012			040	989415	

16 PROJECT NAME _____ NOTEBOOK NO. _____

Date	Length of time	# cycles	Lvmfil	total cycles	Description
7/13/2012			41	1,012,515	
7/16/2012			42	1,055,734	
7/17/2012			44	1,101,166	
7/18/2012			46	1,153,523	
7/19/2012			47	1,176,759	
7/20/2012			48	1,200,000	1/16" horizontal crack on the top web gap.

Map of the cracks after removing composite block.

7/27/2012

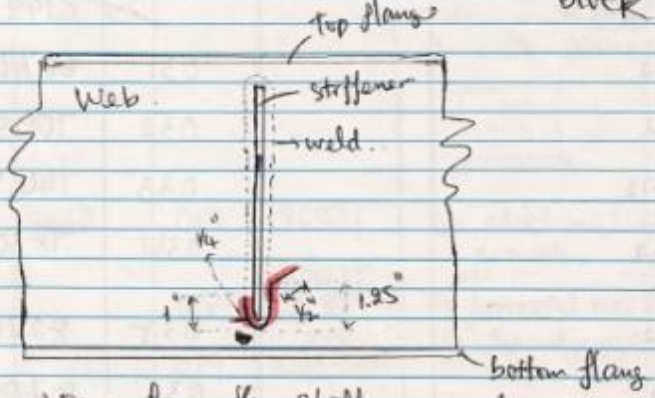

View from the stiffener side.

Stiffener side : left vertical crack = 1"
left spider crack = 1/4"
right vertical crack = 1.25"
right spider crack = 1/2"

fascia side : 1 5/16" horizontal web crack

SIGNATURE _____ DATE _____ 20

Appendix A-2 : Crack Growth Rate Recorded on the Exterior Face of Girder's Web

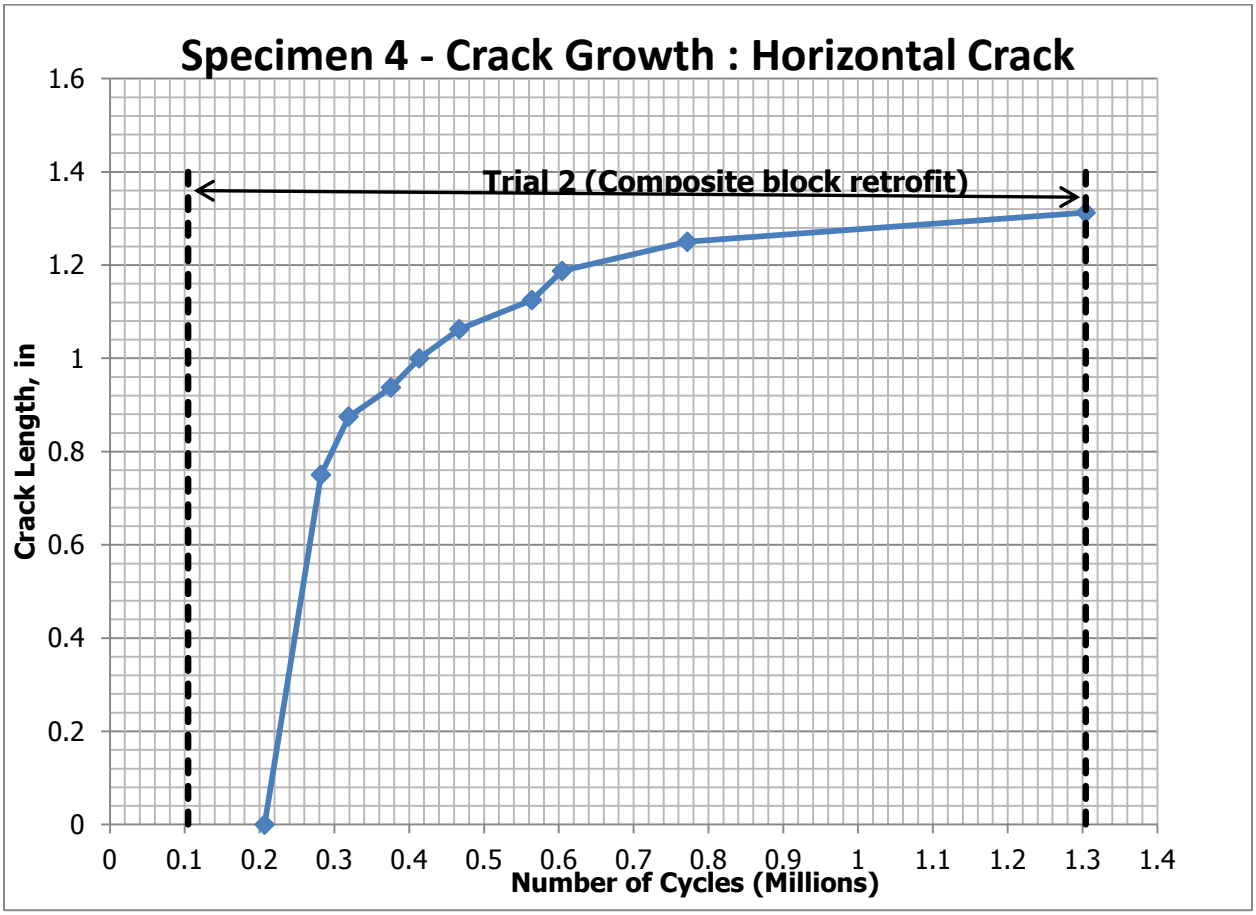

Appendix B-1 : Lab Notes Recorded During Testing CFRP Retrofit

Appendix C-1: Lab Notes Recorded During Testing Crack-arrest Holes

Reaction Frame: IICF actuator Load range: 0.2 – 2.1

DATE	# hours running	Trial #	Cycle # Start	Cycle # End	# cycles	Trial # cycles on Spec #	Description / Figures
2/19/2013	1 hr 23 mn	1	0	10,000	10,000	10,000	horse shoe crack started at the stiffener
2/19/2013	1 hr	1	10,000	16,000	6,000	16,000	No growth
3/04/2013	2 hr 5 mn	1	16,000	31,000	15,000		
3/04/2013	1 hr 23 mn	1	31,000	41,000	10,000	31,000	No growth
3/04/2013	42 mn	1	41,000	46,000	5,000	41,000	No growth
3/06/2013	1 hr 5 mn	1	46,000	60,100	14100	46,000	No growth
3/07/2013	2 hr 12 mn	1	60,100	76,000	15900	60,100	No growth
3/07/2013	2 hr 5 mn	1	76,000	91,000	15,000	76,000	No growth
3/07/2013	42 mn	1	91,000	96,000	5,000	91,000	No crack growth
						96,000	

Drilled crack-arrest holes (2").

$\Delta a = L + 2"$

$= 1\frac{3}{8}" + 2"$

$= 3.\frac{3}{8}"$

SIGNATURE
READ AND UNDERSTOOD
DATE

38 PROJECT NAME Hot Fuse

Continued Load range : 0.7K -> 5.3K

DATE	# hours testing	Trial #	Cycle # Start	Cycle # End	# cycles	Total cycles on spec.
1 4/05/2013	83mn	2	97,467	107,467	10,000	107,467
4/05/2013	83mn	2	10,000	20,000	10,000	117,467
4/11/2013	83mn	2	20,000	30,000	10,000	127,467
	83mn	2	30,000	40,000	10,000	137,467
4/12/2013	83mn	2	40,000	50,000	10,000	147,467
	83mn	2	50,000	60,000	10,000	157,467
4/15/2013	2hr 46mn	2	60,000	80,000	20,000	177,467
	8hr 46mn	2	80,000	100,000	20,000	197,467
4/16/2013	—	2	100,000	120,000	20,000	217,467
	—	2	120,000	140,000	—	237,467
	—	2	140,000	160,000	—	257,467
4/17/2013	—	2	160,000	180,000	—	277,467
	—	2	180,000	200,000	—	297,467
	—	2	200,000	220,000	—	317,467
4/18/2013	—	2	220,000	240,000	—	337,467
	—	2	240,000	260,000	—	357,467
4/19/2013	—	2	260,000	280,000	—	377,467
	—	2	280,000	300,000	—	397,467
4/23/2013	—	2	300,000	320,000	—	417,467

SIGNATURE _____ DATE _____ 20

39 PROJECT NAME _____ NOTEBOOK NO _____

Description / Figures

No growth.

SIGNATURE _____ DATE _____
READ AND UNDERSTOOD _____ DATE _____

PROJECT NAME Pilot Hand Study (#4 Spec #5) NOTEBOOK NO.

Continued

DATE	Hrs Testing	Trial #	Cycle # Start	Cycle # End	# cycles	Last File #	Total cycles on Spec.
4/2/2013	4hr 10mn	1	320,000	350,000	30,000	20	447,467
4/25/2013	4hr 10mn	2	350,000	380,000	30,000	21	477,467
4/26/2013	8h 46mn	2	380,000	400,000	20,000	22	497,467
	8h 48mn	2	400,000	420,000	20,000	23	517,467
4/29/2013	24 46mn	2	420,000	440,000	20,000	24	537,467
	→	2	440,000	460,000	20,000	25	557,467
4/30/2013	→	2	460,000	480,000	20,000	26	577,467
	4hr 30mn	2	480,000	515,000	35,000	27	612,467

SIGNATURE _____ DATE _____ 20 _____
DATE _____ 20 _____

41

Description / Figures

New crack appeared!

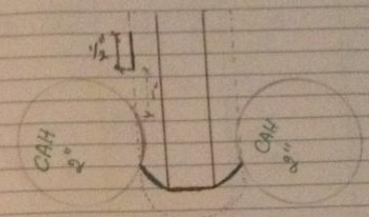

No growth.

the crack above grew to 7/8"

No growth

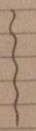

the crack grew to 1 1/8" downwards.
and a new crack on the right stiffener appeared.

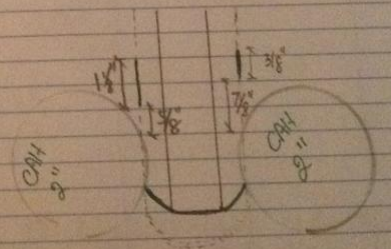

SIGNATURE _____ DATE _____ 20 _____
READ AND UNDERSTOOD _____ DATE _____ 20 _____

42 PROJECT NAME Pool Fund Study (SH- spec #5) NOTEBOOK NO

Continued:...

DATE	# hrs testing	Trial #	Cycles Start	Cycles End	# cycles	Unit #	total cycles on spec
5/01/2013	2hr 46mn	2	515,000	535,000	20,000	28	
	2hr 46mn	2	535,000	555,000	20,000	29	
5/02/2013	2hr 46mn	2	555,000	575,000	20,000	30	
5/07/2013	2hr 46mn	2	575,000	595,000	20,000	31	
5/03/2013	2hr 46mn	2	595,000	615,000	20,000	32	
5/06/2013	2hr 46mn	2	615,000	635,000	20,000	33	
5/06/2013	4h 10mn	2	635,000	665,000	30,000	34	
5/07/2013	2hr 46mn	2	665,000	685,000	20,000	35	
5/08/2013	〃	2	685,000	705,000	〃	36	
	〃	2	705,000	725,000	〃	37	
	〃	2	725,000	745,000	〃	38	

SIGNATURE DATE 20
DATE 20

43 PROJECT NAME NOTEBOOK NO

Description / Figures

No growth

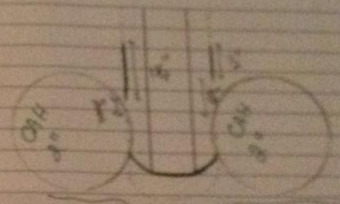

the crack on the right of stiffener grew to 9/16"

The left crack grew to 1 5/8", the right crack grew to 9/16" downwards

The left crack grew to 1 5/8"

The left is 1 3/4" which is 1/8" from CSH

The right is 3/16" which is 3/8" above CSH

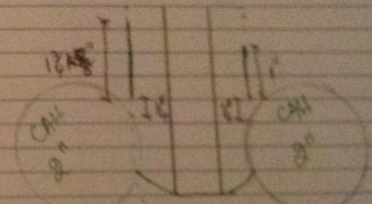

No additional growth

grew! see figure on next

SIGNATURE DATE 20
READ AND UNDERSTOOD DATE 20

44 PROJECT NAME Fatigue Hand Stacking [illegible]

DATE	# hrs testing	Trial #	cycle Start	cycle End	# cycles	Lvm File #	Total cycles on part
5/09/2013	2h 46mn + ~~5h~~ 2h 46mn	2	745,000	785,000	40,000	39	
/10/2013	2h 46mn	2	785,000	805000	20,000	40	

Description / Figures

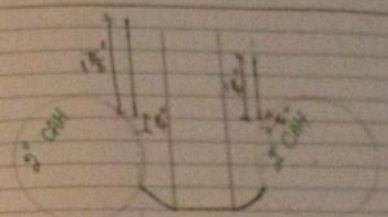

left grew to 2" (⅛" gap above the countersink)
right grew to 1⅝" (¼" gap above the CSK)

No growth

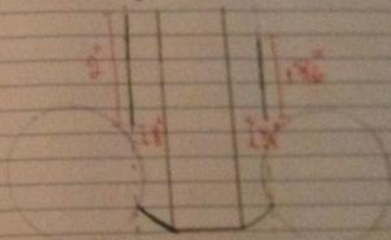

Drilling another ~~set of~~ crack-stop holes

SIGNATURE DATE

DATE 20

48

PROJECT NAME Pool Fund Study (3ft - spec #5) NOTEBOOK NO.

Date	Trial #	cycle start	cycle End	# cycles	Lion File
6/16/2013	3	190,000	210,000	20,000	(15)
6/17/2013	3	210,000	230,000	— " —	
6/18/2013	3	230,000	250,000	— " —	
6/19/2013	3	250,000	270,000	— " —	
6/20/2013	3	270,000	300,000	30,000	
6/21/2013	3	300,000	330,000	30,000	
6/21/2013	3	330,000	360,000	30,000	
6/24/2013	3	360,000	390,000	30,000	
6/26/2013	3	390,000	420,000	— " —	

SIGNATURE DATE 20

49

Description / Figures

No growth

Cracks on the fascia side

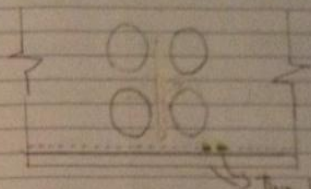

Two horizontal cracks along the weld (Flange-to-web weld) on the right side of fascia side web. The length of the cracks were 1/16"

No growth

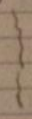

1/16" horizontal crack on left on fascia side about 1/2" from CSH

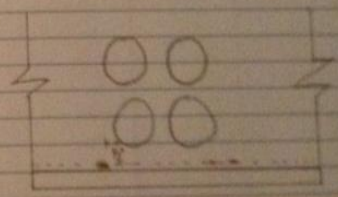

No growth

Two horizontal cracks on stiffener side 0.45" and a 1/16" long with 0.125 apart.

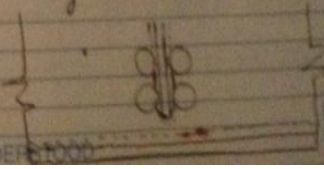

SIGNATURE DATE 20
READ AND UNDER DATE 20

Appendix D-1: Data Acquisition Used During Stringer-floorbeam Testing

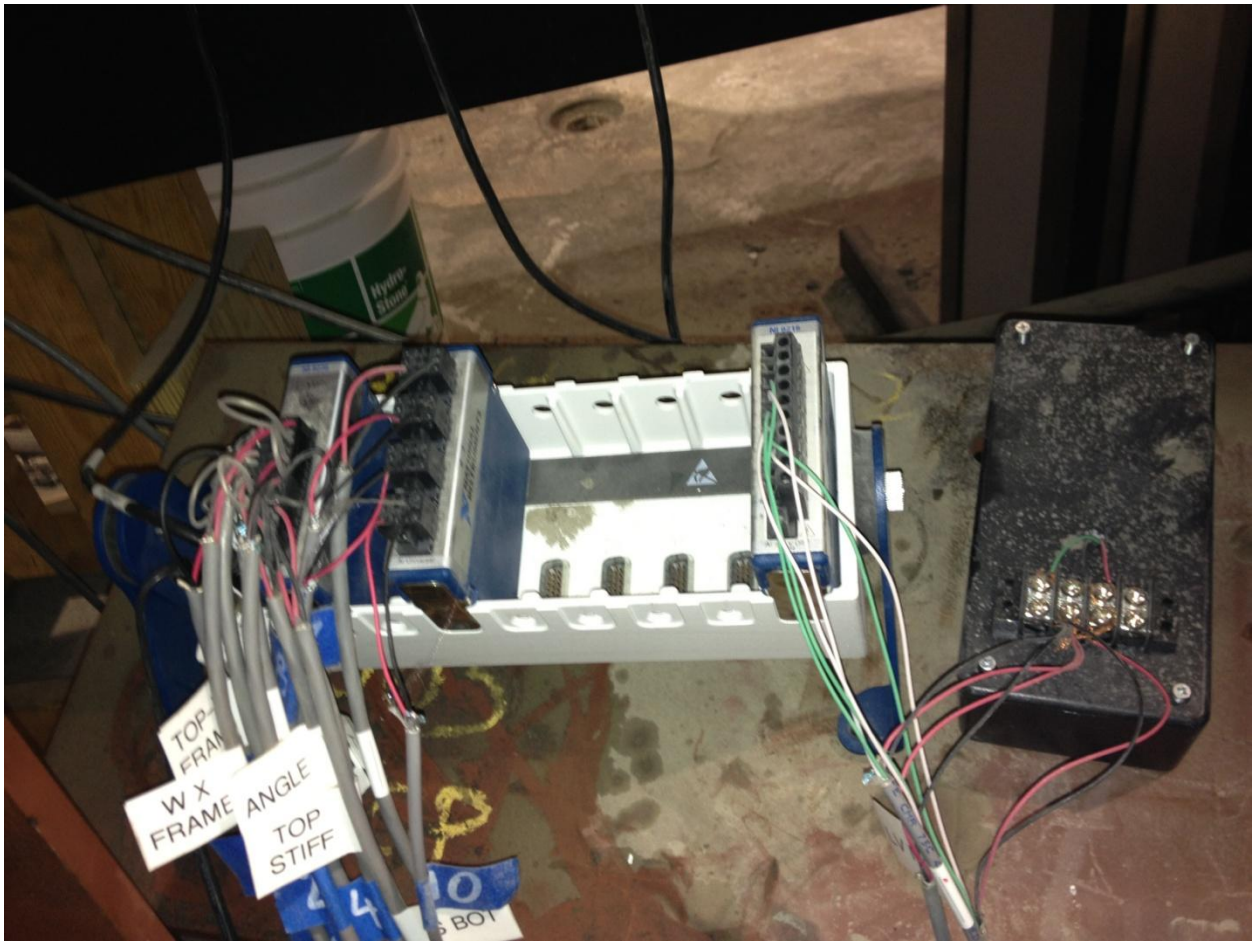

Appendix D-2: Lab Note Recorded During Testing Stringer-floorbeam

54

PROJECT NAME MATC (5+ connection type) NOTEBOOK NO.

Load range : 10% → 4.5%

Date	Load #	Short Cycle	Fatal	* cycles	Loop-Fatal / Partial Fatal cycle of specimen #
	1	0	5000	5,000	5000
	1	5,000	13,000	8,000	13,000
	1	13,000	18,000	5,000	18,000
	1	18,000	23,000	5,000	23,000
7/30/2013	1	23,000	30,000	7,000	30,000
7/31/2013	1	30,000	40,000	10,000	40,000
8/1/2013	1	40,000	50,000	10,000	50,000
8/1/2013	1	50,000	60,000	10,000	60,000

SIGNATURE
READ AND UNDERSTOOD
DATE
DATE
20
20

55

PROJECT NAME NOTEBOOK NO.

Figures / Details

3/16" horseshoe crack on left stiffener (left horseshoe)

3/8" stiffener crack (between weld and stiffener) and 1/4" horseshoe crack on the right stiffener.

stiffener crack = 1/2" ; right horseshoe = 1/16"

No additional growth.

left horseshoe = 3/16"

left horseshoe = 1/2" ; right horseshoe = 3/8"

stiffener crack = 1/2" ; right horseshoe = 7/16"

right horseshoe = 9/16"

SIGNATURE
READ AND UNDERSTOOD
DATE
DATE